



A generalized data selection method for atmospheric carbon dioxide data

Ye Yuan

Vollständiger Abdruck der von der Fakultät Wissenschaftszentrum Weihenstephan für Ernährung, Landnutzung und Umwelt der Technischen Universität München zur Erlangung des akademischen Grades eines

Doktors der Naturwissenschaften (Dr. rer. nat.)

genehmigten Dissertation.

Vorsitzender:

Prof. Dr. Axel Göttlein

Prüfer der Dissertation:

1. Prof. Dr. Annette Menzel
2. Prof. Dr. Michael Leuchner
3. Prof. Dr. Hans Peter Schmid

Die Dissertation wurde am 27.11.2019 bei der Technischen Universität München eingereicht und durch die Fakultät Wissenschaftszentrum Weihenstephan für Ernährung, Landnutzung und Umwelt am 13.08.2020 angenommen.



路漫漫其修远兮，吾将上下而求索。
The road ahead is long and has no ending;
yet high and low I will search with my will
unbending.

屈原《离骚》

Abstract

Data selection or filtering is critical to flag non-representative data in time series of atmospheric constituents measured at Global Atmosphere Watch (GAW) sites. This allows extracting meaningful information on the measuring component and measurement site. For a worldwide database of high-quality measurements with the best possible compatibility, it is of crucial interest to develop an optimal set of automated data selection methods which could be applied at many measurement sites. However, data selection is always customized based on site locations, measurement instruments, and measurement techniques. In order to make the selection routine generalized and derive representative selected results, the most appropriate parameters and threshold criteria are required.

This doctorate study developed the data selection method named Adaptive Diurnal minimum Variation Selection (ADVS) for atmospheric carbon dioxide (CO_2) measurements at elevated mountain stations based on the typical diurnal variation. This statistical selection method was compared and validated with frequently applied conventional methods based on statistical and meteorological properties at European GAW stations at distinct elevations. Later on, the long-term CO_2 records of 36 years at Zugspitze-Schneefernerhaus, Germany, were used to evaluate the efficiency of data selection and examine the difference after selection. In further data analysis routines the respective trend, seasonality, and inter-annual variations were analysed. Furthermore, comparisons of continuous in situ measurements with ground- and satellite-based column-averaged measurements were done to further investigate the comparability of measurements with data selection methods applied.

Results showed that ADVS data selection performed appropriately and rigorously on the mountainous measurement series, only selecting the uninfluenced (most representative) data to obtain the background CO_2 levels in the lower free troposphere (LFT). Measurement site characteristics were clearly differentiated by such a systematic selection routine, particularly referring to the differences in elevation and meteorological parameters influencing air mass transport. Different data selection methods yielded different percentages of selected data exhibiting different levels of acceptance in so-called outliers (or local pollution). After applying a consistent seasonal decomposition technique (STL) to the long-term data series, ADVS data selection resulted in highly comparable annual growth rates across measurement sites and techniques which were in good accordance with global trends. However, ADVS selected data series had considerably smaller seasonal amplitudes indicating less local influences on the selected data. The systematic application of ADVS and STL methods on in situ measurements reached good agreements with column-averaged atmospheric carbon dioxide measurements, indicating a significant representativeness of the GAW measurements for the regional scale as well as providing more reliable ground truth evidence for remote sensing and modelling.

Zusammenfassung

Die Datenauswahl oder -filterung ist entscheidend, um nicht-repräsentative Daten zu kennzeichnen, die in Zeitreihen von atmosphärischen Bestandteilen an Global Atmosphere Watch (GAW) Beobachtungsstationen gemessen wurden. Auf diese Weise lassen sich aussagekräftige Informationen über die Messkomponente am Messort gewinnen. Für eine weltweite Datenbank mit qualitativ hochwertigen Messungen bei bestmöglicher Kompatibilität ist es von entscheidender Bedeutung, einen optimalen Satz von automatisierten Datenauswahlverfahren zu entwickeln, die an vielen Messstellen eingesetzt werden können. Die Datenauswahl wird jedoch immer individuell auf Basis der Standorte, der Messgeräte und der Messtechniken vorgenommen. Um die Auswahlroutine zu verallgemeinern und repräsentativ ausgewählte Ergebnisse abzuleiten, werden die am besten geeigneten Parameter und Schwellenwerte benötigt.

In dieser Promotionsstudie wurde die Datenselektionsmethode "Adaptive Selektion der täglichen minimalen Variation (ADVS)" für atmosphärische Kohlendioxidmessungen (CO_2) an Hochgebirgsstationen auf Basis der typischen Tagesvariation entwickelt. Diese statistische Auswahlmethode wurde mit häufig angewandten konventionellen Methoden verglichen und validiert, die statistische und meteorologische Eigenschaften an europäischen GAW-Stationen in unterschiedlichen Höhenlagen verwenden. Danach wurden die langfristigen, 36-jährigen CO_2 -Messreihen am Zugspitze-Schneefernerhaus genutzt, um die Effizienz der Datenauswahl zu bewerten und Unterschiede in den Zeitreihen vor und nach der Auswahl zu untersuchen. In weiteren Datenanalyseroutinen wurden die jeweiligen Trends, Saisonalität und interannuellen Schwankungen analysiert. Darüber hinaus wurden Vergleiche von kontinuierlichen In-situ-Messungen mit boden- und satellitengestützten säulengemittelten Messungen durchgeführt, um die Vergleichbarkeit von Messungen nach der Anwendung von Datenauswahlmethoden weiter zu untersuchen.

Die Ergebnisse zeigten, dass die ADVS-Datenauswahl mit den Messreihen an Bergstandorten geeignet war, am restriktivsten funktionierte und nur die unbeeinflussten (repräsentativsten) Daten ausgewählt wurden, um die CO_2 Hintergrundkonzentrationen in der unteren freien Troposphäre (LFT) zu erlangen. Die Merkmale der Messstellen wurden durch eine solche systematische Auswahlroutine klar differenziert, insbesondere in Bezug auf die Höhenunterschiede und meteorologischen Parameter, die den Luftmassentransport beeinflussen. Die verschiedenen Datenauswahlverfahren ergaben unterschiedliche Prozentsätze ausgewählter Daten, die sogenannte Ausreißer (oder lokaler Verschmutzung) in unterschiedlichem Ausmaß verwarfen. Nach Anwendung einer konsistenten saisonalen Zerlegungstechnik (STL) auf die Langzeitdatenreihen führte die ADVS-Datenselektion zu hochgradig vergleichbaren jährlichen Wachstumsraten über Messstellen und -techniken hinweg, die den globalen Trends gut entsprachen. Die ausgewählten ADVS-Datenreihen wiesen jedoch deutlich geringere saisonale Amplituden

Zusammenfassung

auf, was auf weniger lokale Einflüsse auf die ausgewählten Daten hinweist. Die systematische Anwendung von ADVS- und STL-Methoden auf In-situ-Messungen ergab gute Übereinstimmungen mit säulengemittelten atmosphärischen Kohlendioxidmessungen, was auf eine signifikante Repräsentativität der GAW-Messungen für den regionalen Maßstab hinweist und zuverlässigere bodengestützte Messdaten (Feldvergleich) für Fernerkundung und Modellierung liefert.

Contents

Abstract	v
Zusammenfassung	vii
Contents	ix
List of Figures	xi
List of Tables	xv
1 Introduction	1
1.1 Atmospheric carbon dioxide	1
1.2 Sources and sinks in the global carbon cycle	2
1.3 Continuity and consistency in measurements	4
1.3.1 Long-term measurements within the global observation network . .	4
1.3.2 Improvements of data processing	6
1.3.2.1 Tracer / chemical data selection	7
1.3.2.2 Meteorological data selection	7
1.3.2.3 Statistical data selection	7
2 Data sets overview	9
2.1 Continuous in situ measurements	9
2.2 Column-averaged measurements	11
2.3 Wind sector	13
3 Methods overview	17
3.1 Variation in time	17
3.2 Diurnal variation and ADVS	19
3.3 Time series analysis	22
3.3.1 STL	23
3.3.2 Curve fitting	25
3.4 Software	26
4 Publication abstracts and contributions	29
4.1 Development of consistent data selection method	30
4.2 Application of data selection on long-term measurements	31
4.3 Comparison of CO ₂ measurements and models	32

Contents

5 Discussion	33
5.1 Data selection	33
5.1.1 Performance	33
5.1.2 Correlation	35
5.1.3 Functionality	36
5.2 Data analysis	36
5.3 Validation with wind sector	38
5.4 Practical implementation of ADVS in the GAW network	39
6 Outlook	45
References	47
Acknowledgment	61
A Publication reprints	63

List of Figures

1.1	Carbon dioxide concentrations of (a) combination of ice-core data before 1958 and Mauna Loa Observatory data after 1958; (b) Mauna Loa Observatory from 1958 until October 22, 2019, i.e., the Keeling Curve (figures adapted from website of the Scripps Institution of Oceanography SIO). The CO ₂ data after 1958 are from the Scripps CO ₂ program (Keeling et al., 2001). The CO ₂ data before 1958 going back 800,000 years are from Lüthi et al. (2008).	2
1.2	Schematic representation of the overall perturbation of the global carbon cycle caused by anthropogenic activities, averaged globally for the decade 2008–2017. The uncertainty in the atmospheric CO ₂ growth rate is very small (± 0.02 GtC yr ⁻¹) and thus neglected. Figure and caption are taken from Figure 2 in Le Quéré et al. (2018).	3
1.3	GAW network with the 31 Global Stations (figure taken from the website of WMO).	5
1.4	Diagram describing the general data processing routine for atmospheric CO ₂ measurements in GAW network.	6
2.1	GAW Global station Zugspitze-Schneefernerhaus (image: L. Ries).	10
2.2	Monthly CO ₂ concentrations at German stations and comparison to the world trend by WMO (figure adapted from the website of Umweltbundesamt with available monthly CO ₂ data sets).	11
2.3	(a) and (b) Global average XCO ₂ by OCO-2; (c) and (d) Monthly global map of XCO ₂ Level 2 data captured by GOSAT; (e) and (f) Monthly global map of XCO ₂ Level 3 data estimated by GOSAT. Time stamps are April and July of 2017 (figures taken from websites of OCO-2 and GOSAT).	13
2.4	Bivariate polar plots of CO ₂ concentrations measured at ZSF (2002–2017). The colour scale shows the concentration of CO ₂ in ppm and the radial scale shows the wind speed (ws, in m s ⁻¹), which increases from the centre of the plot radially outwards. The plotting method and the caption are based on Carslaw and Beevers (2013).	14
3.1	Temporal variation in CO ₂ concentrations in ppm measured at ZSF from 2002 to 2018. The shading shows the 95% confidence intervals in the mean. Times are expressed in UTC + 1.	18

List of Figures

3.2 Schematic representation of a typical mean diurnal cycle based on existing measured CO₂ data at ZSF illustrating the night-day differences at elevated mountain stations. The dark grey shading represents for the nocturnal baseline period (NBP) with blue coloured points indicating air masses in the free lower troposphere. Red coloured points stand for the morning increasing period (MIP) and green coloured points for the afternoon decreasing period (ADP). The light grey shading shows the evening recovery period (ERP). Points always represent the mean hourly value starting at the time stamp. The background picture shows the station ZSF. Figure and caption are adapted from Pal et al. (2015). 20

3.3 Atmospheric CO₂ measurements at ZSF during 2002–2018 with different data selection methods applied. Black data points indicate the selected data while grey points indicate the unselected ones. Percentages of selected data are given at the top of each data record (for data selection methods see Table 3.1). 22

3.4 Monthly time series plot of CO₂ measurements (Data) at ZSF from 2002 to 2018, and its STL decomposed components (Trend, Seasonal, and Remainder) from original measured data (CO₂ in red) and selected data (ADVS in blue). 24

3.5 Fitted components by CCGCRV on the daily averaged atmospheric CO₂ measurements at ZSF from 2002 to 2018. The function fit is shown in red, while the blue line stands for the polynomial part only. The smoothed fit in green is the combination of the function fit and the residuals filtered with short-term cutoff value (80 days). 26

5.1 Linear regressions between the sampling elevations and percentages of selected CO₂ data by four statistical data selection methods for continental sites (excluding IZO, points in open circles). Plotting data are based on Table 2 of Yuan et al. (2018). 34

5.2 Comparisons of **(a)** annual growth rates and **(b)** seasonal amplitudes between the original measured data (CO₂) and selected data (ADVS) at ZSF from 2002 to 2018; between the STL decomposed components and CCGCRV fitted components. 37

5.3 Example of ADVS data selection applied on CO₂ records at ZSF (2002–2018) in the R shiny application using default selection parameters in Yuan et al. (2018). 39

5.4 Example of ADVS data selection applied on CO₂ records at ZSF (2002–2018) in the R shiny application using more conservative selection parameters (length of starting time window = 8 h; standard deviation threshold = 0.5 ppm). 40

5.5 Example of STL-decomposed **(a)** trend, **(b)** seasonal, and **(c)** remainder components from CO₂ records at ZSF (2002–2018) selected by ADVS in the R shiny application. 42

5.6 Example of **(a)** processed annual growth rates and **(b)** seasonal amplitudes from CO₂ records at ZSF (2002–2018) before and after ADVS data selection in the R shiny application. 43

List of Tables

3.1	ADVS and other data selection methods based on statistical properties commonly applied in the atmospheric CO ₂ measurements. SD _{stw} : standard deviation of CO ₂ averages within the starting time window (stw); SD _{hour} : standard deviation of CO ₂ averages within a given hour; DIFF _{hour} : difference in hourly CO ₂ averages from one hour to the next; SD _{6h} : standard deviation of CO ₂ averages for six or more consecutive hours; σ : the scale parameter implemented, i.e., the measurement noise. .	21
5.1	Summary of the operation time (in sec) for all data selection methods implemented in R.	36
5.2	Classification of atmospheric CO ₂ measurements (2002–2018) at ZSF as background by ADVS and wind sector (overall number validated data points: 132,473). Numbers of selected / non-selected data and the corresponding percentages were calculated.	38

Acronyms

ADVS	Adaptive Diurnal Minimum Variation Selection
CBL	Convective Boundary Layer
CRDS	Cavity Ring-Down Spectroscopy
DQO	Data Quality Objective
FFT	Fast Fourier Transform
FTS	Fourier Transform Spectrometer
GAW	Global Atmosphere Watch
GC	Gas Chromatograph
GHG	Greenhouse gas
HPB	Hohenpeissenberg, Germany
IZO	Izaña, Spain
JFJ	Jungfrauoch, Switzerland
LFT	Lower Free Troposphere
MA	Moving Average
MSR	Mean Symmetrized Residual
NDIR	Nondispersive Infrared
PBL	Planetary Boundary Layer
REBS	Robust Extraction of the Baseline Signal
RF	Radiative Forcing
RL	Residual Layer
SI	Steady Interval
SNB	Sonnblick, Austria
SSL	Schauinsland, Germany

Acronyms

STL	Seasonal-Trend Decomposition Procedure Based on Loess
UFS	Umweltforschungsstation Schneefernerhaus
UTC	Coordinated Universal Time
WMO	World Meteorological Organization
ZSF	Zugspitze-Schneefernerhaus, Germany

1 Introduction

The farther backward you can look,
the farther forward you are likely to see.

Winston Churchill

Climate warming is ongoing and drawing much attention. Changes in the Earth's climate and related impacts can be observed in global sea level rise, species loss and extinction, and more intense and frequent weather extremes such as drought and heavy precipitation events. Many impacts can be formally attributed to anthropogenic influences, mainly from burning of fossil fuels and changes in land uses that increase the greenhouse gas levels in the Earth's atmosphere and thus lead to increases in the global mean surface temperature. Global warming due to human activities has been estimated to range from 0.8 °C to 1.2 °C above the pre-industrial levels, with a strong likelihood of reaching 1.5 °C between 2030 and 2052 by the current increasing rate (IPCC, 2018). For a better understanding on the global climate changes and estimation on the future climate-related risks, in-depth research on the atmospheric carbon dioxide (CO₂) with its sources and sinks in the carbon cycle is of great importance.

1.1 Atmospheric carbon dioxide

Atmospheric CO₂ is one of the most important greenhouse gases (GHGs) and plays a key role in global warming. It captures the infrared radiation emitted by the Earth's surface. In terms of radiative forcing (RF), atmospheric CO₂ is the single component with the largest global mean contribution to the global mean RF of $2.83 \pm 0.29 \text{ Wm}^{-2}$ between 1750 and 2011 together with other GHGs such as methane (CH₄), nitrous oxide (N₂O), and halocarbons (Myhre et al., 2013). Regarding the concentration levels of GHGs, IPCC (2014) stated:

“Historical emissions have driven atmospheric concentrations of carbon dioxide, methane and nitrous oxide to levels that are unprecedented in at least the last 800,000 years, leading to an uptake of energy by the climate system.”

As seen in Figure 1.1a, the concentration levels of carbon dioxide measured from ice cores fluctuated between 170 and 280 ppm before the industrial era (Joos and Spahni, 2008; Lüthi et al., 2008). Then, the globally averaged mean CO₂ had increased from approximately 278 ppm in 1750 (Etheridge et al., 1996) to 407.38 ± 0.10 ppm in 2018 estimated by NOAA/ESRL (Dlugokencky and Tans, 2019) showing an increase of 46.5%. The first long-term continuous measurements of atmospheric CO₂ were started by C. D.

1 Introduction

Keeling from the Scripps Institution of Oceanography at the South Pole in 1957 (Keeling et al., 1976a) and at Mauna Loa, Hawaii in 1958 (Keeling et al., 1976b), respectively. Here, the monthly CO_2 concentration in March increased from 315.70 ppm in 1958 (Keeling et al., 2001) to 412.00 ppm in March 2019, with a mean annual growth rate of 1.58 ppm yr^{-1} . This Mauna Loa CO_2 is still updated daily and is known as the “Keeling Curve” (see Figure 1.1b).

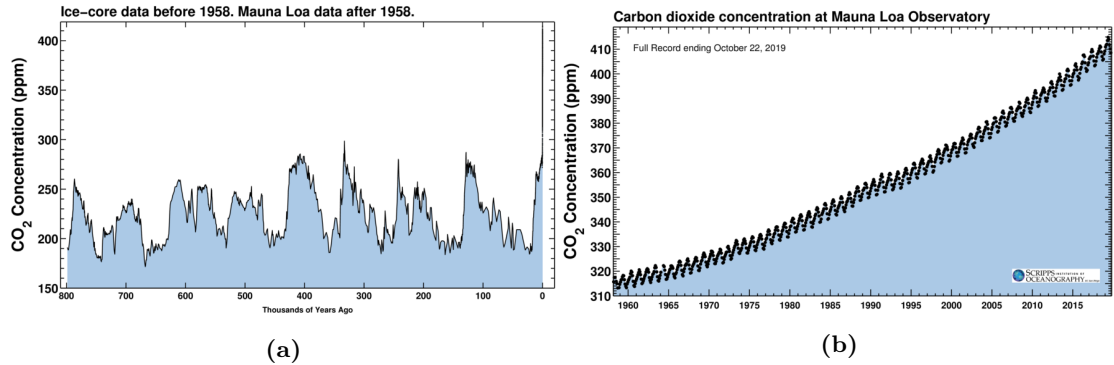


Figure 1.1: Carbon dioxide concentrations of (a) combination of ice-core data before 1958 and Mauna Loa Observatory data after 1958; (b) Mauna Loa Observatory from 1958 until October 22, 2019, i.e., the Keeling Curve (figures adapted from website of the Scripps Institution of Oceanography SIO). The CO_2 data after 1958 are from the Scripps CO_2 program (Keeling et al., 2001). The CO_2 data before 1958 going back 800,000 years are from Lüthi et al. (2008).

1.2 Sources and sinks in the global carbon cycle

The two major sources for atmospheric CO_2 increases are fossil fuel combustion and land use changes (Ciais et al., 2013). In order to understand the perturbation of the CO_2 cycle especially associated with emissions from human activities and transport among atmosphere, land, and ocean, tracking the sources and sinks in the carbon cycle is always required.

The majority of carbon is stored in rocks, with the rest being distributed as gases mostly of CO_2 in the atmosphere amounting to a mass of 860 gigatonnes of carbon (GtC, 10^{15} gC, same as PgC), living biomass in the vegetation (for the amount see Figure 1.2), soils, permafrost, and fossil fuels reserves in forms of gas, oil, and coal in the land, as well as surface sediments and organic and dissolved inorganic carbon in the ocean (Le Quéré et al., 2018). Changes in one reservoir will result in changes in the others.

Fluxes in the carbon cycle are linked to fast and slow processes, the latter one comprising e.g. weathering, erosion, and sediment transport (Sundquist, 1986). This doctorate study deals with processes of the fast carbon cycle, consisting of carbon exchanges through life forms between the atmosphere and the land, as well as the surface sediments

1.2 Sources and sinks in the global carbon cycle

and the ocean in a lifespan from one year to millennia (Ciais et al., 2013). Natural exchanges between the fast and slow carbon cycle are considered to be constant over time despite of potential land use changes by humans (Raymond and Cole, 2003).

The global carbon cycle

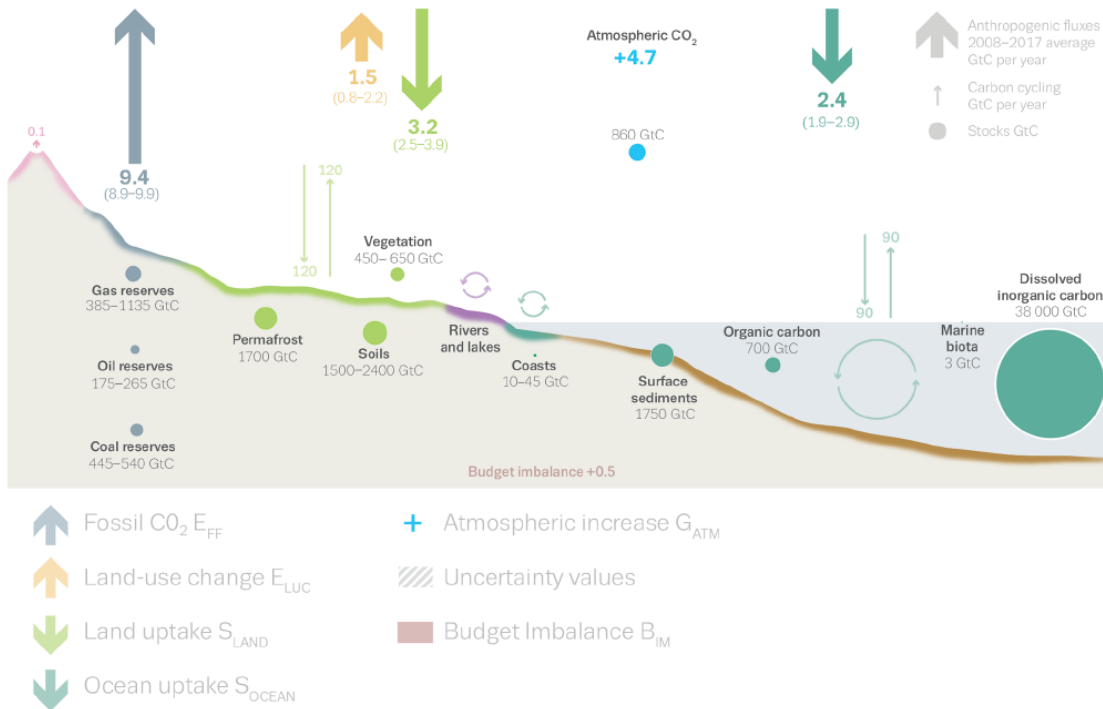
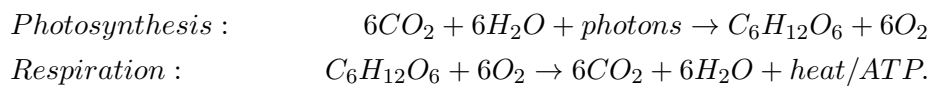


Figure 1.2: Schematic representation of the overall perturbation of the global carbon cycle caused by anthropogenic activities, averaged globally for the decade 2008–2017. The uncertainty in the atmospheric CO₂ growth rate is very small ($\pm 0.02 \text{ GtC yr}^{-1}$) and thus neglected. Figure and caption are taken from Figure 2 in Le Quéré et al. (2018).

Various processes take place in the fast carbon cycle. Vegetation and marine biota (predominantly phytoplankton) take up CO₂ from the atmosphere during photosynthesis. On the contrary, CO₂ is mainly released to the atmosphere by respiration from human, animals, and plants. The corresponding chemical reactions are as follows:



A thorough assessment of atmospheric CO₂ concentration is important to estimate ocean-atmosphere CO₂ fluxes correctly by the partial CO₂ pressure difference (Ciais et al., 2013). The latest updated estimates for the global carbon budget (Le Quéré et al., 2018) reported, for the time period of 2008–2017, anthropogenic activities added

1 Introduction

10.8 ± 0.8 GtC of carbon to the atmosphere per year in combination of fossil fuels combustion (9.4 ± 0.5 GtC yr⁻¹) and land use changes (1.5 ± 0.7 GtC yr⁻¹). The carbon sinks estimated that 22% and 30% of the carbon were absorbed by the ocean (2.4 ± 0.5 GtC yr⁻¹) and the land (3.2 ± 0.7 GtC yr⁻¹), respectively. With a budget imbalance of 5% (0.5 GtC yr⁻¹), the atmospheric increase yielded 4.7 ± 0.02 GtC yr⁻¹ resulting in 44% of the emitted carbon being kept in the atmosphere contributing to global warming. Such estimation of the global carbon budget is updated every year with newly revised methodologies on measurements and modelled data for a better quantification and projection for the coming years. Therefore, real-time atmospheric measurements are always a prerequisite for collecting data representative for the well-mixed background air at the measurement sites as well as being comparable across measurement sites for a better data integration. For such purposes, data processing is very essentially required and preferred with representative data selection and sometimes even further averaging or smoothing on both temporal and spatial scales (e.g. Masarie and Tans, 1995).

1.3 Continuity and consistency in measurements

Atmospheric measurements can be informative both in time and space providing long-term time series signalling the trend, and wider spatial coverage of measurement sites to be more representative for the Earth's atmosphere. Long-term CO₂ measurements in the recent in situ and continuous observing era are briefly introduced. Also, data processing routines in the global observation network are described, while various methods of data selection are highlighted.

1.3.1 Long-term measurements within the global observation network

Long-term measurements of CO₂ and other trace gases have been performed at measurement sites globally. Thus, using the worldwide network of observatories is of great importance in creating a global high quality data base with highly comparable, measured data. The Global Atmosphere Watch (GAW) Programme was developed by the World Meteorological Organization (WMO) in 1992, comprising more than 100 countries with more than 800 stations registered in the GAW Station Information System (GAWSIS). With such contributing networks and collaborations among the stations, it focuses on providing reliable scientific data and information on both natural and anthropogenic changes in atmospheric components, with a better understanding on the global circulation and interactions with the oceans and the biosphere.

GAW observatories are mainly surface-based in situ and remote sensing measurement sites, which can be categorized into Global, Regional, or Contributing stations. While in situ measurements sample the targeted air at certain point levels, remote sensing measurements such as ground-based Fourier Transform Spectrometers (g-b FTSs) retrieve column abundances of CO₂ and others. Figure 1.3 shows the 31 Global stations currently documented in the GAW network. These stations cover at least three of the six GAW focal areas, which are aerosols, greenhouse gases, selected reactive gases, ozone, UV radiation, and atmospheric deposition. They are mostly located along seashores or at

1.3 Continuity and consistency in measurements

elevated mountainous regions. These stations provide long-term records of atmospheric components which are ideally representative for the lower free troposphere (LFT).



Figure 1.3: GAW network with the 31 Global Stations (figure taken from the website of WMO).

Besides Mauna Loa, Hawaii (Thoning et al., 1989), many other GAW Global stations have reported their measured CO_2 levels and studied the increases and changes in CO_2 related to climatic indices (Keeling et al., 1989). The short-term variability since 1976 was studied for Cape Matatula, American Samoa (Halter et al., 1988; Waterman et al., 1989), while continuous CO_2 measurements at Barrow, Alaska starting in 1973 (Peterson et al., 1986) focused on the summer and winter variations (Halter and Harris, 1983). Atmospheric CO_2 has also been monitored at Amsterdam Island since 1980 (Gaudry et al., 1983) and relations of CO_2 changes to the sea surface temperature (SST) of the Pacific Ocean and El Niño Southern Oscillation events (ENSO) have been discussed (Ascencio-Parvy et al., 1984; Gaudry et al., 1987, 1991). Moreover, measurements of CO_2 and ^{222}Rn (radon progeny concentrations) allowed a classification of baseline air mass conditions at Cape Point, South Africa (Brunke et al., 2004). Similar applications of ^{222}Rn have been made for source estimation of CO_2 and other species continuously measured at Mace Head, Ireland (Biraud et al., 2000, 2002; Bousquet et al., 1996). From the long-term continuous CO_2 records at Jungfraujoch of Switzerland beginning in 2005 (Uglietti et al., 2011), different measurement techniques have been compared showing potential offsets as well as improving the compatibility of the data collection system (Schibig et al., 2015; Zellweger et al., 2016). Other long-term CO_2 records exist for GAW Global stations such as Monte Cimone of Italy starting from 1979 (Cundari et al., 1995), the Izaña Observatory on Tenerife, Spain since 1984 (Gomez-Pelaez et al., 2019; Navascués and Rus, 1991), Minamitorishima of Japan since 1993 (Watanabe et al., 2000), and Mount Waliguan of China since 1994 (Zhou et al., 2005). In this doctorate study,

a 36-year long-term continuous CO₂ record at Zugspitze-Schneefernerhaus of Germany since 1981 was analysed (Yuan et al., 2019), showing long-term trends and seasonal variations comparable with global stations, as well as site-specific short-term variations.

1.3.2 Improvements of data processing

During sampling and measurement, a key issue is the data quality assurance. The GAW compatibility goal (or DQO, data quality objective) of atmospheric CO₂ measurements in the Northern Hemisphere is ± 0.10 ppm (WMO, 2016). For further analyses or modelling applications, measurements should be selected for baseline conditions in order to exclude data influenced by local sources and sinks. However, such baseline selections have always been site-specific. The selection procedure is mostly performed personally by scientists in charge at each station before data integration. Thus, in the whole data collection process there is a growing concern on potential errors across measurement sites and data selection methods. This doctorate study aims at improving such introduced incomparability. Given the diagram illustrating the general steps of data processing in Figure 1.4, the representativeness analysis is focused by means of developing a generalized data selection method which can be potentially applicable for different types of measurement sites, with testing on existing long-term atmospheric CO₂ records and evaluating the selection performances with other methods frequently used in the literature.

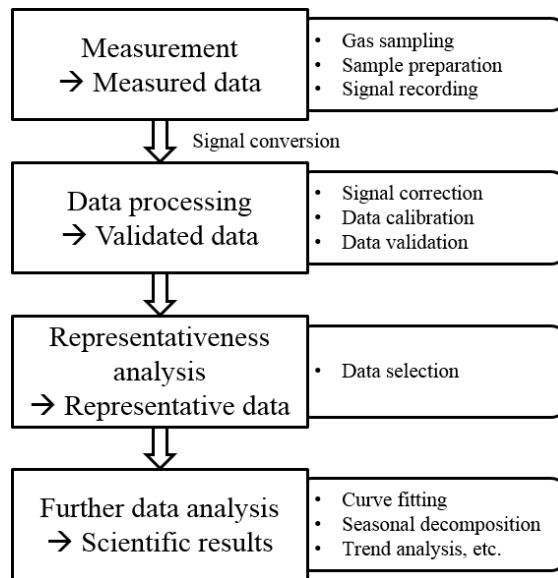


Figure 1.4: Diagram describing the general data processing routine for atmospheric CO₂ measurements in GAW network.

By definition, data selection (or data filtering) is to select a subset of data from the original measurements in order to obtain representativeness for the baseline condition (or background level) unaffected by local conditions of anthropogenic influences or short-term variations (Calvert, 1990; Elliott, 1989). Data selection is mainly performed based

on three properties, i.e., tracer (or chemical), meteorological, and statistical strategies (Ruckstuhl et al., 2012).

1.3.2.1 Tracer / chemical data selection

For identifying the background CO₂ level, data selection can be made based on certain tracers (gases or particles) measured simultaneously at the same site, such as concentration of the tracer or the ratio between the tracer and CO₂. Fang et al. (2015) adopted CH₄ and black carbon to filter observed CO₂ records at Longfengshan, China, based on positive correlations related to common sources such as fossil fuel combustion and biomass burning. Periods likely influenced by local emissions in CH₄ or days with peak values of black carbon were flagged and thus CO₂ data can be excluded for these periods. Similarly Tsutsumi et al. (2006) classified the concentrations of atmospheric CO on Yonagunijima, Japan into local, regional, and background events which were applied to atmospheric CO₂ simultaneously. In Europe, thresholds of 300 ppb for CO and 2000 ppb for CH₄ were applied to remove local influences at Lutjewad of the Netherlands and Mace Head of Ireland (Sirignano et al., 2010). Also, the concentration of ²²²Rn was used for the identification of local and remote influences on the air masses (Chambers et al., 2016).

1.3.2.2 Meteorological data selection

Information on meteorological parameters and conditions is known as very powerful for describing the surrounding environment of measurement sites as well as air mass transport. For example, the “disturbed” free tropospheric (FT) conditions were identified from “undisturbed” FT conditions based on meteorological filters for events of Föhn, synoptical lifting, and thermally induced vertical transport at Jungfraujoeh (Zellweger et al., 2003). Meanwhile, back trajectories and cluster analysis act effectively in detecting the source region of transported air mass reaching the measurement site and in excluding polluted air masses (Balzani Lööv et al., 2008; Pu et al., 2014). Last but not the least, measurement sites can also pre-select the data simply by precipitation (condensation nuclei), wind speed, and wind direction (e.g. Stephens et al., 2013; Buchholz et al., 2016).

1.3.2.3 Statistical data selection

Data selection based on statistical properties is different from other methods since it is independent from other measurements and thus can be adopted in principle at all measurement sites. Statistical data selection typically targets only at the time series of interest by examining the data variability in different temporal scales or between different measurement techniques. Regarding the sampling time resolution of continuous or quasi-continuous atmospheric measurements, the within-hour and the hour-to-hour variability are most commonly examined in terms of standard deviation and difference in hourly values (e.g. Sun et al., 2014; Zhang et al., 2015). Simple statistical measures of median and percentile have been applied as well (Brunke et al., 2004; Chambers et al.,

1 Introduction

2016; Thoning et al., 1989). For measurement sites equipped with various sampling inlets or instrumental setups, inter-comparisons can provide reliable information for data selection (Brooks et al., 2012; Lopez et al., 2015). Furthermore, the curve fitting technique (or smoothing), as a standard statistical approach for time series analysis by fitting mathematical models to separate and study the long-term trend, the seasonal variation, and the local influences, have also been used to aid in the data selection procedure (Conway et al., 1988). What is intended and has been achieved in the doctorate study is a data selection method named ADVS (Adaptive Diurnal minimum Variation Selection) based on statistical properties (Yuan et al., 2018).

By applying the same data selection method, it is able to compare the selected background conditions of multiple stations as well as to evaluate the resulted trend and seasonality across the groups of time series. Data integration after such a consistent data selection would theoretically result in a better performance on further modelling and validation applications. This doctorate study proposes an application of the generalized data selection method consistently on atmospheric CO₂ measurements worldwide. Chapter 2 describes all relevant data sets used for the doctorate study including atmospheric CO₂ and wind records. Chapter 3 explains the statistical theories which are vital to the study with the information of the statistical computing and graphics tool R. Chapter 4 presents the main doctorate outcomes in the form of abstracts of and contributions to three publications (2 published and 1 under review). In Chapter 5, the performance and applicability of the data selection method are discussed with sample atmospheric CO₂ records measured at Zugspitze-Schneefernerhaus of Germany and further wrapped up R application based on the developed data selection method. This doctorate thesis ends by Chapter 6 listing potential research directions followed by such data selection methods.

2 Data sets overview

Primary causes are unknown to us; but are subject to simple and constant laws, which may be discovered by observation, the study of them being the object of natural philosophy. Profound study of nature is the most fertile source of mathematical discoveries.

Joseph Fourier

Two types of atmospheric CO₂ measurements have been used in the study, i.e., continuous in situ measurements and column-averaged measurements from both the space and the ground. An overview of these data sets is given below with the focus on the measurement sites of Germany. In the following, column measurements are introduced by both satellite products and in situ FTS. This chapter ends with a CO₂ related description of the wind sector.

2.1 Continuous in situ measurements

In order to measure atmospheric components without local pollution as well as to provide representative regional data for Germany, the air monitoring network is operated by the Federal Environment Agency (UBA, Umweltbundesamt). The GAW Global station in Germany is Zugspitze / Hohenpeissenberg which consists of two observation platforms and is operated by UBA together with the German Meteorological Service (DWD, Deutscher Wetterdienst). On the platform Zugspitze, GHGs such as CO₂ are measured at the Environmental Research Station Schneefernerhaus (see Figure 2.1, GAW ID: ZSF, or UFS for Umweltforschungsstation Schneefernerhaus). The station ZSF (47°25' N, 10°59' E) is situated at an elevation of 2650 m above sea level (a.s.l.) on the southern slope, around 300 m below the summit of the German highest mountain Zugspitze (Risius et al., 2015). The atmospheric CO₂ record at Zugspitze could be traced back to 1981 when it was performed at a nearby balcony. The measurement had been moved to the Zugspitze summit from 1995 to 2001. Afterwards atmospheric CO₂ has been continuously measured at ZSF from where the validated CO₂ data are available since 2002 (Yuan et al., 2019).

On the other hand, the platform Hohenpeissenberg (HPB, 47°63' N, 11°1' E, 985 m a.s.l.) with continuous meteorological measurements since 1781, has been performing continuous CO₂ measurement at a tall tower in three heights of 50 m, 93 m, and 131 m above ground level (Gilge et al., 2010). Tall towers are designed to achieve a better spatial measurement representativeness, as well as to capture multiple vertical profiles near the ground for different regional influences (Lindauer et al., 2015). Moreover,



Figure 2.1: GAW Global station Zugspitze-Schneefernerhaus (image: L. Ries).

measurements from the GAW Regional station Schauinsland (SSL, $47^{\circ}55'$ N, $7^{\circ}55'$ E, 1205 m a.s.l.) were included as an alternative to evaluate the data selection methods applied on stations representative for regional scales. Station SSL is located in the southern Black Forest, about 10 km southeast of Freiburg, often lying above the ground level mixing layer receiving air masses from both local influences and long-term transport (Ries et al., 2003). Atmospheric CO_2 measurements have been continuously measured at SSL since 1972 with long-term studies on implication to the European CO_2 budget as well as trend of carbon isotopes $^{13}\text{CO}_2$ and $^{14}\text{CO}_2$ records (Levin and Kromer, 1997; Schmidt, 2003; Levin et al., 2013). The long-term CO_2 time series of Zugspitze and Schauinsland are shown in Figure 2.2 with comparison to Mauna Loa, Hawaii as well as the world CO_2 trend calculated by WMO.

In addition, to study the regional characteristics in the central Europe, two more measurement sites have been included for the study, i.e., Hoher Sonnblick in Austria (SNB, $47^{\circ}3'$ N, $12^{\circ}57'$ E, 3106 m a.s.l.) and Jungfraujoch in Switzerland (JFJ, $46^{\circ}33'$ N, $7^{\circ}59'$ E, 3580 m a.s.l.). Together with ZSF and HPB in Germany, a DACH (D – Germany; A – Austria; CH – Switzerland) cooperation has been formed which could be ideally representative for studying the background conditions in this region (Gilge et al., 2010). By the detailed assessment of representativeness Henne et al. (2010) categorized these stations in the following way: HPB and SSL – *rural*; ZSF – *weakly influenced, constant deposition*; SNB and JFJ – *mostly remote*. Therefore, even though all five measurement sites belong to elevated mountain stations, clear differences in the site representativeness could still be indicated by data selection methods (Yuan et al., 2018).

Finally, reference sites / data sets are required for inter-comparison and evaluation of data selection methods. As a result, GAW Global station Izaña (Tenerife, Spain, IZO,

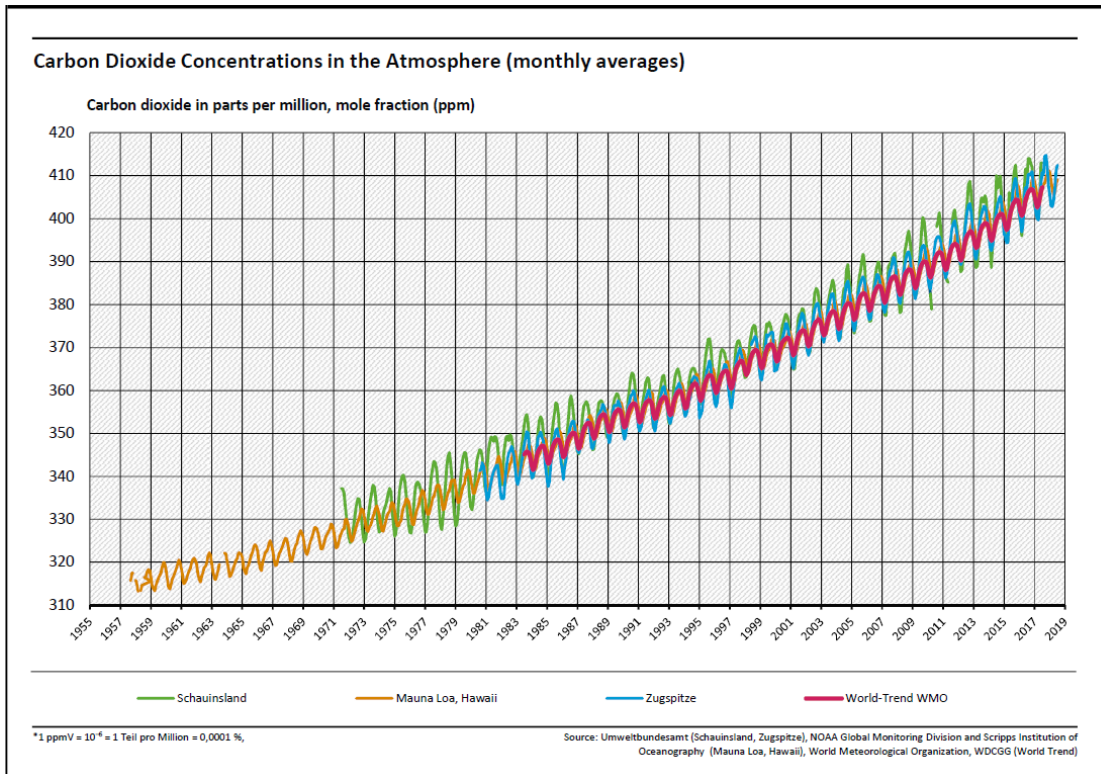


Figure 2.2: Monthly CO₂ concentrations at German stations and comparison to the world trend by WMO (figure adapted from the website of Umweltbundesamt with available monthly CO₂ data sets).

28°19' N, 16°30' W, 2373 m a.s.l.) has been selected as it is located at the summit of a mountain on the island receiving mostly air masses from the North Atlantic atmosphere (Gomez-Pelaez et al., 2019). For a broader view, global means of atmospheric CO₂ have also been compared. Two sources of calculating the global means have been provided by WMO (see world trend in Figure 2.2) and NOAA. The WMO global mean mole fractions of atmospheric CO₂ are calculated from the World Data Centre for Greenhouse Gases (WDCGG), by averaging every 30° zonal means containing synchronized data that are extrapolated from selected stations, in order to cover the same overall time period for global analyses (Tsutsumi et al., 2009; WMO, 2018). On the other hand, the NOAA/ESRL Carbon Cycle Group computes the CO₂ global means based on sites predominantly of well-mixed marine boundary layer (MBL) air masses (Dlugokencky and Tans, 2019), by the data extension method described in Masarie and Tans (1995).

2.2 Column-averaged measurements

Unlike surface-based continuous in situ measurements, column-averaged measurements are often performed based on space remote sensing techniques in order to provide global

2 Data sets overview

insights on carbon fluxes and budgets (Butz et al., 2011; Miao et al., 2013). Satellite products can provide the column abundances of GHG species such as CO_2 and CH_4 , defined as the number of the gas molecules in a vertical unit column stretching from the ground surface to the top of the atmosphere (Morino et al., 2011). Various satellites have been launched which are able to retrieve the column-average dry mole fractions of atmospheric carbon dioxide (XCO_2) and other GHGs based on the near-infrared spectral region of the lower troposphere, such as the Scanning Imaging Absorption Spectrometer for Atmospheric Cartography of the Environmental Satellite SCIAMACHY/ENVISAT (Bovensmann et al., 1999; Burrows et al., 1995), the Thermal and Near-infrared Sensor for Carbon Observation in the Greenhouse Gases Observing Satellite TANSO/GOSAT (Kuze et al., 2009), and the NASA Orbiting Carbon Observatory-2 (OCO-2) mission (Boesch et al., 2011; Hakkarainen et al., 2019).

In Figure 2.3 the monthly global maps of XCO_2 retrieved from GOSAT and OCO-2 are shown for April and July 2017 as examples for XCO_2 levels in both peaks and troughs. From Figure 2.3a and 2.3c clearly high levels of XCO_2 (shown in red) can be observed from both satellite products in April. In contrast, due to carbon sinks by photosynthesis in summer months, lower concentrations can be detected (in blue) especially in the continental areas of the Northern Hemisphere (see Figure 2.3b and 2.3d). However, detection gaps through measurement orbits or cloudiness are inevitable, and differences in detection resolutions should always be noted using different satellite products (Yoshida et al., 2011). From Figure 2.3a to 2.3d the vertical profile of CO_2 concentrations derived and processed from the satellites (Level 2 data) are presented, while Figure 2.3e and 2.3f illustrate the Level 3 data, the global monthly XCO_2 map after data processing (interpolation, extrapolation, and smoothing). Since the accuracy of satellite Level 2 data is vital to generate the Level 3 data, validation is highly required where the in situ remote sensing measurements of XCO_2 are usually compared, e.g. g-b FTSs in the Total Carbon Column Observing Network (TCCON). TCCON measurements are performed worldwide which retrieve column abundances of GHGs in a highly accurate and precise way (Wunch et al., 2011).

In the study, a merged XCO_2 satellite product of SCIAMACHY/ENVISAT and TANSO/GOSAT has been included in the form of a Level 3 product named Obs4MIPs Version 3.0, which is available at <https://cds.climate.copernicus.eu/> (Buchwitz et al., 2018). The OCO-2 satellite data has also been used to cover a longer time period for inter-comparison with continuous CO_2 records. The inter-comparison between OCO-2 and GOSAT revealed similar latitudinal gradients, seasonal amplitudes, and annual growth trends of the monthly mean XCO_2 (Liang et al., 2017). Satellite retrieved XCO_2 concentrations from these three satellites were extracted for the corresponding grid values representative for Mount Zugspitze, together with FTS observations at the TCCON stations Garmisch and Zugspitze, available at <https://tccodata.org/> (Sussmann and Rettinger, 2018a,b). In addition, data sets of modelled CO_2 mole fractions were used for validation, e.g. NOAA's CarbonTracker, version CT2017 (Peters et al., 2007, with updates documented at <http://carbontracker.noaa.gov>).

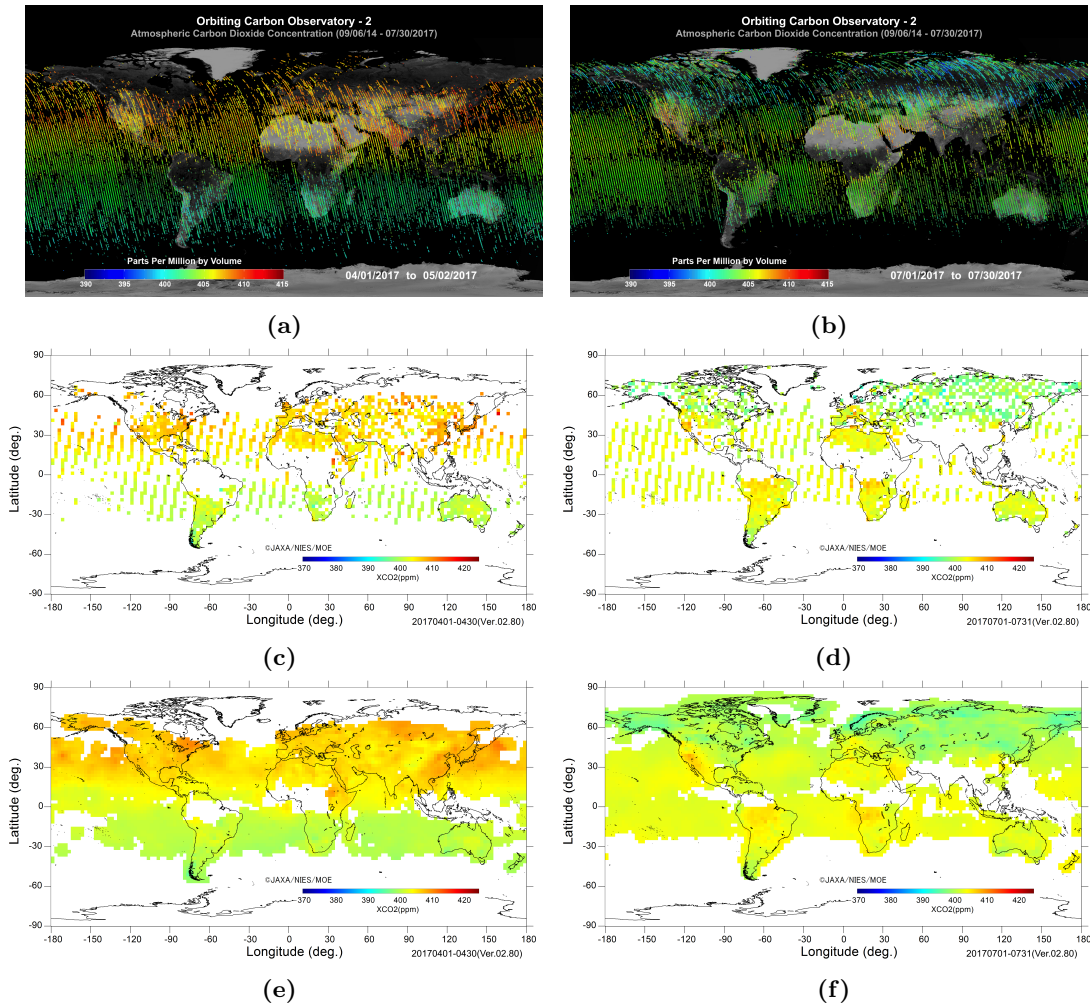


Figure 2.3: (a) and (b) Global average XCO₂ by OCO-2; (c) and (d) Monthly global map of XCO₂ Level 2 data captured by GOSAT; (e) and (f) Monthly global map of XCO₂ Level 3 data estimated by GOSAT. Time stamps are April and July of 2017 (figures taken from websites of OCO-2 and GOSAT).

2.3 Wind sector

Meteorological parameters can be very helpful in understanding the conditions at the measurement sites, as well as serving as inputs for trajectory analyses by clustering air mass transports or identifying sources of polluted air masses. Data sets of wind sector have been used frequently in atmospheric CO₂ research showing predominant wind speeds and directions and providing evidence for representative CO₂ background levels (e.g. Massen and Beck, 2011). A CO₂ versus wind speed plot is very informative not only for estimating the background CO₂ levels at more regional sites despite of local influences, but also for validation of historical CO₂ levels. Figure 2.4 shows a yearly

2 Data sets overview

CO₂ distribution combined with wind speeds and directions using the wind sector data at ZSF.

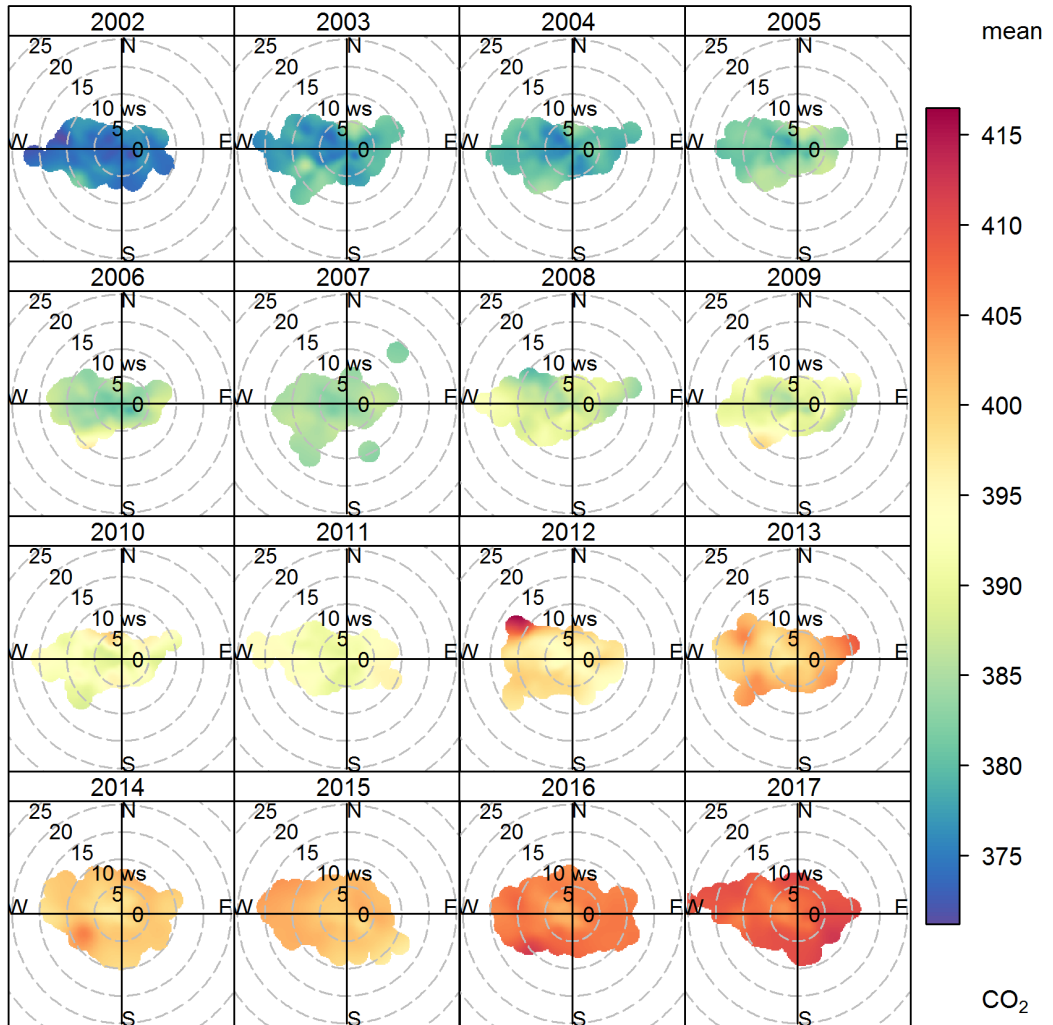


Figure 2.4: Bivariate polar plots of CO₂ concentrations measured at ZSF (2002–2017). The colour scale shows the concentration of CO₂ in ppm and the radial scale shows the wind speed (ws, in m s⁻¹), which increases from the centre of the plot radially outwards. The plotting method and the caption are based on Carslaw and Beevers (2013).

Together with continuously increasing CO₂ concentrations throughout the years, clear patterns in the predominant wind profiles in relation to CO₂ peaks and troughs can be observed. Winds reaching at ZSF are mainly from the west where the famous western glacier ridge “Schneefernerkopf” lowers the ridge height significantly due to the erosion

effect (Risius et al., 2015). Consequently, air masses of high to intermediate wind speeds (up to 20 m s^{-1}) with intermediate CO_2 concentrations (peak values only in 2012 and 2014) are shown in Figure 2.4 from the west. From the north and the south, the ZSF is protected by ridges (e.g. northern ridge about 290 m straight above ZSF), and thus only low wind speeds ($< 10 \text{ m s}^{-1}$) and comparably low CO_2 concentrations are detected. Two major sources of high wind speeds with high CO_2 levels can be identified as from the east and the southeast with upwind channels from valleys Reintal and Inntal (Gantner et al., 2003; Yuan et al., 2019). The wind sector data have been used in the study in combination with data selection methods.

3 Methods overview

All models are wrong; some models are useful.

George E. P. Box

The main methods described include fundamentals and development of data selection method ADVS and retrospective approaches in Section 3.1 and Section 3.2, time series analyses with seasonal decomposition and curve fitting techniques in Section 3.3, and used packages in the programming language R in Section 3.4.

3.1 Variation in time

Data selection is critical for extracting representative data which then describe the background condition at measurement sites. Different properties can be taken into consideration (see Section 1.3.2), but only statistical data selection has the potential for consistent applications and inter-comparisons among records at various measurement sites. From this perspective, variations of the measured records in time, especially time of the day and day of the week, can provide insights about the background / influenced time periods, acting as a “time filter” on the time series. Monthly to weekly (daily) variations in atmospheric CO₂ at ZSF can be seen in Figure 3.1.

From the monthly cycle (lower centre of Figure 3.1), atmospheric CO₂ at ZSF exhibits clearly seasonal variations with monthly maximum (395.7 ± 0.2 ppm) in March and monthly minimum (382.9 ± 0.2 ppm) in August. Such a fluctuation has already been reported by Keeling (1960) as the “sawtooth” pattern due to the activity of terrestrial vegetation via photosynthesis especially in the Northern Hemisphere because of the greater land area in combination with the result of CO₂ production. The monthly CO₂ maximum and minimum correspond well with the start and end of the growing season. Therefore, an elevated mountain station remote from local sources and sinks such as ZSF is still influenced to a certain extent (mean seasonal amplitude up to 15 ppm) by seasonal vegetation activity. For measurement sites located at more populated regions, such local pollution is assumed to be stronger with larger seasonal amplitudes measured.

The variation of CO₂ time series in the temporal scale of a week (7 days) reveals anthropogenic influences, because such a weekly cycle cannot be explained by natural variability (Bäumer and Vogel, 2007; Cerverny and Balling Jr., 1998). Interesting results have been shown in the upper and lower right sub-panels of Figure 3.1 as well as in Yuan et al. (2019), that distinct CO₂ levels can be observed between weekends and weekdays. The mean weekly CO₂ maximum over the 17 years (2002–2018) is noted on Thursday (391.1 ± 0.1 ppm) while the mean weekly minimum results on Saturday (390.3 ± 0.2

3 Methods overview

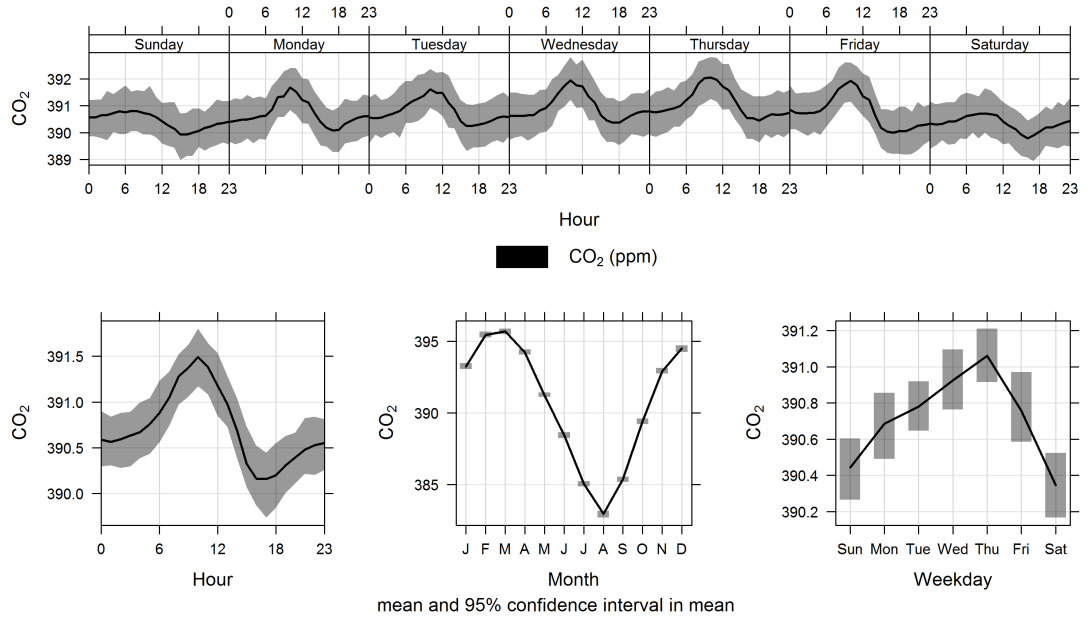


Figure 3.1: Temporal variation in CO₂ concentrations in ppm measured at ZSF from 2002 to 2018. The shading shows the 95% confidence intervals in the mean. Times are expressed in UTC + 1.

ppm). Such a difference of 0.8 ppm is worth noting concerning the DQO of ± 0.1 ppm, indicating potentially intensive human activities accumulating and peaking in the middle of the week. For a systematic evaluation of such a weekly periodicity in the atmospheric CO₂ record at Mount Zugspitze since 1981, the statistical method Mean Symmetrized Residual (MSR) has been applied (Cerveny and Coakley, 2002; Yuan et al., 2019). The MSR method can be seen as a generalization of the residual from the weekly average. Using daily CO₂ records, a moving seven-day time window is applied to calculate all distinct seven-day mean values containing the day of interest. Residuals are defined as the daily CO₂ value of interest minus these seven-day mean values, and then averaged to derive of the so-called MSR:

$$MSR(i) = \sum_{m=-6}^6 h(m)x(i+m), \quad (3.1)$$

where

$$h(m) = \begin{cases} -\frac{7-|m|}{49} & \text{if } m \neq 0 \\ \frac{42}{49} & \text{if } m = 0 \end{cases} \quad (3.2)$$

and $x(i)$ denotes the CO₂ observation on the i^{th} (absolute) day. MSRs are aggregated into an overall mean MSR for each day of the week, and allow as assessment of the

weekly cycle at the measurement site based on the 95% confidence intervals with respect to the overall daily MSRs. If a significant difference is observed between weekdays and weekends, both the systematic measurement errors and variations in real measurements should be considered above all as potential causes. However with highly automated atmospheric CO₂ measurement devices, such a weekly cycle is more likely to be attributed to local influences and thus additional climatic and atmospheric measurements are needed for investigations.

3.2 Diurnal variation and ADVS

What is left undiscussed in Figure 3.1 is the mean diurnal cycle of atmospheric CO₂ exhibiting a typical diurnal pattern representative for elevated mountain stations. This pattern is the fundamental on the development of the statistical data selection method ADVS. Figure 3.2 exclusively illustrates its mechanism based on the sample CO₂ record at ZSF from 2002 to 2018. Colours indicate the different phases of air masses from night to day reaching the measurement site. The diurnal cycle can be characterized by a CO₂ increase after the sunrise and a decrease during the afternoon until the sunset. Such variations depend largely on the synoptic conditions and the planetary boundary layer (PBL) movement (Collaud Coen et al., 2014; Denning et al., 1995). During the night, the station ZSF is always situated above the PBL with the least CO₂ variations, well representative for the lower free troposphere (NBP, nocturnal baseline period). Starting from sunrise with the PBL growing, air masses with higher CO₂ concentrations from plant respiration and potential anthropogenic sources (such as morning traffic) in the residual layer (RL) are travelling and reaching the station, resulting in increasing atmospheric CO₂ in the morning (MIP, morning increasing period). At the same time, from the lower levels of the PBL, the convective boundary layer (CBL) also starts to develop filled with CO₂ depleted air masses from plant photosynthesis. Until late in the morning till noon, air masses in and above the CBL are vertically well mixed, and the upflow wind brings up air masses with lower CO₂ concentrations above the CBL and RL to the station lowering down the measured CO₂ levels. Such a dilution effect lasts till sunset in the late afternoon (ADP, afternoon decreasing period). Afterwards, air masses stabilize from the CO₂ depletion from RL and below, and come close to the nocturnal baseline conditions of the lower free troposphere eventually in the late evening (ERP, evening recovery period).

Therefore, data selection can be performed based on the corresponding time window of NBP. However variations and lengths of NBP may differ from day to day because of local synoptic conditions, or from season to season mainly due to solar radiation. An adaptive solution is to select the representative NBP for each day individually in order to have the most representative baseline conditions with highest amounts of suitable data remaining. Thus, concepts have been established based on the definition of NBP by certain thresholds in data variability, and selection rules of how to select the CO₂ data adaptively for every day. The data selection routine ADVS was developed with two selection steps, i.e., starting selection and adaptive selection. The starting selection

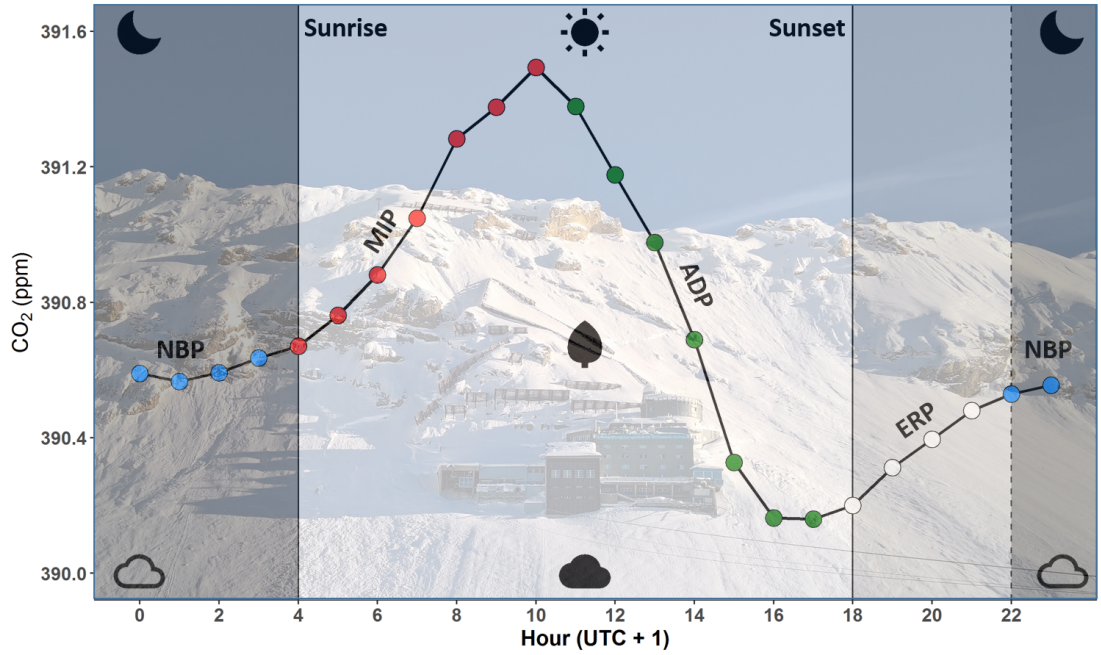


Figure 3.2: Schematic representation of a typical mean diurnal cycle based on existing measured CO_2 data at ZSF illustrating the night-day differences at elevated mountain stations. The dark grey shading represents the nocturnal baseline period (NBP) with blue coloured points indicating air masses in the free lower troposphere. Red coloured points stand for the morning increasing period (MIP) and green coloured points for the afternoon decreasing period (ADP). The light grey shading shows the evening recovery period (ERP). Points always represent the mean hourly value starting at the time stamp. The background picture shows the station ZSF. Figure and caption are adapted from Pal et al. (2015).

determines a starting time window for all days by extracting a 6-hour time window with the least standard deviations from the overall mean de-trended diurnal cycle. Afterwards, the adaptive selection is performed by examining every single data point whether it could be included in the selected time window during the current and previous 24 hours centred at the starting time window. Such a time length is required because data selection is performed both backward and forward from the starting time window. The threshold criterion is based on:

$$|x_i - \bar{x}| \leq \kappa * s \quad (3.3)$$

where x_i is the data point to be examined, \bar{x} is the mean value of the current selected time window for the day, κ is the threshold parameter, and s is the standard deviation of the current selected time window. At the end, the final selected data set comprises all the selected data merged from forward and backward adaptive selection. More details are described in Yuan et al. (2018). For consistency ADVS has been compared with other data selection methods based on statistical properties as well (see Table 3.1).

Table 3.1: ADVS and other data selection methods based on statistical properties commonly applied in the atmospheric CO₂ measurements. SD_{stw} : standard deviation of CO₂ averages within the starting time window (stw); SD_{hour} : standard deviation of CO₂ averages within a given hour; $\text{DIFF}_{\text{hour}}$: difference in hourly CO₂ averages from one hour to the next; $SD_{6\text{h}}$: standard deviation of CO₂ averages for six or more consecutive hours; σ : the scale parameter implemented, i.e., the measurement noise.

Selection method	Reference	Selection criteria
ADVS	Yuan et al. (2018)	$SD_{\text{stw}} \leq 0.3$ ppm
NOAA/ESRL (THO)	Thoning et al. (1989)	$SD_{\text{hour}} < 0.3$ ppm $\text{DIFF}_{\text{hour}} < 0.25$ ppm
Steady interval (SI)	Stephens et al. (2013)	$SD_{6\text{h}} \leq 0.3$ ppm
Moving average (MA)	Satar et al. (2016)	30-day moving window $\pm 2*SD$
Robust extraction of the baseline signal (REBS)	Ruckstuhl et al. (2012)	Robust local regression fit 90-day bandwidth $\pm 3*\sigma$

The statistical data selection methods can be summarized into two approaches. One measure is to evaluate the data variability regarding standard deviation (SD) or absolute difference (DIFF) between neighbouring data points locally. Elsewise, data points are filtered based on certain threshold criteria by fixed parameters multiplied by 2 or 3 times allowing for accepted variations or residuals. Parameters have been carefully chosen and tested for all methods in the study to derive the best representativeness for remote elevated mountain stations. However, for measurement sites with intensive regional influences or located on islands, parameters are thought to be adapted accordingly.

After data selection, results can be clearly viewed overlapping with original data sets and calculating the percentage of selected data points. In Figure 3.3 the CO₂ measurements at ZSF have been selected based on all methods shown with the percentages of selected CO₂ data. The method ADVS seems to be the most stringent method allowing only 15.3% of measured data considered to be “clean”. Both THO and SI result similar selected percentages of more than 40% likely due to the variation threshold of around 0.3 ppm. The number of selected data by MA increases largely with three quarters of the data remaining. Only less than 4% of the data are discarded as being polluted by REBS. From the selected data distribution in Figure 3.3 it is clearly observed that MA and REBS selection follow the certain boundary rules ($2*SD$ and $3*\sigma$) and that neither the data above nor below such a threshold are selected. The other three methods (ADVS, THO, and SI) allow more peak values due to their selection rules.

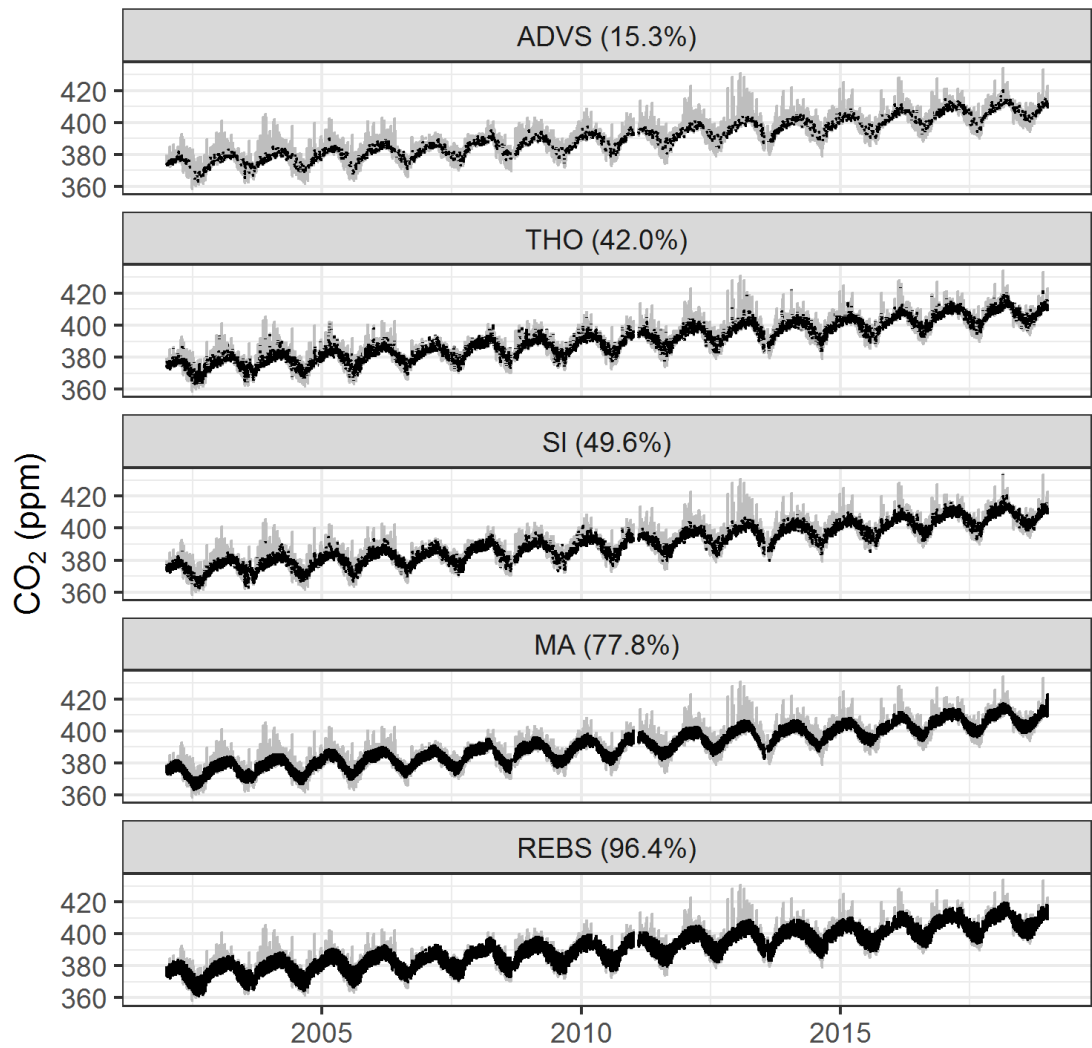


Figure 3.3: Atmospheric CO₂ measurements at ZSF during 2002–2018 with different data selection methods applied. Black data points indicate the selected data while grey points indicate the unselected ones. Percentages of selected data are given at the top of each data record (for data selection methods see Table 3.1).

3.3 Time series analysis

Time series analysis is commonly performed on measurement series for extracting useful information on the changes over years, seasons, and months. Changes over years comprise annual increases in atmospheric CO₂ as well as inter-annual variations related to years of extreme concentrations. In terms of seasons and months, the seasonality is always studied with its peaks as well as changes in the seasonal amplitude. The two

approaches used in the study are described in detail, i.e., the seasonal decomposition technique STL and the curve fitting technique.

3.3.1 STL

Cleveland et al. (1990) developed the filtering approach STL to decompose a time series into trend, seasonal, and remainder components. STL stands for a seasonal-trend decomposition procedure based on the locally weighted regression (loess), which performs regression analysis by local fitting (Cleveland and Devlin, 1988). It divides a single time series into parts with variations in different frequencies. The trend component T represents any potential long-term changes at the low frequency of the time series, while the seasonal component S illustrates changes in the data annually. The remaining variation from the trend and seasonal components combined is defined as the remainder component R , indicating any unexplained changes beyond. At any time stamp $v = 1$ to N , the data Y_v can be represented as,

$$Y_v = T_v + S_v + R_v. \quad (3.4)$$

The loess regression curve $\hat{g}(x)$ is calculated for any y given x (Cleveland et al., 1990). By selecting a number of x_i closest to x , the distance $\lambda_q(x)$ of each x_i from x is calculated in a tricube weight function $W(u)$ as a neighborhood weight $v_i(x)$. A polynomial fitting (locally-linear or locally-quadratic) is then applied with such a weight to derive $\hat{g}(x)$ at x .

$$W(u) = \begin{cases} (1 - u^3)^3 & \text{for } 0 \leq u < 1 \\ 0 & \text{for } u \geq 1 \end{cases} \quad (3.5)$$

$$v_i(x) = W\left(\frac{|x_i - x|}{\lambda_q(x)}\right) \quad (3.6)$$

Thus the loess smoother works as a moving average technique on the time series at different frequencies of interest (Carslaw, 2005; Pickers and Manning, 2015). Two recursive loops are performed in the STL procedure, i.e., an inner loop within an outer loop. The inner loop smooths firstly the seasonal component with cycle-subseries (time series for each month, such as January values and February values) and then the trend component by a series of means such as loess, detrending, and deseasonalizing. Afterwards, the remainder component can be estimated and a robustness weight ρ_v is defined based on how the extremes in remainder component behave in the outer loop.

$$\rho_v = B\left(\frac{|R_v|}{h}\right) \quad (3.7)$$

$$B(u) = \begin{cases} (1 - u^2)^2 & \text{for } 0 \leq u < 1 \\ 0 & \text{for } u > 1 \end{cases} \quad (3.8)$$

$$h = 6 \text{ median}(|R_v|) \quad (3.9)$$

3 Methods overview

Such values will be used for the next run of the inner loop until convergence is met (Pickers and Manning, 2015). At the end, a post-smoothing by loess on the seasonal component is necessary when the smoothness from one day to the next is required.

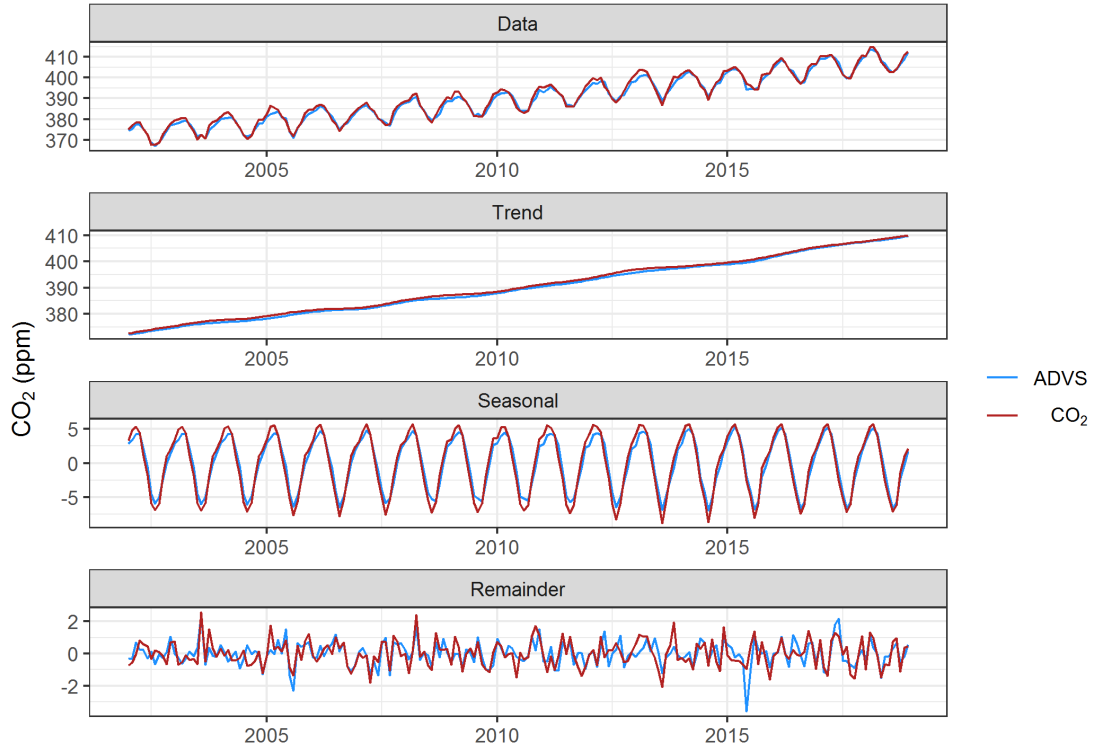


Figure 3.4: Monthly time series plot of CO₂ measurements (Data) at ZSF from 2002 to 2018, and its STL decomposed components (Trend, Seasonal, and Remainder) from original measured data (CO₂ in red) and selected data (ADVS in blue).

For STL decomposition, smoothing parameters for both the seasonal and trend components have to be set. The smoothing parameters define the smoothness of both variation in the time series and are important for both inner and outer loops. Since the purpose of smoothing differs between these two components, they should not compete for variation in the data (Cleveland et al., 1990). The choices for both $n_{(s)}$ and $n_{(t)}$ have to be odd, and $n_{(s)}$ is defined to be at least 7 (Cleveland et al., 1990). Considering that the remainder component should only consist of extremes instead of peaks and troughs, $n_{(t)}$ needs to be small but it cannot be too small to interfere with the seasonal component. Requirements for selecting $n_{(s)}$ and $n_{(t)}$ are summarized as

$$n_{(t)} \geq \frac{1.5n_{(p)}}{1 - 1.5n_{(s)}^{-1}}; \quad (3.10)$$

$$n_{(s)} \geq 7, \quad (3.11)$$

where $n_{(p)}$ is the number of observations per seasonal cycle. For the study, given that the seasonality plays a major part in the CO₂ time series due to respiration and photosynthesis, $n_{(s)} = 7$ is chosen. Using monthly time series of CO₂ and ADVS selected data (see Figure 3.4) $n_{(p)} = 12$ is taken. As a result, the constraint can be derived as $n_{(t)} \geq 22.9$ so that 23 is used for $n_{(t)}$ shown in Figure 3.4.

3.3.2 Curve fitting

As an alternative in time series analysis, curve fitting techniques have been frequently used especially for atmospheric CO₂ measurements, such as an oscillating power function by Keeling et al. (1976a) or least squares cubic splines by Wong et al. (1984). Similar to STL, the CO₂ time series can be seen as summing up a long-term trend, a yearly cycle, and short-term variations (Thoning et al., 1989). Throughout the development of atmospheric CO₂ studies, the understanding of the CO₂ trend and seasonality has also been improved. One of the most widely applied curve fitting methods CCGCRV (e.g. Curcoll et al., 2019; Fang et al., 2016; Zhu and Yoshikawa-Inoue, 2015) is a function fit with digital filtering on the residuals from the fit, which is used by NOAA/ESRL based on Thoning et al. (1989).

Steps of CCGCRV are briefly described here with fitted results on sample CO₂ data measured at ZSF shown in Figure 3.5. Firstly, a function fit consisting of a polynomial function for the trend and a harmonic function for the seasonality is applied on the data by general linear least squares regression based on Press et al. (1988) as

$$f(t) = a_0 + a_1t + a_2t^2 + \dots + a_{(k-1)}t^{(k-1)} + \sum_{n=1}^{nh} c_n[\sin(2n\pi t + \varphi_n)], \quad (3.12)$$

where k and nh stand for the number of polynomial terms and harmonics, respectively. Typical values of $k = 3$ and $nh = 4$ are used indicating a quadratic polynomial function with four harmonic terms. Residuals calculated from the function fit to the data are then filtered by converting the data from the time domain into the frequency domain by the fast Fourier transform (FFT) algorithm and later applying a low-pass filter for the separation of inter-annual and short-term variations. Afterwards, the filtered data is transformed back to the time domain by an inverse FFT. The function of the low-pass filter is

$$H(f) = \exp[-\ln(2) * (\frac{f}{f_c})^6], \quad (3.13)$$

where f_c is the cutoff frequency in cycles year⁻¹ representing the number of days. The residuals are filtered firstly with $f_c = 4.56$ (80 days) for smoothing the short-term variations, and secondly with $f_c = 0.55$ (667 days) for excluding all remaining seasonal variations but keeping any potential inter-annual variations not explained in the fitted polynomial function (Pickers and Manning, 2015; Thoning et al., 1989). At the end, different components of interest can be combined in order to represent e.g. trend (polynomial function fit plus long-term cutoff filtered residuals), or seasonality (harmonic function fit plus short-term cutoff filtered residuals). More explana-

3 Methods overview

tions on the estimation of uncertainties are available at the website of NOAA/ESRL (<https://www.esrl.noaa.gov/gmd/ccgg/mbl/crvfit/crvfit.html>).

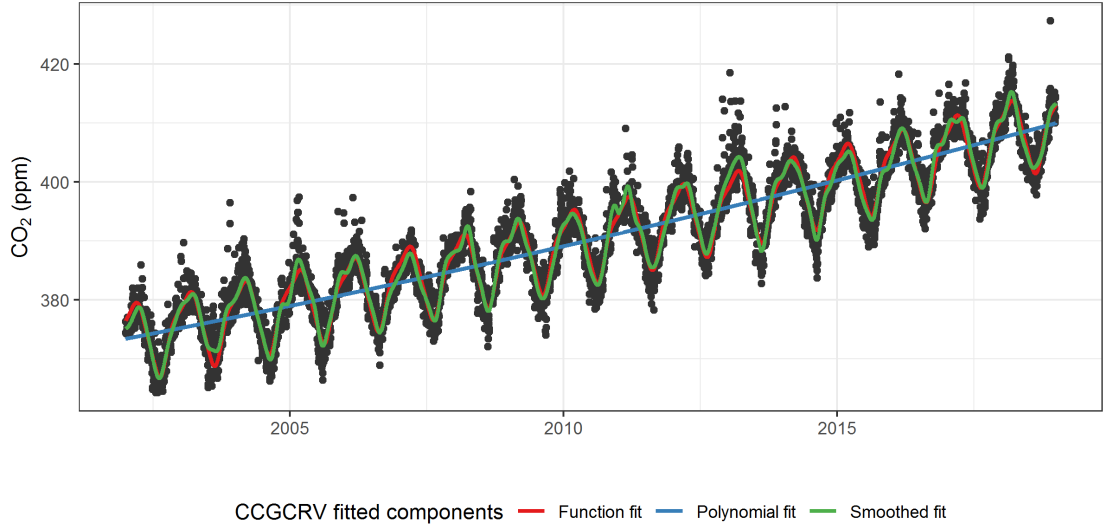


Figure 3.5: Fitted components by CCGCRV on the daily averaged atmospheric CO₂ measurements at ZSF from 2002 to 2018. The function fit is shown in red, while the blue line stands for the polynomial part only. The smoothed fit in green is the combination of the function fit and the residuals filtered with short-term cutoff value (80 days).

For column-averaged XCO₂ series from g-b FTSs and satellite observations, similar curve fitting methods were also applied successfully. For instance, Lindqvist et al. (2015) fitted a function in form of a linear trend and a sine curve to nicely capture the increasing trend and seasonal cycle of XCO₂ as

$$f(t) = a_0 + a_1 t + a_2 \sin(\omega[t - a_3] + \cos^{-1}[a_4 \cos(\omega[t - a_5])]). \quad (3.14)$$

As a result, STL and curve fitting techniques are helpful for data processing by examining the data variability especially regarding local fluctuations (Conway et al., 1988). Based on a good knowledge of the measurements, curve fitting can be extremely important for interpolation of missing or unevenly spaced data, and predictions of upcoming trends by extrapolation of the fitted functions. However, the most valuable result from time series analysis is the information of all pre-defined components, providing insights into the compatibility across measurement sites as well as comparison among data selection methods.

3.4 Software

All data sets used in the study were imported and analysed in the free software environment for statistical computing and graphics R with its integrated development

environment (IDE) RStudio (R Core Team, 2019). Data selection methods (including ADVS) and STL were implemented into R functions and scripts for processing. The most frequently used R packages are listed below:

- `openair` (Carslaw and Ropkins, 2012): open-source tools for analysing air pollution data
- `data.table` (Dowle and Srinivasan, 2019), `reshape2` (Wickham, 2007), and `plyr` (Wickham, 2011): fast manipulation for large data
- `zoo` (Zeileis and Grothendieck, 2005): regular and irregular time series analysis
- `raster` (Hijmans, 2019): gridded spatial data processing
- `ggplot2` (Wickham, 2016): elegant graphics for data analysis.

The curve fitting technique CCGCRV was applied using the python code downloaded from NOAA/ESRL (<https://www.esrl.noaa.gov/gmd/ccgg/mbl/crvfit/crvfit.html>).

4 Publication abstracts and contributions

玉不琢，不成器。

No jade crude, shows craft good.

三字经

The thesis is based on three publications (I, II, and III).

- I Yuan, Y., Ries, L., Petermeier, H., Steinbacher, M., Gómez-Peláez, A. J., Leuenberger, M. C., Schumacher, M., Trickl, T., Couret, C., Meinhardt, F., and Menzel, A. (2018). Adaptive selection of diurnal minimum variation: a statistical strategy to obtain representative atmospheric CO₂ data and its application to European elevated mountain stations. *Atmos. Meas. Tech.*, 11(3): 1501–1514.
- II Yuan, Y., Ries, L., Petermeier, H., Trickl, T., Leuchner, M., Couret, C., Sohmer, R., Meinhardt, F., and Menzel, A. (2019). On the diurnal, weekly, and seasonal cycles and annual trends in atmospheric CO₂ at Mount Zugspitze, Germany, during 1981–2016. *Atmos. Chem. Phys.*, 19(2): 999–1012.
- III Yuan, Y., Sussmann, R., Rettinger, M., Ries, L., Petermeier, H., and Menzel, A. (2019). Comparison of continuous in-situ CO₂ measurements with co-located column-averaged XCO₂ TCCON/satellite observations and CarbonTracker model over the Zugspitze region. *Remote Sens.*, 11(24): 2981.

Abstracts and author contributions for all publications are given. Abbreviations with initials of the first name and the family name are used in the contributions for authors, e.g. YY for Ye Yuan. When duplicated, the second letter of the family name is added in lowercase. The full copies are presented in Appendix ??.

4.1 Development of consistent data selection method

Yuan, Y., Ries, L., Petermeier, H., Steinbacher, M., Gómez-Peláez, A. J., Leuenberger, M. C., Schumacher, M., Trickl, T., Couret, C., Meinhardt, F., and Menzel, A. (2018). Adaptive selection of diurnal minimum variation: a statistical strategy to obtain representative atmospheric CO₂ data and its application to European elevated mountain stations. *Atmos. Meas. Tech.*, 11(3): 1501–1514.

Abstract

Critical data selection is essential for determining representative baseline levels of atmospheric trace gases even at remote measurement sites. Different data selection techniques have been used around the world, which could potentially lead to reduced compatibility when comparing data from different stations. This paper presents a novel statistical data selection method named adaptive diurnal minimum variation selection (ADVS) based on CO₂ diurnal patterns typically occurring at elevated mountain stations. Its capability and applicability were studied on records of atmospheric CO₂ observations at six Global Atmosphere Watch stations in Europe, namely, Zugspitze-Schneefernerhaus (Germany), Sonnblick (Austria), Jungfraujoch (Switzerland), Izaña (Spain), Schauinsland (Germany), and Hohenpeissenberg (Germany). Three other frequently applied statistical data selection methods were included for comparison. Among the studied methods, our ADVS method resulted in a lower fraction of data selected as a baseline with lower maxima during winter and higher minima during summer in the selected data. The measured time series were analyzed for long-term trends and seasonality by a seasonal-trend decomposition technique. In contrast to unselected data, mean annual growth rates of all selected datasets were not significantly different among the sites, except for the data recorded at Schauinsland. However, clear differences were found in the annual amplitudes as well as the seasonal time structure. Based on a pairwise analysis of correlations between stations on the seasonal-trend decomposed components by statistical data selection, we conclude that the baseline identified by the ADVS method is a better representation of lower free tropospheric (LFT) conditions than baselines identified by the other methods.

Contributions

YY, LR, and AM formulated the overall research goals. LR and YY developed the methodology. YY performed the formal analysis and programming code advice by LR and HP. Atmospheric CO₂ measurements were monitored and data were provided by LR, MSt, AG, ML, MSc, TT, CC, and FM. YY visualized the work results and drafted the manuscript with contributions from all co-authors.

4.2 Application of data selection on long-term measurements

Yuan, Y., Ries, L., Petermeier, H., Trickl, T., Leuchner, M., Couret, C., Sohmer, R., Meinhardt, F., and Menzel, A. (2019). On the diurnal, weekly, and seasonal cycles and annual trends in atmospheric CO₂ at Mount Zugspitze, Germany, during 1981–2016. *Atmos. Chem. Phys.*, 19(2): 999–1012.

Abstract

A continuous, 36-year measurement composite of atmospheric carbon dioxide (CO₂) at three measurement locations on Mount Zugspitze, Germany, was studied. For a comprehensive site characterization of Mount Zugspitze, analyses of CO₂ weekly periodicity and diurnal cycle were performed to provide evidence for local sources and sinks, showing clear weekday to weekend differences, with dominantly higher CO₂ levels during the daytime on weekdays. A case study of atmospheric trace gases (CO and NO) and the passenger numbers to the summit indicate that CO₂ sources closeby did not result from tourist activities but instead obviously from anthropogenic pollution in the near vicinity. Such analysis of local effects is an indispensable requirement for selecting representative data at orographic complex measurement sites. The CO₂ trend and seasonality were then analyzed by background data selection and decomposition of the long-term time series into trend and seasonal components. The mean CO₂ annual growth rate over the 36-year period at Zugspitze is 1.8 ± 0.4 ppm yr⁻¹, which is in good agreement with Mauna Loa station and global means. The peak-to-trough amplitude of the mean CO₂ seasonal cycle is 12.4 ± 0.6 ppm at Mount Zugspitze (after data selection: 10.5 ± 0.5 ppm), which is much lower than at nearby measurement sites at Mount Wank (15.9 ± 1.5 ppm) and Schauinsland (15.9 ± 1.0 ppm), but following a similar seasonal pattern.

Contributions

YY, LR, HP, and AM designed the study and YY performed the data analyses with help from LR and HP for the data processing and code validation. Atmospheric measurement data were collected, pre-processed, and provided by LR, TT, CC, RS, and FM. Information about data quality assurance and measurement site was provided by LR. YY prepared the manuscript with contributions from all co-authors.

4.3 Comparison of CO₂ measurements and models

Yuan, Y., Sussmann, R., Rettinger, M., Ries, L., Petermeier, H., and Menzel, A. (2019). Comparison of continuous in-situ CO₂ measurements with co-located column-averaged XCO₂ TCCON/satellite observations and CarbonTracker model over the Zugspitze region. *Remote Sens.*, 11(24): 2981.

Abstract

Atmospheric CO₂ measurements are important in understanding the global carbon cycle and in studying local sources and sinks. Ground and satellite-based measurements provide information on different temporal and spatial scales. However, the compatibility of such measurements at single sites is still underexplored, and the applicability of consistent data processing routines remains a challenge. In this study, we present an inter-comparison among representative surface and column-averaged CO₂ records derived from continuous in-situ measurements, ground-based Fourier transform infrared measurements, satellite measurements, and modelled results over the Mount Zugspitze region of Germany. The mean annual growth rates agree well with around 2.2 ppm yr⁻¹ over a 17-year period (2002–2018) while the mean seasonal amplitudes show distinct differences (surface: 11.7 ppm/column-averaged: 6.6 ppm) due to differing air masses. We were able to demonstrate that, using consistent data processing routines with proper data retrieval and gap interpolation algorithms, the trend and seasonality can be well extracted from all measurement data sets.

Contributions

The research aim were developed by YY, LR, and AM; Formal analysis, methodology, and implementation of the programming algorithm were done by YY under the supervision of LR, HP, RS, and AM; The ground-based FTS measurements were performed and collected by RS and MR; The original draft was prepared by YY and reviewed and edited by all co-authors.

5 Discussion

一花独放不是春，百花齐放春满园。
A single flower does not make spring,
while one hundred flowers in full
blossom bring spring to the garden.

古今贤文

From the publication-based results on the developed data selection method ADVS and its application on long-term atmospheric CO₂ measurements and comparisons, the performances of ADVS data selection mainly on the applicability are discussed in Section 5.1. The differences in data analysis routines STL and curve fitting are presented in Section 5.2. Further discussion focuses on the difference between ADVS and wind sector in Section 5.3, and the web application of data selections and analyses by R shiny in Section 5.4.

5.1 Data selection

The data selection method ADVS (Adaptive Diurnal minimum Variation Selection) was developed based on the diurnal variation exhibited in the atmospheric CO₂ records at elevated mountain stations Yuan et al. (2018). The main research goal of the study is to evaluate whether such a data processing approach can be consistently applicable on atmospheric CO₂ measurements from the perspectives of remote – urban; short-term – long-term; continuous – discrete; point – column.

5.1.1 Performance

The location of measurement site is critical as data selection and processing is always site-specific. The difficulty of generalized data selection is reflected by the site characteristics experiencing distinct meteorological conditions and measurement techniques (e.g. instrumentation, sampling time resolutions / lengths). Therefore, tracer / chemical and meteorological data selection are feasible only based on additional measurements on the same site. Even by statistical data selection, site-related threshold criteria are required (including ADVS).

Yuan et al. (2018) showed the comparison of atmospheric CO₂ records from various types of stations by ADVS data selection under the same threshold criterion (0.3 ppm for the standard deviation threshold of the starting time window), reporting increasing percentages of selected data to the original data sets with sampling elevations (see

red points and line in Figure 5.1). Lower elevated measurement sites (HPB and SSL) exhibiting more regional influences and thus larger data variations resulted in lower percentages (vice versa for the higher elevated alpine stations ZSF, SNB, and JFJ). Similar patterns were found for data selection methods SI and THO, but not MA. From the selection mechanism (see Table 3.1), both SI and THO apply similar statistical criteria (0.3 ppm) but with respect to different standard deviations (SD_{hour} and $SD_{6\text{h}}$). However, the MA technique selects data within the statistical boundary ($2*SD$), indicating that the selection criteria for MA varies based on the data variability only, despite of the knowledge of the CO_2 concentration levels and changes in the atmosphere. Therefore, such data selection is capable of detecting obvious outliers resulting in similar percentages for all sites but difficulties remain for identifying the real background levels of atmospheric CO_2 . Moreover, at IZO (open circles in Figure 5.1) percentages of selected CO_2 data in ADVS, SI, and THO were much higher than at other stations, but not for MA. The measurement site IZO is located seaside on the Island of Tenerife above the strong subtropical temperature inversion layer exhibiting extremely low data variations (comparable to the seaside station MLO). Consequently the selection criteria performed by MA data selection acts too strictly (Yuan et al., 2018).

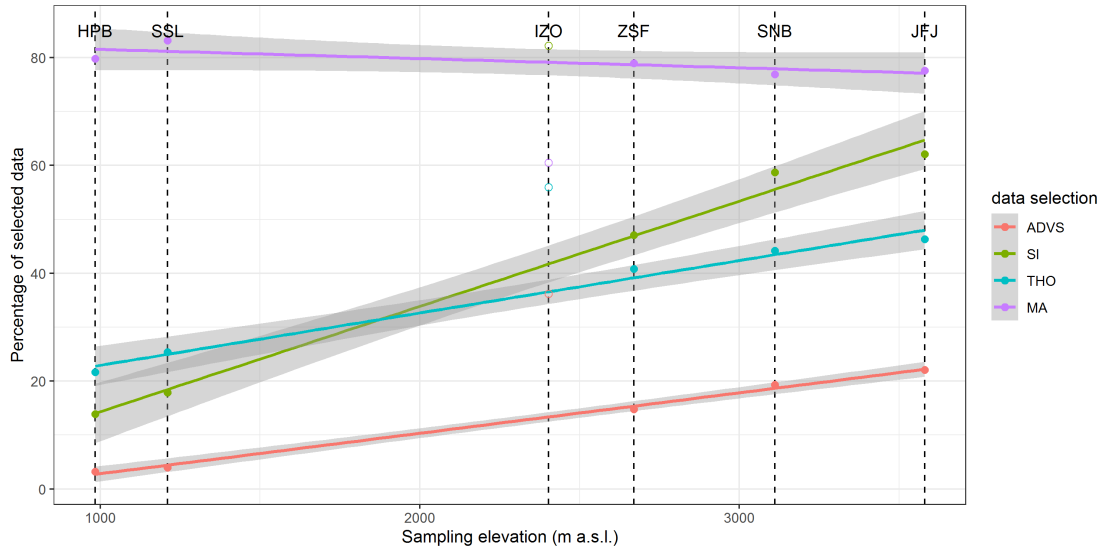


Figure 5.1: Linear regressions between the sampling elevations and percentages of selected CO_2 data by four statistical data selection methods for continental sites (excluding IZO, points in open circles). Plotting data are based on Table 2 of Yuan et al. (2018).

Nevertheless, data selection based on standard deviation is still of the most interest to researchers or station managers. El Yazidi et al. (2018) tried to identify the local emission by positive spike detection in the time series of GHGs. Similar data selection methods were compared, including coefficient of variation (COV), REBS, and standard deviation of the background (SD). Their conclusion revealed that REBS and SD were performed successfully in detecting most of the manual spikes identified, particularly SD

was preferred and had been proposed to atmospheric network such as ICOS (Integrated Carbon Observation System), due to its easy and efficient implementation in automatic data processing. At the end, external and empirical knowledge is necessary and even crucial for data selection with preferred practical statistical threshold settings implemented. In addition to the standard deviation of 0.3 ppm frequently used for remote stations (e.g. Francey et al., 2010; Nakazawa et al., 1991; Watanabe et al., 2000), a value of 1.0 ppm was often applied for regional to urban stations (e.g. Brooks et al., 2012; Zhang et al., 2015; Zhou et al., 2003).

Data selection is also potentially influenced by different measurement techniques and instruments. The highly accurate continuous in situ CO₂ measurements were mainly performed by nondispersive infrared (NDIR) analyser, gas chromatographs using the flame ionization detector (GC-FID), and cavity ring-down spectroscopy (CRDS) technique (Chen et al., 2010; van der Laan et al., 2009). Schibig et al. (2015) calculated a difference of 0.03 ± 0.25 ppm between two measurement systems (NDIR and CRDS) at JFJ, and revealed a good agreement in terms of trend and seasonality calculations, as well as short-term variations. Another good agreement was also reported by Yuan et al. (2019) between one NDIR and one GC-FID analysers at measurement sites within 300 m in elevation (Zugspitze summit and Schneefernerhaus) exhibiting a difference of 0.1 ± 0.4 ppm. Given that only validated CO₂ data sets were used in this study fulfilling the compatibility goal of GAW (DQO: ± 0.10 ppm), differences are more likely to be found regarding sampling resolution or time length of measurements. Unlike discrete sampling or campaign (weekly / daily / sub-daily), continuous in situ measurements are always available at least with hourly or finer scale (also up to seconds for CRDS). It was tested in Yuan et al. (2018) that the percentages of ADVS selected CO₂ data were always higher for hourly averages compared with sub-hourly data (10 / 20 / 30-min) at both ZSF and JFJ. This is clear because data series exhibits smaller variations after averaging and thus fulfilling better with threshold conditions. Besides, hourly statistical measures (i.e., hourly standard deviation, hour-to-hour variability) are taken in statistical data selection as well as in ADVS (diurnal variations). On the other hand, time length of data series is also important since data selection based on curve fitting techniques with certain threshold boundaries (e.g. Kilkki et al., 2015; Sirignano et al., 2010) often requires a relatively longer time period for a better fitting performance of the function. It is also suggested by NOAA/ESRL that for the function fit (similar to Equation 3.12) it is better to use a linear term instead of the polynomial fit when the data set is shorter than three years to prevent outlier influences from the seasonal cycle due to least squares fit. However since ADVS data selection only focused on changes in the diurnal cycle, it is theoretically applicable for data sets covering time periods of years to months and even to days. Therefore it is recommended here to apply data selection methods especially ADVS on the hourly validated data sets.

5.1.2 Correlation

The correlation analysis was adopted in the study as a measure of comparing CO₂ data sets among measurement series (see Section 4.3) and among data selection methods

(Yuan et al., 2018). By correlating CO₂ / XCO₂ measurements and modelled data sets, clear improvements in both coefficients and significance levels were derived after ADVS data selection applied, matching better with other global studies (e.g. Buchwitz et al., 2018; Schibig et al., 2016). On the other hand, by the seasonal decomposition technique STL correlations of the atmospheric CO₂ series between measurement sites across data selection methods were performed resulting in significant and high coefficients ranging from 0.68 to 1.00. Afterwards, STL decomposed remainder components exhibited largely decreased coefficients between measurement sites as well as less pairs with significance. In particular, ADVS data selection included the most significant correlation pairs (seven out of ten) in the trend and seasonal components and the least significant correlation pairs (only two) in the remainder component, representing the best fit for the smoothed CO₂ levels while excluding the most of local variations in the residuals.

5.1.3 Functionality

The functionality described here only refers to the operation time of running data selection methods implemented in R scripts. The CO₂ data set at ZSF was tested by applying all data selection methods implemented in the study with three subsetting time lengths (5 / 10 / 15 years). The summary in Table 5.1 shows that the SI data selection was performing the fastest because of one single selection criteria (see Table 3.1). The MA and REBS required almost one minute for the 15-yr hourly data set related to outlier rejection mechanisms from the fit. The ADVS method managed to perform the data selection on a daily basis but still exhibiting intermediately fast computation speed similar to THO. These results suggest that ADVS can be performed efficiently for the purpose of data processing on a routinely basis.

Table 5.1: Summary of the operation time (in sec) for all data selection methods implemented in R.

Time period (length)	ADVS	THO	SI	MA	REBS
2014–2018 (5 yrs)	3.91	3.17	0.98	25.46	19.39
2009–2018 (10 yrs)	8.16	6.89	1.95	60.57	38.45
2004–2018 (15 yrs)	13.96	10.44	2.81	67.21	57.93

5.2 Data analysis

With the appropriate data selection method applied, further data analysis routine is required to extract useful information from the validated and representative atmospheric data set. Throughout the study, the seasonal decomposition technique STL was performed to separate CO₂ series into parts representing sources local and non-local (Yuan et al., 2018) as well as to study the inter-annual variations / anomalies due to vegetation dynamics (photosynthesis / respiration). This gave valuable insights into trend and seasonality under the influence of climate change (Forkel et al., 2016; Yuan et al.,

2019, also see Section 4.3). Nevertheless, Pickers and Manning (2015) recommended to employ more than one data analysis routine for unduly bias. They compared STL with two curve fitting techniques (CCGCRV and another parametric curve fitting program named HPspline used at Scripps) using long-term records of CO₂, CH₄, and ozone (O₃). However, there were no clear conclusions on which routine performed the best as each of them was appropriate for certain types of data sets. And also as shown in Figure 3.4, clear differences can be observed between original CO₂ and ADVS-selected data set, especially for the seasonal components. For a better quantification and characterization of those signal differences, both STL and CCGCRV methods were applied here on the CO₂ records from 2002 to 2018 at ZSF to compare annual growth rates and seasonal amplitudes (see Figure 5.2).

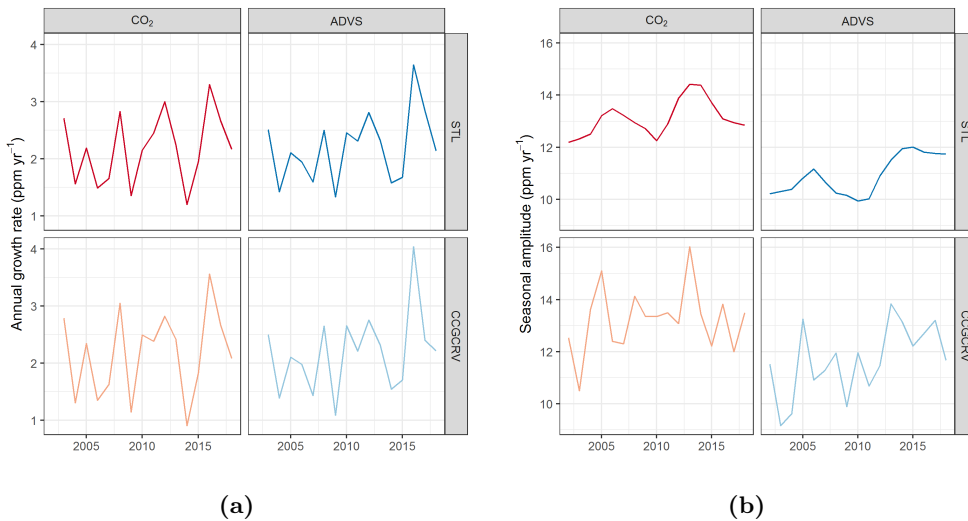


Figure 5.2: Comparisons of (a) annual growth rates and (b) seasonal amplitudes between the original measured data (CO₂) and selected data (ADVS) at ZSF from 2002 to 2018; between the STL decomposed components and CCGCRV fitted components.

As noted in Yuan et al. (2018) and Yuan et al. (2019), the ADVS data selection results in similar levels of annual growth rates as the original CO₂ data set but exhibits much smaller seasonal amplitudes (around 2.0 ppm in Figure 5.2). However, no clear differences were found in the annual growth rates by both STL and CCGCRV techniques. Here the annual growth rate was calculated on a monthly basis, deriving the growth rate by differentiating between one monthly value and the value of the same month from the previous year. Then, all 12-month growth rates were averaged for each year as the annual growth rate. Seasonal amplitudes were defined as the difference between the monthly maximum and minimum for each year. Surprisingly the annual variation of seasonal amplitudes (see Figure 5.2b) was different. Compared to STL, more fluctuations were present with CCGCRV while both techniques captured nicely the main peaks (2006, 2013) and troughs (2010). Such a difference agreed well with Pickers and Manning (2015) noting that STL assigned less variation to the seasonal component and more variation to

the trend compared to CCGCRV. They further suggested that both STL and CCGCRV were recommended for studies aiming at accurate extraction of year-to-year variations in the trend and seasonal components; magnitude or timing of the seasonal cycles; and inter-annual variations of the long-term trends especially with variable growth rates. Nevertheless, gaps or unevenly spaced time series need to be analysed with caution by these two routines, potentially pre-processed by gap filling (interpolation) techniques. What's more, potential improvements on the methodological model are possible, such as the time series analysis model used in Belikov et al. (2019) similar to STL applied an additional holiday component emphasizing the effects on irregular schedules over one or more days.

5.3 Validation with wind sector

For the ADVS statistical data selection developed in the study, it is important to examine the agreement with methods based on meteorological parameters. Wind sectors have been used to assign the atmospheric measurements to predominant wind directions with comparably high wind speeds representing long distance air mass transport. It has been confirmed by Stavert et al. (2019) that more noises (higher data variability) are observed for atmospheric CO₂ measurements at lower wind speeds, indicating the influence from local fluxes. Wind directions between 45° to 135° (28.8% of the data) and 225° to 315° (47.5%) were selected as described in Section 2.3. With respect to wind speeds, thresholds have been applied differently worldwide for different types of measurement sites. Both Brunke et al. (2004) and Francey et al. (2010) required wind speeds > 5 m s⁻¹ for the maritime wind sector while even 6 m s⁻¹ was chosen at Mace Head, Ireland (Biraud et al., 2000; Derwent et al., 2002). Also note that measurements with wind speed less than 1.5 m s⁻¹ was flagged as local events by Fang et al. (2016) for the Shangdianzi GAW Regional station in China and 0.4 m s⁻¹ was used for the Southern Hemisphere urban site Wollongong, Australia (Buchholz et al., 2016). Thus, a threshold of above or equal 3 m s⁻¹ (31.6% of the data) was determined empirically for ZSF concerning the specific alpine characteristics similar to Schmidt (2003). By combining wind direction and speed criteria 30.3% of the CO₂ data at ZSF were selected.

Table 5.2: Classification of atmospheric CO₂ measurements (2002–2018) at ZSF as background by ADVS and wind sector (overall number validated data points: 132,473). Numbers of selected / non-selected data and the corresponding percentages were calculated.

Classification		ADVS	
		selected	non-selected
Wind Sector	selected	7394 (5.6%)	32776 (24.7%)
	non-selected	12886 (9.7%)	79417 (59.9%)

The CO₂ data selected by both ADVS and wind sector amounted only 5.6% of the original data set (see Table 5.2). Around 25% of the data were selected by wind sector but not ADVS. Combining with the wind sector distribution at ZSF, CO₂ data from this category (ADVS non-selected; Wind sector selected) could be attributed to those extremes shown in Figure 2.4 as well as certain time periods with high CO₂ variability. Moreover, nearly 10% of ADVS selected data were not considered by the selected wind sector, indicating that such selections of wind direction and speed are not sufficient. More measured stable conditions of air masses should be included. From this perspective, it is not recommended for data selection by only using wind sector data especially considering the complex topography at elevated mountain stations.

5.4 Practical implementation of ADVS in the GAW network

Adaptive Diurnal minimum Variation Selection (ADVS)

Data selection method for atmospheric CO₂ at elevated mountain stations.

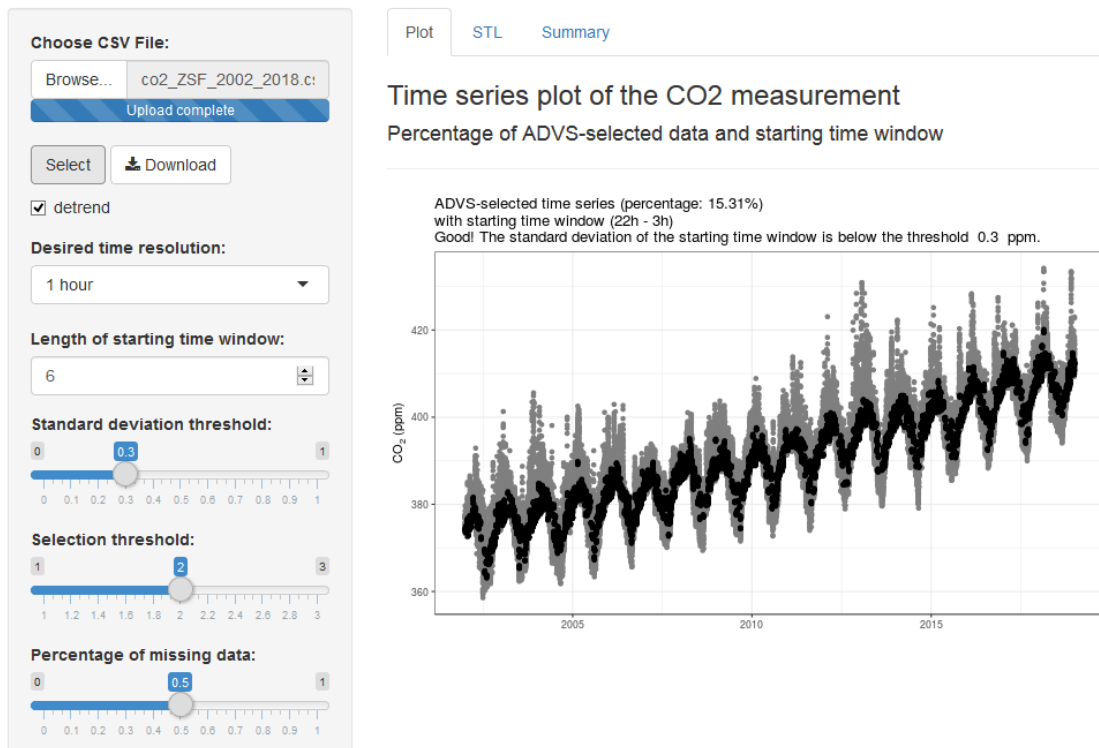


Figure 5.3: Example of ADVS data selection applied on CO₂ records at ZSF (2002–2018) in the R shiny application using default selection parameters in Yuan et al. (2018).

A web application with the user friendly interface for data processing with ADVS and further data analysis routines has been developed and integrated in R with the package shiny (Chang et al., 2019). The application with training data is available at the web page

5 Discussion

of standardized data quality assurance at GAW stations (www.gawstat.de), together with a data processing routine Dafit to be used for data processing at GAW stations and projects (Ries, 2013). Figure 5.3 presents the interface of ADVS data selection application. On the left side panel it consists of CO₂ data import and adjustment of selection parameters. The sample data (i.e., atmospheric CO₂ at ZSF from 2002 to 2018) were used here. All default selection parameters are chosen based on Yuan et al. (2018), which can be freely adjusted by users. The selected result will be shown on the right after clicking on the “Select” button, with a further option to obtain the selected data set using “Download” button. The percentage of selected data (15.31%) and the starting time window (22:00h–03:00h LT) are listed together with the information whether the standard deviation threshold (SD_{stw} in Table 3.1) is fulfilled or not.

For a more conservative data selection, different selection parameters can be used. For instance, in Figure 5.4, a longer length of starting time window and a larger threshold for standard deviation were applied, resulting in 28.13% of CO₂ data selected with a broader starting time window from 21:00h to 04:00h. For such adjustments further knowledge of the measurement sites and empirical experiments on the selection parameters are required.

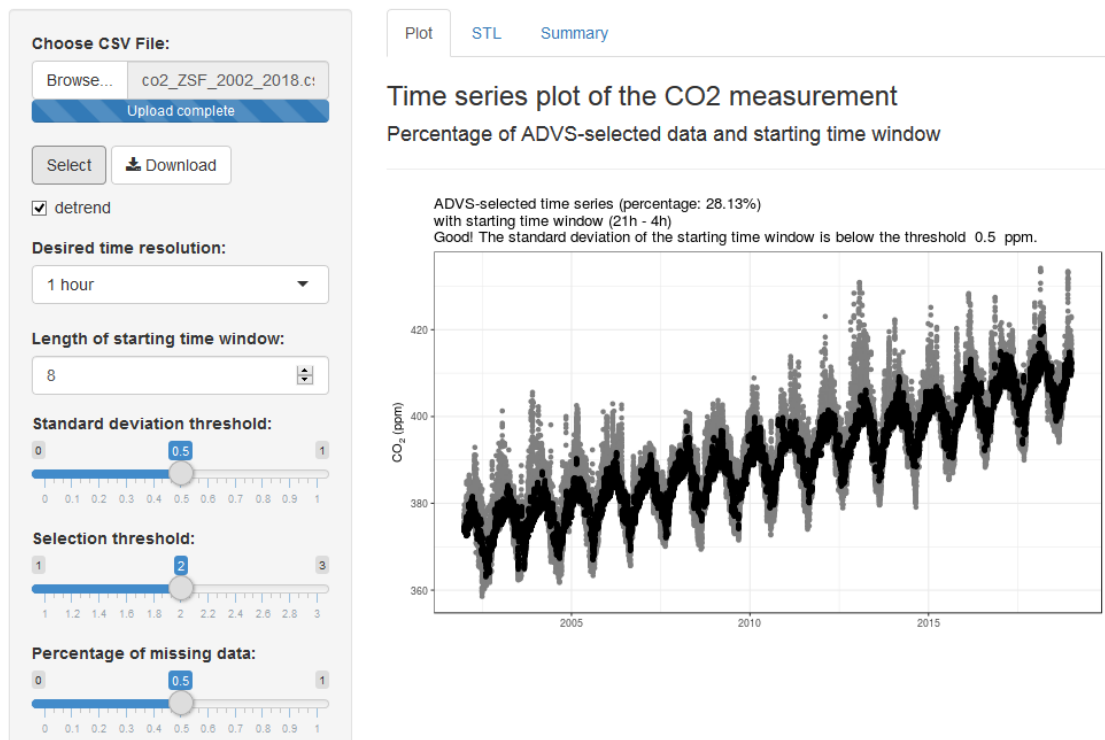


Figure 5.4: Example of ADVS data selection applied on CO₂ records at ZSF (2002–2018) in the R shiny application using more conservative selection parameters (length of starting time window = 8 h; standard deviation threshold = 0.5 ppm).

5.4 Practical implementation of ADVS in the GAW network

There are two more panels named “STL” and “Summary” in the application, which illustrate the time series analyses and statistics in more details for the selected data. Further parameters regarding STL decomposition can be chosen for the smoothing parameters of trend and seasonal, with the functional buttons “Decompose” and “Download”. The decomposed trend, seasonal, and remainder components of ADVS selected CO₂ can be seen in Figure 5.5. In the web application, every single data point in the time series can be examined in value when being clicked, and the time length can be freely extracted for a better view in the details. Moreover, further analyses of annual growth rates and mean seasonal amplitudes are available (see Figure 5.6), showing a clear difference between the CO₂ data before and after ADVS data selection.

5 Discussion

Seasonal decomposition technique (STL)

To decompose time series into trend, seasonal, and remainder components.

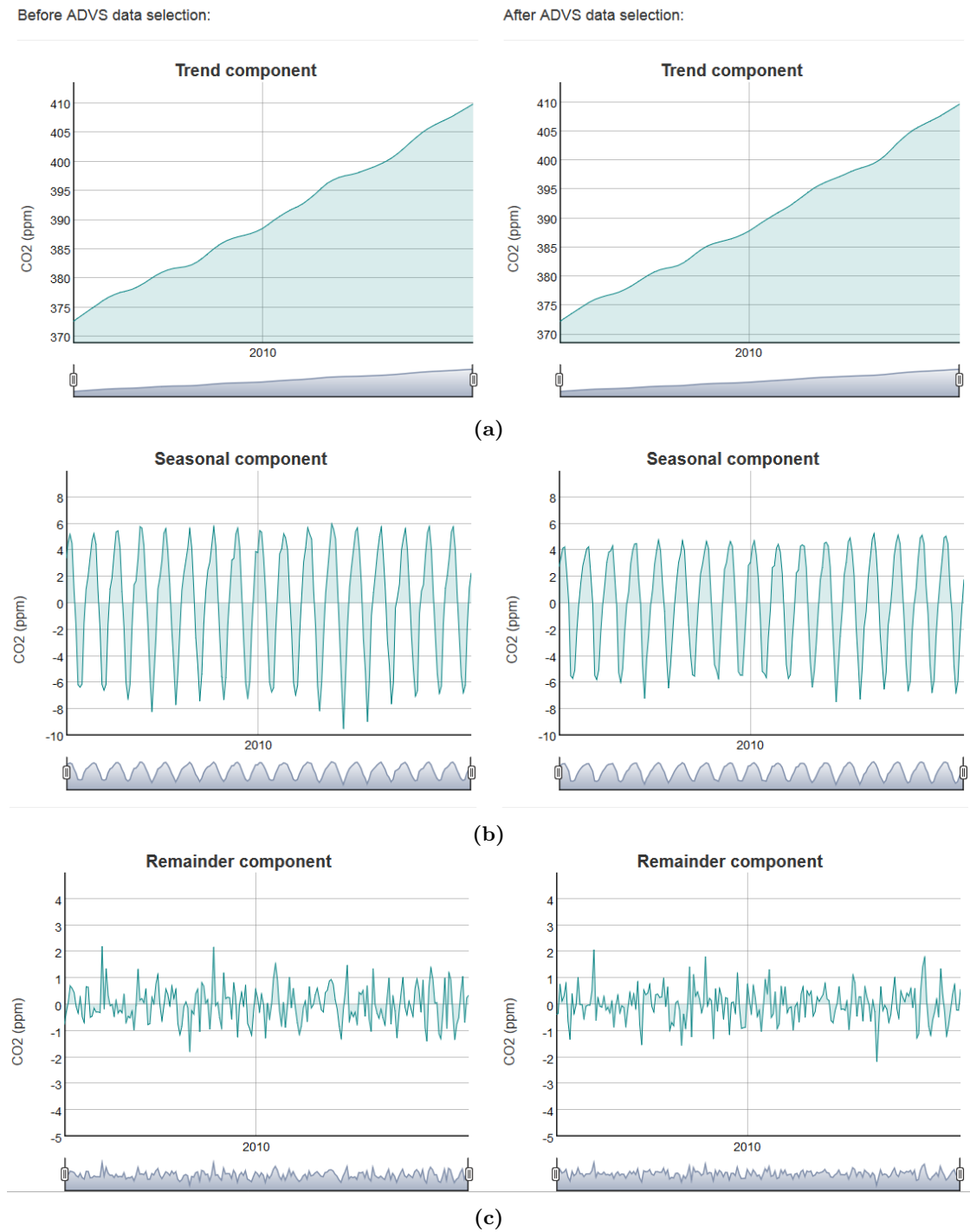


Figure 5.5: Example of STL-decomposed (a) trend, (b) seasonal, and (c) remainder components from CO₂ records at ZSF (2002–2018) selected by ADVS in the R shiny application.

5.4 Practical implementation of ADVS in the GAW network

Statistical summary of time series

Annual growth rate, seasonal amplitude and so on

Before ADVS data selection:

1. Annual mean mole fraction (annual growth rate)

Show entries Search:

	year ↕	co2 ↕	gr ↕
1	2002	373.89	0
2	2003	376.55	2.67
3	2004	378.16	1.61
4	2005	380.31	2.15
5	2006	381.81	1.5
6	2007	383.5	1.69
7	2008	386.27	2.77
8	2009	387.67	1.4
9	2010	389.82	2.16
10	2011	392.27	2.45

Showing 1 to 10 of 17 entries

Previous 2 Next

After ADVS data selection:

1. Annual mean mole fractions (annual growth rate)

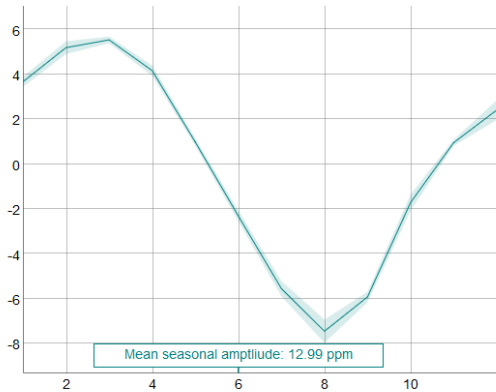
Show entries Search:

	year ↕	co2 ↕	gr ↕
1	2002	373.45	0
2	2003	375.87	2.42
3	2004	377.3	1.43
4	2005	379.45	2.15
5	2006	381.32	1.87
6	2007	383.05	1.73
7	2008	385.51	2.46
8	2009	386.83	1.32
9	2010	389.03	2.2
10	2011	391.54	2.51

Showing 1 to 10 of 17 entries

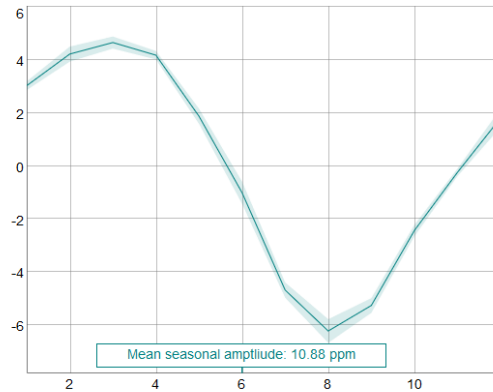
Previous 2 Next

2. Mean seasonal cycle



(a)

2. Mean seasonal cycle



(b)

Figure 5.6: Example of (a) processed annual growth rates and (b) seasonal amplitudes from CO₂ records at ZSF (2002–2018) before and after ADVS data selection in the R shiny application.

6 Outlook

This doctorate study developed and practically applied the statistical data selection method ADVS on atmospheric CO₂ measurements at European mountain stations. Research outcomes such as the resulting trend and seasonality were validated across measurement sites and measurement techniques. Apadula et al. (2019) selected atmospheric background CO₂ hourly concentrations at the high Plateau Rosa mountain station by means of a BaDS (Background Data Selection) filter with similar statistical criteria as ADVS and THO while focusing more on the moving median / average techniques. The importance of identifying the representative “background conditions” for the measurement sites was mentioned in Diémoz et al. (2019) using the example differentiating between the local and regional pollution levels in Yuan et al. (2018). Moreover, the characteristics of measurement site ZSF was described in detail for studies of atmospheric aerosol particles (Schnaiter et al., 2019) with insights from the weekday-weekend analysis from Yuan et al. (2019). Recently a multivariate statistical air mass classification performed at ZSF (Sigmund et al., 2019) suggested that 14% of the air masses belong to the class UFT/SIN (undisturbed free troposphere or stratospheric intrusion) which was highly comparable to the percentages of ADVS selected data (around 14%) reported in Yuan et al. (2018) and Yuan et al. (2019). Apart from these, knowledge of the long-term CO₂ measurements and diurnal variation are also helpful in understanding measurements of the carbon isotope ($\delta^{13}\text{C}$) with identification of pollution events (Ghasemifard et al., 2019a,b), and identification of typical diurnal patterns (Ghada et al., 2019).

In the meantime, potential applications of ADVS data selection can be foreseen. Instead of elevated mountain stations, both seaside and regional / urban stations are worth testing with more appropriate constraints of the threshold criteria. Seaside stations experience mostly long distance transport of air masses over the ocean and thus data variability is assumed to be noticeably smaller, such as at IZO or MLO. For regional or urban stations not only larger data variability is expected due to closer distance to carbon sources and sinks, but also distinct diurnal patterns are possible. Likely, afternoon time can be selected instead of night time for the well-mixed conditions at urban stations (e.g. Guha and Ghosh, 2015; Lauvaux et al., 2013). On the other hand, besides atmospheric CO₂ any measurements with typical diurnal patterns are theoretically applicable by ADVS. Airborne aerosols and black carbon (BC) are a good start exhibiting clear diurnal peaks during the daytime due to traffic and new particle formation (Backman et al., 2012; Ma and Birmili, 2015). Last but not least, for further validation of ADVS data selection, ²²²Rn could be used with statistical percentile approach for improving the selection performances (Brunke et al., 2004; Chambers et al., 2016).

References

- Apadula, F., Cassardo, C., Ferrarese, S., Heltai, D., and Lanza, A. (2019). Thirty Years of Atmospheric CO₂ Observations at the Plateau Rosa Station, Italy. *Atmosphere*, 10(7):418.
- Ascencio-Parvy, J. M., Gaudry, A., and Lambert, G. (1984). Year-to-year CO₂ variations at Amsterdam Island in 1980–83. *Geophys. Res. Lett.*, 11(12):1215–1217.
- Backman, J., Rizzo, L. V., Hakala, J., Nieminen, T., Manninen, H. E., Morais, F., Aalto, P. P., Siivola, E., Carbone, S., Hillamo, R., Artaxo, P., Virkkula, A., Petäjä, T., and Kulmala, M. (2012). On the diurnal cycle of urban aerosols, black carbon and the occurrence of new particle formation events in springtime São Paulo, Brazil. *Atmos. Chem. Phys.*, 12:11733–11751.
- Balzani Lööv, J. M., Henne, S., Legreid, G., Staehelin, J., Reimann, S., Prévôt, A. S. H., Steinbacher, M., and Vollmer, M. K. (2008). Estimation of background concentrations of trace gases at the Swiss Alpine site Jungfraujoch (3580 m asl). *J. Geophys. Res.*, 113(D22):3017.
- Belikov, D., Arshinov, M., Belan, B., Davydov, D., Fofonov, A., Sasakawa, M., and Machida, T. (2019). Analysis of the Diurnal, Weekly, and Seasonal Cycles and Annual Trends in Atmospheric CO₂ and CH₄ at Tower Network in Siberia from 2005 to 2016. *Atmosphere*, 10(11):689.
- Biraud, S., Ciais, P., Ramonet, M., Simmonds, P., Kazan, V., Monfray, P., O’Doherty, S., Spain, G., and Jennings, S. G. (2002). Quantification of carbon dioxide, methane, nitrous oxide and chloroform emissions over Ireland from atmospheric observations at Mace Head. *Tellus B*, 54(1):41–60.
- Biraud, S., Ciais, P., Ramonet, M., Simmonds, P., Kazan, V., Monfray, P., O’Doherty, S., Spain, T. G., and Jennings, S. G. (2000). European greenhouse gas emissions estimated from continuous atmospheric measurements and radon 222 at Mace Head, Ireland. *J. Geophys. Res. Atmos.*, 105(D1):1351–1366.
- Boesch, H., Baker, D., Connor, B., Crisp, D., and Miller, C. (2011). Global Characterization of CO₂ Column Retrievals from Shortwave-Infrared Satellite Observations of the Orbiting Carbon Observatory-2 Mission. *Remote. Sens.*, 3(2):270–304.
- Bousquet, P., Gaudry, A., Ciais, P., Kazan, V., Monfray, P., Simmonds, P. G., Jennings, S. G., and O’Connor, T. C. (1996). Atmospheric CO₂ concentration variations

References

- recorded at Mace Head, Ireland, from 1992 to 1994. *Phys. Chem. Earth.*, 21(5):477–481.
- Bovensmann, H., Burrows, J. P., Buchwitz, M., Frerick, J., Noël, S., Rozanov, V. V., Chance, K. V., and Goede, A. P. H. (1999). SCIAMACHY: Mission Objectives and Measurement Modes. *J. Atmos. Sci.*, 56(2):127–150.
- Brooks, B.-G. J., Desai, A. R., Stephens, B. B., Bowling, D. R., Burns, S. P., Watt, A. S., Heck, S. L., and Sweeney, C. (2012). Assessing filtering of mountaintop CO₂ mole fractions for application to inverse models of biosphere-atmosphere carbon exchange. *Atmos. Chem. Phys.*, 12(4):2099–2115.
- Brunke, E. G., Labuschagne, C., Parker, B., Scheel, H. E., and Whittlestone, S. (2004). Baseline air mass selection at Cape Point, South Africa: application of ²²²Rn and other filter criteria to CO₂. *Atmos. Environ.*, 38(33):5693–5702.
- Buchholz, R. R., Paton-Walsh, C., Griffith, D., Kubistin, D., Caldow, C., Fisher, J. A., Deutscher, N. M., Kettlewell, G., Riggensbach, M., Macatangay, R., Krummel, P. B., and Langenfelds, R. L. (2016). Source and meteorological influences on air quality (CO, CH₄ & CO₂) at a Southern Hemisphere urban site. *Atmos. Environ.*, 126:274–289.
- Buchwitz, M., Reuter, M., Schneising, O., Noël, S., Gier, B., Bovensmann, H., Burrows, J. P., Boesch, H., Anand, J., Parker, R. J., Somkuti, P., Detmers, R. G., Hasekamp, O. P., Aben, I., Butz, A., Kuze, A., Suto, H., Yoshida, Y., Crisp, D., and O’Dell, C. (2018). Computation and analysis of atmospheric carbon dioxide annual mean growth rates from satellite observations during 2003–2016. *Atmos. Chem. Phys.*, 18(23):17355–17370.
- Burrows, J. P., Hölzle, E., Goede, A., Visser, H., and Fricke, W. (1995). SCIAMACHY—scanning imaging absorption spectrometer for atmospheric cartography. *Acta Astronaut.*, 35(7):445–451.
- Butz, A., Guerlet, S., Hasekamp, O., Schepers, D., Galli, A., Aben, I., Frankenberg, C., Hartmann, J.-M., Tran, H., Kuze, A., Keppel-Aleks, G., Toon, G., Wunch, D., Wennberg, P., Deutscher, N., Griffith, D., Macatangay, R., Messerschmidt, J., Notholt, J., and Warneke, T. (2011). Toward accurate CO₂ and CH₄ observations from GOSAT. *Geophys. Res. Lett.*, 38(14).
- Bäumer, D. and Vogel, B. (2007). An unexpected pattern of distinct weekly periodicities in climatological variables in Germany. *Geophys. Res. Lett.*, 34(3).
- Calvert, J. G. (1990). Glossary of atmospheric chemistry terms. *Pure Appl. Chem.*, 62:2167–2219.
- Carlsaw, D. C. (2005). On the changing seasonal cycles and trends of ozone at Mace Head, Ireland. *Atmos. Chem. Phys.*, 5(12):3441–3450.

- Carslaw, D. C. and Beevers, S. D. (2013). Characterising and understanding emission sources using bivariate polar plots and k-means clustering. *Environ. Model. Softw.*, 40:325–329.
- Carslaw, D. C. and Ropkins, K. (2012). openair — An R package for air quality data analysis. *Environ. Model Softw.*, 27–28(0):52–61.
- Cerveny, R. S. and Balling Jr., R. C. (1998). Weekly cycles of air pollutants, precipitation and tropical cyclones in the coastal NW Atlantic region. *Nature*, 394.
- Cerveny, R. S. and Coakley, K. J. (2002). A weekly cycle in atmospheric carbon dioxide. *Geophys. Res. Lett.*, 29(2):967.
- Chambers, S. D., Williams, A. G., Conen, F., Griffiths, A. D., Reimann, S., Steinbacher, M., Krummel, P. B., Steele, L. P., van der Schoot, M. V., Galbally, I. E., Molloy, S. B., and Barnes, J. E. (2016). Towards a Universal “Baseline” Characterisation of Air Masses for High- and Low-Altitude Observing Stations Using Radon-222. *Aerosol Air. Qual. Res.*, 16(3):885–899.
- Chang, W., Cheng, J., Allaire, J. J., Xie, Y., and McPherson, J. (2019). shiny: Web Application Framework for R.
- Chen, H., Winderlich, J., Gerbig, C., Hofer, A., Rella, C. W., Crosson, E. R., Van Pelt, A. D., Steinbach, J., Kolle, O., Beck, V., Daube, B. C., Gottlieb, E. W., Chow, V. Y., Santoni, G. W., and Wofsy, S. C. (2010). High-accuracy continuous airborne measurements of greenhouse gases (CO₂ and CH₄) using the cavity ring-down spectroscopy (CRDS) technique. *Atmos. Meas. Tech.*, 3:375–386.
- Ciais, P., Sabine, C., Bala, G., Bopp, L., Brovkin, V., Canadell, J., Chhabra, A., DeFries, R., Galloway, J., Heimann, M., Jones, C., Quéré, C. L., Myneni, R., Piao, S., and Thornton, P. (2013). Carbon and Other Biogeochemical Cycles. In Stocker, T., Qin, D., Plattner, G.-K., Tignor, M., Allen, S., Boschung, J., Nauels, A., Xia, Y., Bex, V., and Midgley, P., editors, *Climate Change 2013: The Physical Science Basis. Contribution of Working Group I to the Fifth Assessment Report of the Intergovernmental Panel on Climate Change*, page 467. Cambridge University Press, Cambridge, United Kingdom and New York, NY, USA.
- Cleveland, R. B., Cleveland, W. S., McRae, J. E., and Terpenning, I. (1990). STL: a seasonal-trend decomposition procedure based on loess. *J. Off. Stat.*, 6(1):3–73.
- Cleveland, W. S. and Devlin, S. J. (1988). Locally Weighted Regression: An Approach to Regression Analysis by Local Fitting. *J. Am. Stat. Assoc.*, 83(403):596–610.
- Collaud Coen, M., Praz, C., Haeefe, A., Ruffieux, D., Kaufmann, P., and Calpini, B. (2014). Determination and climatology of the planetary boundary layer height above the Swiss plateau by in situ and remote sensing measurements as well as by the COSMO-2 model. *Atmos. Chem. Phys.*, 14(23):13205–13221.

References

- Conway, T. J., Tans, P., Waterman, L. S., Thoning, K. W., Masarie, K. A., and Gammon, R. H. (1988). Atmospheric carbon dioxide measurements in the remote global troposphere, 1981–1984. *Tellus B*, 40B(2):81–115.
- Cundari, V., Colombo, T., and Ciattaglia, L. (1995). Thirteen years of atmospheric carbon dioxide measurements at Mt. Cimone station, Italy. *Nuovo Cimento C*, 18(1):33–47.
- Curcoll, R., Camarero, L., Bacardit, M., Àgueda, A., Grossi, C., Gacia, E., Font, A., and Morgu , J.-A. (2019). Atmospheric Carbon Dioxide variability at Aig estortes, Central Pyrenees, Spain. *Reg. Environ. Change*, 19(2):313–324.
- Denning, A., Fung, I., and Randall, D. (1995). Latitudinal gradient of atmospheric CO₂ due to seasonal exchange with land biota. *Nature*, 386:240–243.
- Derwent, R. G., Ryall, D. B., Manning, A. J., Simmonds, P. G., O’Doherty, S., Biraud, S., Ciais, P., Ramonet, M., and Jennings, S. G. (2002). Continuous observations of carbon dioxide at Mace Head, Ireland from 1995 to 1999 and its net European ecosystem exchange. *Atmos. Environ.*, 36:2799–2807.
- Di moz, H., Gobbi, G. P., Magri, T., Pession, G., Pittavino, S., Tombolato, I. K. F., Campanelli, M., and Barnaba, F. (2019). Transport of Po Valley aerosol pollution to the northwestern Alps – Part 2: Long-term impact on air quality. *Atmos. Chem. Phys.*, 19(15):10129–10160.
- Dlugokencky, E. and Tans, P. (2019). NOAA/ESRL. available at www.esrl.noaa.gov/gmd/ccgg/trends/ (access date: 2019-08-29).
- Dowle, M. and Srinivasan, A. (2019). data.table: Extension of data.frame.
- El Yazidi, A., Ramonet, M., Ciais, P., Broquet, G., Pison, I., Abbaris, A., Brunner, D., Conil, S., Delmotte, M., Gheusi, F., Guerin, F., Hazan, L., Kachroudi, N., Kouvarakis, G., Mihalopoulos, N., Rivier, L., and Ser a, D. (2018). Identification of spikes associated with local sources in continuous time series of atmospheric CO, CO₂ and CH₄. *Atmos. Meas. Tech.*, 11(3):1599–1614.
- Elliott, W. P. (1989). (Ed.) The Statistical treatment of CO₂ data records, NOAA Technical Memorandum ERL ARL, 173.
- Etheridge, D., Steele, L., Langenfelds, R., Francey, R., Barnola, J., and Morgan, V. (1996). Natural and anthropogenic changes in atmospheric CO₂ over the last 1000 years from air in Antarctic ice and firn. *J. Geophys. Res. Atmos.*, 101(D2):4115–4128.
- Fang, S.-X., Luan, T., Zhang, G., Wu, Y.-L., and Yu, D.-J. (2015). The determination of regional CO₂ mole fractions at the Longfengshan WMO/GAW station: A comparison of four data filtering approaches. *Atmos. Environ.*, 116:36–43.

- Fang, S.-X., Tans, P. P., Dong, F., Zhou, H.-G., and Luan, T. (2016). Characteristics of atmospheric CO₂ and CH₄ at the Shangdianzi regional background station in China. *Atmos. Environ.*, 131:1–8.
- Forkel, M., Carvalhais, N., Rödenbeck, C., Keeling, R., Heimann, M., Thonicke, K., Zaehle, S., and Reichstein, M. (2016). Enhanced seasonal CO₂ exchange caused by amplified plant productivity in northern ecosystems. *Science*, 351(6274):696–699.
- Francey, R. J., Trudinger, C. M., Van Der Schoot, M., Krummel, P. B., Steele, L. P., and Langenfelds, R. L. (2010). Differences between trends in atmospheric CO₂ and the reported trends in anthropogenic CO₂ emissions. *Tellus B*, 62(5):316–328.
- Gantner, L., Hornsteiner, M., Egger, J., and Hartjenstein, G. (2003). The diurnal circulation of Zugspitzplatt: observations and modeling. *Meteorologische Zeitschrift*, 12(2):95–102.
- Gaudry, A., Ascencio, J. M., and Lambert, G. (1983). Preliminary study of CO₂ variations at Amsterdam Island (Territoire des Terres Australes et Antarctiques Françaises). *J. Geophys. Res.*, 88(C2):1323–1329.
- Gaudry, A., Monfray, P., Polian, G., Bonsang, G., Ardouin, B., Jegou, A., and Lambert, G. (1991). Non-seasonal variations of atmospheric CO₂ concentrations at Amsterdam Island. *Tellus B Chem. Phys. Meteorol.*, 43(2):136–143.
- Gaudry, A., Monfray, P., Polian, G., and Lambert, G. (1987). The 1982–1983 El Niño: a 6 billion ton CO₂ release. *Tellus B*, 39B(1-2):209–213.
- Ghada, W., Yuan, Y., Wastl, C., Estrella, N., and Menzel, A. (2019). Precipitation Diurnal Cycle in Germany Linked to Large-Scale Weather Circulations. *Atmosphere*, 10(9):545.
- Ghasemifard, H., Vogel, F. R., Yuan, Y., M., L., Chen, J., Ries, L., Leuchner, M., Schunk, C., Vardag, S. N., and Menzel, A. (2019a). Pollution Events at the High-Altitude Mountain Site Zugspitze-Schneefernerhaus (2670 m a.s.l.), Germany. *Atmosphere*, 10:330.
- Ghasemifard, H., Yuan, Y., M., L., Schunk, C., Chen, J., Ries, L., Leuchner, M., and Menzel, A. (2019b). Atmospheric CO₂ and $\delta^{13}\text{C}$ Measurements from 2012 to 2014 at the Environmental Research Station Schneefernerhaus, Germany: Technical Corrections, Temporal Variations and Trajectory Clustering. *Aerosol Air. Qual. Res.*, 19:657–670.
- Gilge, S., Plass-Duelmer, C., Fricke, W., Kaiser, A., Ries, L., Buchmann, B., and Steinbacher, M. (2010). Ozone, carbon monoxide and nitrogen oxides time series at four alpine GAW mountain stations in central Europe. *Atmos. Chem. Phys.*, 10(24):12295–12316.

References

- Gomez-Pelaez, A. J., Ramos, R., Cuevas, E., Gomez-Trueba, V., and Reyes, E. (2019). Atmospheric CO₂, CH₄, and CO with the CRDS technique at the Izaña Global GAW station: instrumental tests, developments, and first measurement results. *Atmos. Meas. Tech.*, 12(4):2043–2066.
- Guha, T. and Ghosh, P. (2015). Diurnal and seasonal variation of mixing ratio and $\delta^{13}\text{C}$ of air CO₂ observed at an urban station Bangalore, India. *Environ. Sci. Pollut. Res.*, 22:1877–1890.
- Hakkarainen, J., Ialongo, I., Maksyutov, S., and Crisp, D. (2019). Analysis of Four Years of Global XCO₂ Anomalies as Seen by Orbiting Carbon Observatory-2. *Remote. Sens.*, 11(7):850.
- Halter, B. and Harris, J. M. (1983). On the variability of atmospheric carbon dioxide concentration at Barrow, Alaska during winter. *J. Geophys. Res.*, 88(C11):6858–6864.
- Halter, B. C., Harris, J. M., and Conway, T. J. (1988). Component signals in the record of atmospheric carbon dioxide concentration at American Samoa. *J. Geophys. Res.*, 93(D12):15914–15918.
- Henne, S., Brunner, D., Folini, D., Solberg, S., Klausen, J., and Buchmann, B. (2010). Assessment of parameters describing representativeness of air quality in-situ measurement sites. *Atmos. Chem. Phys.*, 10(8):3561–3581.
- Hijmans, R. J. (2019). raster: Geographic Data Analysis and Modeling.
- IPCC (2014). Climate Change 2014: Synthesis Report. In Team, C. W., Pachauri, R., and Meyer, L., editors, *Contribution of Working Groups I, II and III to the Fifth Assessment Report of the Intergovernmental Panel on Climate Change*, page 44. World Meteorological Organization, Geneva, Switzerland.
- IPCC (2018). Summary for Policymakers. In Masson-Delmotte, V., Zhai, P., Pörtner, H.-O., Roberts, D., Skea, J., Shukla, P., Pirani, A., Moufouma-Okia, W., Péan, C., Pidcock, R., Connors, S., Matthews, J., Chen, Y., Zhou, X., Gomis, M., Lonnoy, E., Maycock, T., Tignor, M., and T., W., editors, *Global Warming of 1.5°C. An IPCC Special Report on the impacts of global warming of 1.5°C above pre-industrial levels and related global greenhouse gas emission pathways, in the context of strengthening the global response to the threat of climate change, sustainable development, and efforts to eradicate poverty*, page 6. World Meteorological Organization, Geneva, Switzerland.
- Joos, F. and Spahni, R. (2008). Rates of change in natural and anthropogenic radiative forcing over the past 20,000 years. *Proc. Natl. Acad. Sci. U. S. A.*, 105:1425–1430.
- Keeling, C., Piper, S., Bacastow, R., Wahlen, M., Whorf, T., Heimann, M., and Meijer, H. (2001). Exchanges of atmospheric CO₂ and ¹³CO₂ with the terrestrial biosphere and oceans from 1978 to 2000. I. Global aspects. SIO Reference Series, No. 01–06. Scripps Institution of Oceanography, San Diego, 88 pages, <http://escholarship.org/uc/item/09v319r9>.

- Keeling, C. D. (1960). The Concentration and Isotopic Abundances of Carbon Dioxide in the Atmosphere. *Tellus*, 12(2):200–203.
- Keeling, C. D., Adams, Jr., J. A., Ekdahl, Jr., C. A., and Guenther, P. R. (1976a). Atmospheric Carbon Dioxide Variations at the South Pole. *Tellus*, 28(6):552–564.
- Keeling, C. D., Bacastow, R. B., Bainbridge, A. E., Ekdahl, Jr., C. A., Guenther, P. R., Waterman, L. S., and Chin, J. F. S. (1976b). Atmospheric Carbon Dioxide Variations at Mauna Loa Observatory, Hawaii. *Tellus*, 28(6):538–551.
- Keeling, C. D., Bacastow, R. B., Carter, A. F., Piper, S. C., Whorf, T. P., Heimann, M., Mook, W. G., and Roeloffzen, H. (1989). A three-dimensional model of atmospheric CO₂ transport based on observed winds: 1. Analysis of observational data. In Peterson, D. H., editor, *Aspects of climate variability in the Pacific and the western Americas*, volume 261 of *Geophysical monograph*, pages 165–236. American Geophysical Union, Washington, DC, U.S.A.
- Kilkki, J., Hatakka, J., Portin, H., and Laurila, T. (2015). Atmospheric CO₂ observations at Finnish urban and rural sites. *Boreal Environment Research*, 20:227–242.
- Kuze, A., Suto, H., Nakajima, M., and Hamazaki, T. (2009). Thermal and near infrared sensor for carbon observation Fourier-transform spectrometer on the Greenhouse Gases Observing Satellite for greenhouse gases monitoring. *Appl. Opt.*, 48(35):6716.
- Lauvaux, T., Miles, N. L., Richardson, S. J., Deng, A., Stauffer, D. R., Davis, K. J., Jacobson, G., Rella, C., Calonder, G.-P., and DeCola, P. L. (2013). Urban Emissions of CO₂ from Davos, Switzerland: The First Real-Time Monitoring System Using an Atmospheric Inversion Technique. *J. Appl. Meteorol. Climatol.*, 52:2654–2668.
- Le Quéré, C., Andrew, R. M., Friedlingstein, P., Sitch, S., Hauck, J., Pongratz, J., Pickers, P. A., Korsbakken, J. I., Peters, G. P., Canadell, J. G., Arneeth, A., Arora, V. K., Barbero, L., Bastos, A., Bopp, L., Chevallier, F., Chini, L. P., Ciais, P., Doney, S. C., Gkritzalis, T., Goll, D. S., Harris, I., Haverd, V., Hoffman, F. M., Hoppema, M., Houghton, R. A., Hurtt, G., Ilyina, T., Jain, A. K., Johannessen, T., Jones, C. D., Kato, E., Keeling, R. F., Goldewijk, K. K., Landschützer, P., Lefèvre, N., Lienert, S., Liu, Z., Lombardozzi, D., Metzl, N., Munro, D. R., Nabel, J. E. M. S., Nakaoka, S., Neill, C., Olsen, A., Ono, T., Patra, P., Peregón, A., Peters, W., Peylin, P., Pfeil, B., Pierrot, D., Poulter, B., Rehder, G., Resplandy, L., Robertson, E., Rocher, M., Rödenbeck, C., Schuster, U., Schwinger, J., Séférian, R., Skjelvan, I., Steinhoff, T., Sutton, A., Tans, P. P., Tian, H., Tilbrook, B., Tubiello, F. N., van der Laan-Luijkx, I. T., van der Werf, G. R., Viovy, N., Walker, A. P. and Wiltshire, A. J., Wright, R., Zaehle, S., and Zheng, B. (2018). Global Carbon Budget 2018. *Earth Syst. Sci. Data*, 10(4):2141–2194.
- Levin, I. and Kromer, B. (1997). Twenty Years of Atmospheric ¹⁴CO₂ Observations At Schauinsland Station, Germany. *Radiocarbon*, 39(2):205–218.

References

- Levin, I., Kromer, B., and Hammer, S. (2013). Atmospheric delta $^{14}\text{CO}_2$ trend in Western European background air from 2000 to 2012. *Tellus B Chem. Phys. Meteorol.*, 65(1):20092.
- Liang, A., Gong, W., Han, G., and Xiang, C. (2017). Comparison of Satellite-Observed XCO₂ from GOSAT, OCO-2, and Ground-Based TCCON. *Remote Sens.*, 9(10):1033.
- Lindauer, M., Schumacher, M., and Koch, T. (2015). Network of ICOS stations for measuring climate-relevant trace gases in Germany. GAW Letter of DWD No 66.
- Lindqvist, H., O'Dell, C. W., Basu, S., Boesch, H., Chevallier, F., Deutscher, N., Feng, L., Fisher, B., Hase, F., Inoue, M., Kivi, R., Morino, I., Palmer, P. I., Parker, R., Schneider, M., Sussmann, R., and Yoshida, Y. (2015). Does GOSAT capture the true seasonal cycle of carbon dioxide? *Atmos. Chem. Phys.*, 15(22):13023–13040.
- Lopez, M., Schmidt, M., Ramonet, M., Bonne, J.-L., Colomb, A., Kazan, V., Laj, P., and Pichon, J.-M. (2015). Three years of semicontinuous greenhouse gas measurements at the Puy de Dôme station (central France). *Atmos. Meas. Tech.*, 8(9):3941–3958.
- Lüthi, D., Floch, M., Bereiter, B., Blunier, T., Barnola, J.-M., Siegenthaler, U., Raynaud, D., Jouzel, J., Fischer, H., Kawamura, K., and Stocker, T. (2008). High-resolution carbon dioxide concentration record 650,000–800,000 years before present. *Nature*, 453:379–382.
- Ma, N. and Birmili, W. (2015). Estimating the contribution of photochemical particle formation to ultrafine particle number averages in an urban atmosphere. *Sci. Total Environ.*, 512–513:154–166.
- Masarie, K. A. and Tans, P. P. (1995). Extension and integration of atmospheric carbon dioxide data into a globally consistent measurement record. *J. Geophys. Res.*, 100(D6):11593–11610.
- Massen, F. and Beck, E.-G. (2011). Accurate estimation of CO₂ background level from near ground measurements at non-mixed environments. In Filho, W. L., editor, *The Economic, Social and Political Elements of Climate Change*. Springer.
- Miao, R., Lu, N., Yao, L., Zhu, Y., Wang, J., and Sun, J. (2013). Multi-Year Comparison of Carbon Dioxide from Satellite Data with Ground-Based FTS Measurements (2003–2011). *Remote. Sens.*, 5(7):3431–3456.
- Morino, I., Uchino, O., Inoue, M., Yoshida, Y., Yokota, T., Wennberg, P. O., Toon, G. C., Wunch, D., Roehl, C. M., Notholt, J., Warneke, T., Messerschmidt, J., Griffith, D. W. T., Deutscher, N. M., Sherlock, V., Connor, B., Robinson, J., Sussmann, R., and Rettinger, M. (2011). Preliminary validation of column-averaged volume mixing ratios of carbon dioxide and methane retrieved from GOSAT short-wavelength infrared spectra. *Atmos. Meas. Tech.*, 4(6):1061–1076.

- Myhre, G., Shindell, D., Bréon, F.-M., Collins, W., Fuglestedt, J., Huang, J., Koch, D., Lamarque, J.-F., Lee, D., Mendoza, B., Nakajima, T., Robock, A., Stephens, G., T., T., and H., Z. (2013). Anthropogenic and Natural Radiative Forcing. In Stocker, T., Qin, D., Plattner, G.-K., Tignor, M., Allen, S., Boschung, J., Nauels, A., Xia, Y., V., B., and P.M., M., editors, *Climate Change 2013: The Physical Science Basis. Contribution of Working Group I to the Fifth Assessment Report of the Intergovernmental Panel on Climate Change*, page 661. Cambridge University Press, Cambridge, United Kingdom and New York, NY, USA.
- Nakazawa, T., Aoki, S., Murayama, S., Fukabori, M., Yamanouchi, T., Murayama, H., Shiobara, M., Hashida, G., Kawaguchi, S., and Tanaka, M. (1991). The concentration of atmospheric carbon dioxide at the Japanese Antarctic Station, Syowa. *Tellus*, 43B:126–135.
- Navascués, B. and Rus, C. (1991). Carbon dioxide observations at Izaña baseline station, Tenerife (Canary Islands): 1984–1988. *Tellus B*, 43(2):118–125.
- Pal, S., Lopez, M., Schmidt, M., Ramonet, M., Gibert, F., Xueref-Remy, I., and Ciais, P. (2015). Investigation of the atmospheric boundary layer depth variability and its impact on the ^{222}Rn concentration at a rural site in France. *J. Geophys. Res. Atmos.*, 120(2):623–643.
- Peters, W., Jacobson, A. R., Sweeney, C., Andrews, A. E., Conway, T. J., Masarie, K., Miller, J. B., Bruhwiler, L. M. P., Pétron, G., Hirsch, A. I., Worthy, D. E. J., van der Werf, G. R., Randerson, J. T., Wennberg, P. O., Krol, M. C., and Tans, P. P. (2007). An atmospheric perspective on North American carbon dioxide exchange: CarbonTracker. *Proc. Natl. Acad. Sci. U. S. A.*, 104(48):18925–18930.
- Peterson, J. T., Komhyr, W. D., Waterman, L. S., Gammon, R. H., Thoning, K. W., and Conway, T. J. (1986). Atmospheric CO_2 variations at Barrow, Alaska, 1973–1982. *J. Atmos. Chem.*, 4(4):491–510.
- Pickers, P. A. and Manning, A. C. (2015). Investigating bias in the application of curve fitting programs to atmospheric time series. *Atmos. Meas. Tech.*, 8(3):1469–1489.
- Press, W., Teukolsky, S., Vetterling, W., and Flannery, B. (1988). *Numerical Recipes in C: The Art of Scientific Computing (1st ed.)*. Cambridge University Press, New York.
- Pu, J.-J., Xu, H.-H., He, J., Fang, S.-X., and Zhou, L.-X. (2014). Estimation of regional background concentration of CO_2 at Lin’an Station in Yangtze River Delta, China. *Atmos. Environ.*, 94:402–408.
- R Core Team (2019). R: A language and environment for statistical computing.
- Raymond, P. A. and Cole, J. J. (2003). Increase in the export of alkalinity from North America’s largest river. *Science*, 301:88–91.

References

- Ries, L. (2013). Dafit - a new workflow oriented approach for time efficient data preparation, validation and flagging of time series data from environmental monitoring. In *Proceedings of the 27th conference on Environmental informatics – Informatics for Environmental Protection, Sustainable Development and Risk Management, Part II*, pages 651–656. Shaker Verlag.
- Ries, L., Graul, R., and Gilge, S. (2003). CO₂ Measurements at the Zugspitze and Schauinsland GAW Stations. GAW Letter of DWD No. 19.
- Risius, S., Xu, H., Di Lorenzo, F., Xi, H., Siebert, H., Shaw, R. A., and Bodenschatz, E. (2015). Schneefernerhaus as a mountain research station for clouds and turbulence. *Atmos. Meas. Tech.*, 8(8):3209–3218.
- Ruckstuhl, A. F., Henne, S., Reimann, S., Steinbacher, M., Vollmer, M. K., O’Doherty, S., Buchmann, B., and Hueglin, C. (2012). Robust extraction of baseline signal of atmospheric trace species using local regression. *Atmos. Meas. Tech.*, 5(11):2613–2624.
- Satar, E., Berhanu, T. A., Brunner, D., Henne, S., and Leuenberger, M. (2016). Continuous CO₂/CH₄/CO measurements (2012–2014) at Beromünster tall tower station in Switzerland. *Biogeosciences*, 13:2623–2635.
- Schibig, M. F., Mahieu, E., Henne, S., Lejeune, B., and Leuenberger, M. C. (2016). Inter-comparison of in situ NDIR and column FTIR measurements of CO₂ at Jungfraujoch. *Atmos. Chem. Phys.*, 16:9935–9949.
- Schibig, M. F., Steinbacher, M., Buchmann, B., van der Laan-Luijkx, I. T., van der Laan, S., Ranjan, S., and Leuenberger, M. C. (2015). Comparison of continuous in situ CO₂ observations at Jungfraujoch using two different measurement techniques. *Atmos. Meas. Tech.*, 8(1):57–68.
- Schmidt, M. (2003). The Schauinsland CO₂ record: 30 years of continental observations and their implications for the variability of the European CO₂ budget. *J. Geophys. Res.*, 108(D19):535.
- Schnaiter, M., Linke, C., Ibrahim, I., Kiselev, A., Waitz, F., Leisner, T., Norra, S., and Rehm, T. (2019). Specifying the light-absorbing properties of aerosol particles in fresh snow samples, collected at the Environmental Research Station Schneefernerhaus (UFS), Zugspitze. *Atmos. Chem. Phys.*, 19(16):10829–10844.
- Sigmund, A., Freier, K., Rehm, T., Ries, L., Schunk, C., Menzel, A., and Thomas, C. K. (2019). Multivariate statistical air mass classification for the high-alpine observatory at the Zugspitze Mountain, Germany. *Atmos. Chem. Phys.*, 19:12477–12494.
- Sirignano, C., Neubert, R. E. M., Rödenbeck, C., and Meijer, H. A. J. (2010). Atmospheric oxygen and carbon dioxide observations from two European coastal stations 2000–2005: continental influence, trend changes and APO climatology. *Atmos. Chem. Phys.*, 10(4):1599–1615.

- Stavert, A. R., Law, R. M., van der Schoot, M., Langenfelds, R. L., Spencer, D. A., Krummel, P. B., Chambers, S. D., Williams, A. G., Werczynski, S., Francey, R. J., and Howden, R. T. (2019). The Macquarie Island (LoFlo2G) high-precision continuous atmospheric carbon dioxide record. *Atmos. Meas. Tech.*, 12(2):1103–1121.
- Stephens, B. B., Brailsford, G. W., Gomez, A. J., Riedel, K., Mikaloff Fletcher, S. E., Nichol, S., and Manning, M. (2013). Analysis of a 39-year continuous atmospheric CO₂ record from Baring Head, New Zealand. *Biogeosciences*, 10(4):2683–2697.
- Sun, Y., Bian, L., Tang, J., Gao, Z., Lu, C., and Schnell, R. (2014). CO₂ Monitoring and Background Mole Fraction at Zhongshan Station, Antarctica. *Atmosphere*, 5(3):686–698.
- Sundquist, E. T. (1986). Geologic analogs: Their value and limitations in carbon dioxide research. In Trabalka, J. R. and Reichle, D. E., editors, *The Changing Carbon Cycle*, pages 371–402. Springer-Verlag, New York.
- Sussmann, R. and Rettinger, M. (2018a). TCCON data from Garmisch (DE), Release GGG2014.R2 [Data set].
- Sussmann, R. and Rettinger, M. (2018b). TCCON data from Zugspitze (DE), Release GGG2014.R1 [Data set].
- Thoning, K. W., Tans, P. P., and Komhyr, W. D. (1989). Atmospheric carbon dioxide at Mauna Loa Observatory: 2. Analysis of the NOAA GMCC data, 1974–1985. *J. Geophys. Res.*, 94(D6):8549–8565.
- Tsutsumi, Y., Mori, K., Hirahara, T., Ikegami, M., and Conway, T. J. (2009). Technical Report of Global Analysis Method for Major Greenhouse Gases by the World Data Center for Greenhouse Gases. GAW Report No.184.
- Tsutsumi, Y., Mori, K., Ikegami, M., Tashiro, T., and Tsuboi, K. (2006). Long-term trends of greenhouse gases in regional and background events observed during 1998–2004 at Yonagunijima located to the east of the Asian continent. *Atmos. Environ.*, 40(30):5868–5879.
- Uglietti, C., Leuenberger, M., and Brunner, D. (2011). European source and sink areas of CO₂ retrieved from Lagrangian transport model interpretation of combined O₂ and CO₂ measurements at the high alpine research station Jungfraujoch. *Atmos. Chem. Phys.*, 11(15):8017–8036.
- van der Laan, S., Neubert, R. E. M., and Meijer, H. A. J. (2009). A single gas chromatograph for accurate atmospheric mixing ratio measurements of CO₂, CH₄, N₂O, SF₆ and CO. *Atmos. Meas. Tech.*, 2:549–559.
- Watanabe, F., Uchino, O., Joo, Y., Aono, M., Higashijima, K., Hirano, Y., Tsuboi, K., and Suda, K. (2000). Interannual Variation of Growth Rate of Atmospheric Carbon Dioxide Concentration Observed at the JMA’s Three Monitoring Stations. *Journal of the Meteorological Society of Japan. Ser. II*, 78(5):673–682.

References

- Waterman, L. S., Nelson, D. W., Komhyr, W. D., Harris, T. B., Thoning, K. W., and Tans, P. P. (1989). Atmospheric carbon dioxide measurements at Cape Matatula, American Samoa, 1976–1987. *J. Geophys. Res.*, 94(D12):14817–14829.
- Wickham, H. (2007). Reshaping Data with the reshape Package. *J. Stat. Softw.*, 21(12):1–20.
- Wickham, H. (2011). The Split-Apply-Combine Strategy for Data Analysis. *J. Stat. Softw.*, 40(1):1–29.
- Wickham, H. (2016). *ggplot2: Elegant Graphics for Data Analysis*. Springer-Verlag New York.
- WMO (2016). Expert group recommendations, 18th WMO/IAEA Meeting on Carbon Dioxide, Other Greenhouse Gases and Related Tracers Measurement Techniques (GGMT-2015), La Jolla, CA, USA, 13–17 September 2015. GAW Report No. 229.
- WMO (2018). Greenhouse Gas Bulletin: The State of Greenhouse Gases in the Atmosphere Based on Global Observations through 2017. No. 14.
- Wong, C. S., Chan, Y.-H., Page, J. S., Bellagay, R. D., and Pettit, K. G. (1984). Trends of Atmospheric CO₂ Over Canadian WMO Background Stations at Ocean Weather Station P, Sable Island, and Alert. *J. Geophys. Res.*, 89(D6):9527–9539.
- Wunch, D., Toon, G. C., Blavier, J.-F. L., Washenfelder, R. A., Notholt, J., Connor, B. J., Griffith, D. W. T., Sherlock, V., and Wennberg, P. O. (2011). The total carbon column observing network. *Philos. Trans. A Math. Phys. Eng. Sci.*, 369(1943):2087–2112.
- Yoshida, Y., Ota, Y., Eguchi, N., Kikuchi, N., Nobuta, K., Tran, H., Morino, I., and Yokota, T. (2011). Retrieval algorithm for CO₂ and CH₄ column abundances from short-wavelength infrared spectral observations by the Greenhouse gases observing satellite. *Atmos. Meas. Tech.*, 4(4):717–734.
- Yuan, Y., Ries, L., Petermeier, H., Steinbacher, M., Gómez-Peláez, A. J., Leuenberger, M. C., Schumacher, M., Trickl, T., Couret, C., Meinhardt, F., and Menzel, A. (2018). Adaptive selection of diurnal minimum variation: a statistical strategy to obtain representative atmospheric CO₂ data and its application to European elevated mountain stations. *Atmos. Meas. Tech.*, 11(3):1501–1514.
- Yuan, Y., Ries, L., Petermeier, H., Trickl, T., Leuchner, M., Couret, C., Sohmer, R., Meinhardt, F., and Menzel, A. (2019). On the diurnal, weekly, and seasonal cycles and annual trends in atmospheric CO₂ at Mount Zugspitze, Germany, during 1981–2016. *Atmos. Chem. Phys.*, 19(2):999–1012.
- Zeileis, A. and Grothendieck, G. (2005). zoo: S3 Infrastructure for Regular and Irregular Time Series. *J. Stat. Softw.*, 14(6):1–27.

- Zellweger, C., Emmenegger, L., Firdaus, M., Hatakka, J., Heimann, M., Kozlova, E., Spain, T. G., Steinbacher, M., van der Schoot, M. V., and Buchmann, B. (2016). Assessment of recent advances in measurement techniques for atmospheric carbon dioxide and methane observations. *Atmos. Meas. Tech.*, 9(9):4737–4757.
- Zellweger, C., Forrer, J., Hofer, P., Nyeki, S., Schwarzenbach, B., Weingartner, E., Ammann, M., and Baltensperger, U. (2003). Partitioning of reactive nitrogen (NO_y) and dependence on meteorological conditions in the lower free troposphere. *Atmos. Chem. Phys.*, 3(3):779–796.
- Zhang, F., Fukuyama, Y., Wang, Y., Fang, S., Li, P., Fan, T., Zhou, L., Liu, X., Meinhardt, F., and Emiliani, P. (2015). Detection and attribution of regional CO_2 concentration anomalies using surface observations. *Atmos. Environ.*, 123:88–101.
- Zhou, L., Conway, T. J., White, J. W. C., Mukai, H., Zhang, X., Wen, Y., Li, J., and MacClune, K. (2005). Long-term record of atmospheric CO_2 and stable isotopic ratios at Waliguan Observatory: Background features and possible drivers, 1991–2002. *Global Biogeochem. Cycles*, 19(3).
- Zhou, L., Tang, J., Wen, Y., Li, J., Yan, P., and Zhang, X. (2003). The impact of local winds and long-range transport on the continuous carbon dioxide record at Mount Waliguan, China. *Tellus*, 55B:145–158.
- Zhu, C.-M. and Yoshikawa-Inoue, H. (2015). Seven years of observational atmospheric CO_2 at a maritime site in northernmost Japan and its implications. *Sci. Total Environ.*, 524–525:331–337.

Acknowledgment

Life is full of surprises. Back to 1998, when a teacher asked the most boring and out-of-date question in the class about “what do you want to be in the future?”, the teenager answering “a scientist!” never thought this would actually become true. But here he is, at the age of 30 (*almost*), trying to finish his doctorate study as a summary for the past few years (*4.27 years to be specific*).

Life is about experiencing, and so does pursuing a Ph.D. Throughout the adventure, it will not be as much striking and memorable as it is without knowing all of you and enjoying life with you. Thank you (*names listed alphabetically*): Brigitte, for being the one and only everyone needs regarding administrative affairs; Christian, for being the omnipotent person that I can look up to; Eli, for your optimistic and warm spirit; Gourav, for being very humorous at heart for me; Hannes, for really showing me the extent of working; Homa, for sharing the most similar topics in the chair and being always nice for discussion; Marvin, for being so efficient and practical at all time; Michael, for triggering my interests in statistics and programming; Nicole, for providing me with knowledge of phenology and meteorology; Nik, for being well-prepared for any kinds of computer emergencies; Stephan, for having the most time spent in the study (MICMoR or not) and growing up as the PhD candidate since the very beginning; Upsee, for always lighting up the office with your smile; Wael, for being the ruthless research machine of publications and attending courses that can always astonish me; and many more. Also, the earnest greetings to my friends Hongchang, Sam, and Haowen for being there for me no matter what happens.

This doctorate study would not be possible without the guidance of my mentors. First of all, thank you Annette Menzel, for providing this opportunity to me; leading me into phenology; supervising me with valuable characteristics in science; always encouraging me and pushing me to a better researcher. The most heartfelt thanks to you, Ludwig Ries, who not only acted as my supervisor in the field of atmospheric measurements, but also as my mentor of life. Your dedication for work, passion for life, and care for people will always motivate me. Also, special thanks to Michael Leuchner for being my examiner, and Hannes Petermeier for fruitful discussion about statistics. This is for all of you:

志于道，据于德，依于仁，游于艺。

Let the will be set on the path of duty;

Let every attainment in what is good be firmly grasped;

Let perfect virtue be accorded with;

Let relaxation and enjoyment be found in the arts.

孔子 *Analects of Confucius*

Acknowledgment

I would also like to thank the funding from China Scholarship Council (CSC) for covering the study period, and supports from Mechanisms and Interactions of Climate Change in Mountain Regions (MICMoR) fellowship for attending conferences and activities. In the meantime, I would like to express my great respect to the colleagues (Cedric, Ralf, and more) at Zugspitze-Schneefernerhaus for making the measurements running continuously, providing convincing data, and helping me with everything during the visits.

At the end, my sincere thanks go to my parents, who allow me to do whatever I want and support me in all directions; my wife, for what a journey it has been with you and will be in the future; and my son, Caleb, for being the cutest little one ever and bringing full of joy and vitality to the family.

A Publication reprints

The next pages show the publication reprints in the doctorate study (see Chapter 4), which can be found at pages:

I 64–77

II 78–91

III 92–107

No restrictions to reprint apply to I, II, and III since they are open access, using the Creative Commons Attribution (CC-BY) License.

Atmos. Meas. Tech., 11, 1501–1514, 2018
https://doi.org/10.5194/amt-11-1501-2018
© Author(s) 2018. This work is distributed under
the Creative Commons Attribution 4.0 License.



Atmospheric
Measurement
Techniques
Open Access
EGU

Adaptive selection of diurnal minimum variation: a statistical strategy to obtain representative atmospheric CO₂ data and its application to European elevated mountain stations

Ye Yuan¹, Ludwig Ries², Hannes Petermeier³, Martin Steinbacher⁴, Angel J. Gómez-Peláez^{5,a},
Markus C. Leuenberger⁶, Marcus Schumacher⁷, Thomas Trickl⁸, Cedric Couret², Frank Meinhardt⁹, and
Annette Menzel^{1,10}

¹Department of Ecology and Ecosystem Management, Technical University of Munich (TUM), Freising, Germany

²German Environment Agency (UBA), Zugspitze, Germany

³Department of Mathematics, Technical University of Munich (TUM), Freising, Germany

⁴Empa, Laboratory for Air Pollution/Environmental Technology, Dübendorf, Switzerland

⁵Izaña Atmospheric Research Center, Meteorological State Agency of Spain (AEMET), Santa Cruz de Tenerife, Spain

⁶Climate and Environmental Physics Division, Physics Institute and Oeschger Centre for Climate Change Research, University of Bern, Bern, Switzerland

⁷Meteorological Observatory Hohenpeissenberg, Deutscher Wetterdienst (DWD), Hohenpeissenberg, Germany

⁸Institute of Meteorology and Climate Research, Atmospheric Environmental Research (IMK-IFU),

Karlsruhe Institute of Technology, Garmisch-Partenkirchen, Germany

⁹German Environment Agency (UBA), Schauinsland, Germany

¹⁰Institute for Advanced Study, Technical University of Munich (TUM), Garching, Germany

^anow at: Meteorological State Agency of Spain (AEMET), Delegation in Asturias, Oviedo, Spain

Correspondence: Ye Yuan (yuan@wzw.tum.de)

Received: 29 August 2017 – Discussion started: 12 September 2017

Revised: 1 February 2018 – Accepted: 11 February 2018 – Published: 15 March 2018

Abstract. Critical data selection is essential for determining representative baseline levels of atmospheric trace gases even at remote measurement sites. Different data selection techniques have been used around the world, which could potentially lead to reduced compatibility when comparing data from different stations. This paper presents a novel statistical data selection method named adaptive diurnal minimum variation selection (ADVS) based on CO₂ diurnal patterns typically occurring at elevated mountain stations. Its capability and applicability were studied on records of atmospheric CO₂ observations at six Global Atmosphere Watch stations in Europe, namely, Zugspitze-Schneefernerhaus (Germany), Sonnblick (Austria), Jungfrauoch (Switzerland), Izaña (Spain), Schauinsland (Germany), and Hohenpeissenberg (Germany). Three other frequently applied statistical data selection methods were included for comparison. Among the studied methods, our ADVS method resulted in a lower fraction of data selected as a baseline with lower max-

ima during winter and higher minima during summer in the selected data. The measured time series were analyzed for long-term trends and seasonality by a seasonal-trend decomposition technique. In contrast to unselected data, mean annual growth rates of all selected datasets were not significantly different among the sites, except for the data recorded at Schauinsland. However, clear differences were found in the annual amplitudes as well as the seasonal time structure. Based on a pairwise analysis of correlations between stations on the seasonal-trend decomposed components by statistical data selection, we conclude that the baseline identified by the ADVS method is a better representation of lower free tropospheric (LFT) conditions than baselines identified by the other methods.

Published by Copernicus Publications on behalf of the European Geosciences Union.

1 Introduction

Continuous in situ measurements of greenhouse gases (GHGs) at remote locations have been established since 1958 (Keeling, 1960). Knowledge of background atmospheric GHG concentrations is key to understanding the global carbon cycle and its effect on climate, as well as the GHG responses to a changing climate. A critical issue when using data from remote stations remains the identification of time periods that are representative of larger spatial areas and their differentiation from periods influenced by local and regional pollution. If these two regimes are well disaggregated, the available datasets can represent more reliable information about long-term changes of undisturbed atmospheric GHG levels or be used to investigate local and regional GHG sources and sinks when specifically analyzing deviations from baseline conditions. In this study, the baseline conditions refer to a selected subset of data from the validated dataset, representing well-mixed air masses with minimized short-term external influences (Elliott, 1989; Calvert, 1990; Balzani Lööv et al., 2008; Chambers et al., 2016).

Measurement results depend on sampling methods, analytical instrumentation, and data processing. Validated data (labeled as VAL in this study to differentiate from the selected data) are usually obtained after signal correction, for example due to interferences from other GHGs such as water vapor, calibration accounting for sensitivity changes of the analyzer, and validation based on plausibility checks. Baseline data selection starts with validated data and identifies in subsequent steps a final subset of the validated dataset based on predefined criteria for specific qualities such as representativeness. These data will be referred to as “selected baseline data” or simply as “selected data” in the following.

Data selection methods can be categorized into meteorological, tracer, and statistical selection methods (Ruckstuhl et al., 2012; Fang et al., 2015). Meteorological data selection makes use of the meteorological information at the measurement sites, which provides valuable information about the surrounding environment as well as air mass transport (Carnuth and Trickl, 2000; Carnuth et al., 2002). Forrer et al. (2000), Zellweger et al. (2003), and Kaiser et al. (2007) intensively studied the relationship between measured trace gases (such as O₃, CO, and NO_x) and meteorological processes at Zugspitze, Jungfraujoch, Sonnblick, and Hohenpeissenberg. For CO₂, the most common parameters applied in the literature are wind speed and wind direction. They can provide information on critical variations at stations with sources and sinks in their vicinity, while these parameters are less suited at stations in largely pristine environments. For example, Lowe et al. (1979) performed a pre-selection on the CO₂ record at Baring Head (New Zealand) using periods with southerly winds only (clean marine air). Massen and Beck (2011) found that the CO₂ versus wind speed plot can be valuable for baseline CO₂ estimation without a local influence of continental measurements. Another widely used

data filtering method is fixed time window selection, by selecting data in a certain time interval of the day based on local and mesoscale mechanisms of air mass transport. For selecting well-mixed air at elevated mountain sites, nighttime is usually chosen with a special focus on the exclusion of afternoon periods due to the influence of convective upward transport (Bacastow et al., 1985). Brooks et al. (2012), for example, limited their mountaintop CO₂ results in the Rocky Mountains (USA) by “time-of-day” from 0 a.m. till 4 a.m. local time (LT) to increase the likelihood of sampling the free tropospheric environment at the station. Apart from this, modeling techniques such as backward trajectories are very helpful for analyzing the origins and transport processes of air masses arriving at the station in detail (Cui et al., 2011). Uglietti et al. (2011) focused on the origins of atmospheric CO₂ at Jungfraujoch (Switzerland) by the FLEXible PARTicle dispersion model. Using tracers, data selection can be performed by investigating the correlations between the air components of interest. Many tracers have been tested and compared with CO₂. Threshold limits of 300 ppb for CO and 2000 ppb for CH₄ were defined by Sirignano et al. (2010) to perform a regional analysis of CO₂ data at Lutjewad (the Netherlands) and Mace Head (Ireland). Similar approaches with black carbon and CH₄ were performed by Fang et al. (2015) at Lin’an (China). Moreover, Chambers et al. (2016) applied a data selection technique to identify baseline air masses using atmospheric radon measurements at the stations Cape Grim (Australia), Mauna Loa (Hawaii, USA), and Jungfraujoch (Switzerland).

Unlike most of the methods mentioned above, which require additional data or advanced transport modeling, statistical data selection only relies on the time series of interest and typically investigates the variability of signal. It is usually assumed that the most representative CO₂ data are found during well-mixed conditions revealing small variations in time (Peterson et al., 1982) and in space (Sepúlveda et al., 2014). For continuous measurements, it is possible to investigate within-hour and hour-to-hour variability in the datasets. The within-hour variability is often expressed as the standard deviation of the measured data within 1 h. The hour-to-hour variability compares the differences between hourly averaged concentrations either during a certain time period, or from one hour to the next. Pales and Keeling (1965) marked ambient data as “variable” when the within-hour variability for the air sample was significantly larger than the within-hour variability for the reference gas. Consequently, they only considered CO₂ data to belong to background conditions when the concentrations were in “steady” conditions for 6 h or more. Similarly, Peterson et al. (1982) rejected sampled CO₂ data values for adjacent hours when the hour-to-hour variability exceeded 0.25 ppm. Thoning et al. (1989) combined these two strategies using an iterative approach by selecting data according to deviations of daily averages from a spline curve fit. Ruckstuhl et al. (2012) developed a method based on robust local regression, called “Robust Extraction

of Baseline Signal”, to estimate the baseline curves generalized for atmospheric compounds, which is available in the R package IDPmisc (Locher and Ruckstuhl, 2012).

The present study focuses on the comparison of results from previous statistical data selection methods with the new adaptive diurnal minimum variation selection (ADVS) method proposed in this study. The ADVS is seen as a possible alternative to already known data selection methods as discussed above. The results obtained with ADVS for the atmospheric CO₂ records from six European mountain stations are compared with those derived from three other statistical data selection methods. To investigate the potential influences of trend and seasonality, further analyses focus on the decomposition of validated and selected datasets into trend and seasonal components. Finally, differences between ADVS and other data selection methods are assessed by correlation analysis.

2 Methods

2.1 CO₂ measurements at elevated European sites

CO₂ measurements from six European mountain stations (see Fig. 1) within the Global Atmosphere Watch (GAW) network were used. The data were taken from mountain stations due to their remote locations, being subjected to limited anthropogenic influence and this provided increased representativeness. Three high alpine measurement sites were included: Zugspitze-Schneefernerhaus (ZSF, DE, 47°25′ N, 10°59′ E, 2670 m a.s.l.), Jungfraujoch (JFJ, CH, 46°33′ N, 7°59′ E, 3580 m a.s.l.), and Sonnblick (SNB, AT, 47°03′ N, 12°57′ E, 3106 m a.s.l.). They are often above the planetary boundary layer (PBL) and thus exposed to free and presumably clean lower tropospheric air masses, but periodically influenced by regional emissions from lower altitudes. Additionally, to test data selection for a less remote environment, CO₂ measurements were investigated from Schauinsland (SSL, DE, 47°55′ N, 7°55′ E, 1205 m a.s.l.) at a much lower elevation, in the mid-range Black Forest. Data selection was also applied to three recently started CO₂ time series from different sampling heights above ground on a tall tower at the Hohenpeissenberg observatory (HPB, DE, 47°63′ N, 11°01′ E, 934 m a.s.l.), located in the northern foothills of the Alps. Henne et al. (2010) presented a method of categorizing site representativeness based on the influence and variability of population and deposition by the surface fluxes. JFJ and SNB were classified as “mostly remote,” while ZSF was considered as “weakly influenced, constant deposition,” and SSL and HPB were considered as “rural” (Henne et al., 2010). Finally, the station Izaña on Tenerife Island (IZO, ES, 28°19′ N, 16°30′ W, 2373 m a.s.l.) in the North Atlantic was chosen as a reference due to its location above the subtropical temperature inversion layer, which means that the station

is rarely affected by any local or regional CO₂ sources and sinks (Gomez-Pelaez et al., 2013).

For this study, unless otherwise indicated, hourly data were used consistently for the purpose of evaluating the data selection method since the method should be easily applicable to data obtained from standard data centers such as the World Data Centre for Greenhouse Gases (WDCGG) where data are commonly stored with hourly resolution. The validated CO₂ hourly averages from all stations were downloaded from WDCGG (<http://ds.data.jma.go.jp/gmd/wdcgg/>). Data with higher time resolution required for some sensitivity analysis in this study were provided directly by the station investigators. All time stamps refer to the beginning of the averaging interval. Descriptions of the sampling elevation and time period of available data are given in Table 1. Further information on each station can be found in Schmidt et al. (2003) for SSL, Gilge et al. (2010) for HPB and SNB, Gomez-Pelaez et al. (2010) for IZO, Risius et al. (2015) for ZSF, and Schibig et al. (2015) for JFJ. Practical data selections and analyses in this study were performed using the R Statistical Environment (R Core Team, 2017).

2.2 ADVS

ADVS is a tool for automated and systematic analysis of diurnal CO₂ cycles at elevated mountain stations in order to select consecutive time sequences with minimum variation, which can be regarded as representing well-mixed air conditions. Even though such measurement sites are remotely located, the CO₂ levels are still influenced by local sources and sinks. For example, at ZSF, these can be characterized by episodic CO₂ enhancements due to anthropogenic emissions, detectable especially in winter during the day, whereas in summer the convective upwind transport results in episodes with depleted CO₂ concentrations due to photosynthetic uptake of CO₂ at lower altitudes. Although high altitude mountain stations do not have vegetation in their surroundings, mountain stations at lower altitudes that are still in the vegetation zone may be influenced by plant respiration, especially at night. As these effects of upward transport photosynthesis and respiration all vary diurnally, the basic strategy that we follow in this study is to identify the most stable time periods of the day, i.e., periods with minimum variation, which in turn can be used for selecting representative data. However, the duration of this time window during the day varies with the season and from day to day because of variations in the dynamics of transport to the site (e.g., Birmili et al., 2009; Herrmann et al., 2015). In summer, larger variabilities in the CO₂ signal are observed due to more prevalent convective boundary-layer air-mass injections influencing the diurnal pattern, resulting in shorter periods of stable conditions, whereas in winter, significantly longer stable periods occur. No upwind air masses with depleted CO₂ levels due to photosynthesis by vegetation are recorded in winter. To preserve as much representative data as possible, it is desirable to se-

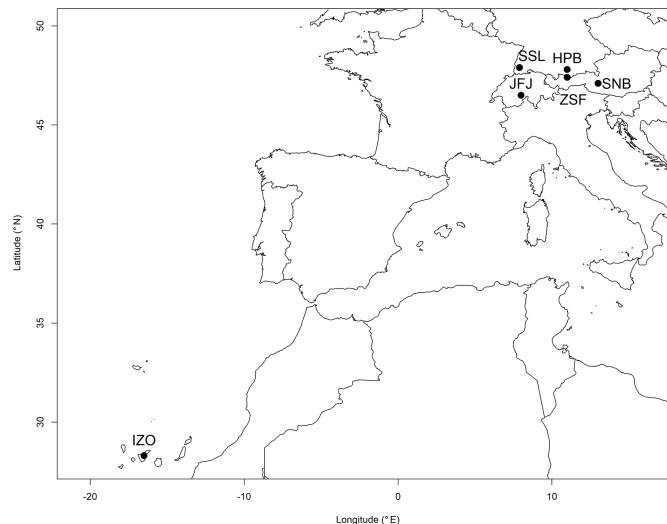


Figure 1. Locations of six European elevated mountain stations. Symbols from left to right stand for: IZO – Izaña, Spain; SSL – Schauinsland, Germany; JFJ – Jungfrauoch, Switzerland; HPB – Hohenpeissenberg, Germany; ZSF – Schneefernerhaus-Zugspitze, Germany; SNB – Sonnblick, Austria.

Table 1. Information of measured CO₂ datasets at six GAW mountain stations.

Station (GAW ID)	Sampling elevation (a.s.l.)	Time period (yyyy.mm)	Data provider
Hohenpeissenberg (HPB)	984/1027/1065 m	2015.09–2016.06	DWD
Schauinsland (SSL)	1210 m	2010.01–2015.12	UBA-De
Izaña (IZO)	2403 m	2010.01–2015.12	AEMET
Zugspitze-Schneefernerhaus (ZSF)	2670 m	2010.01–2015.12	UBA-De
Sonnblick (SNB)	3111 m	2010.01–2015.12	UBA-At
Jungfrauoch (JFJ)	3580 m	2010.01–2015.12	Empa

lect the time window dynamically. ADVS is constructed to select a subset from the measured data, being best representative for baseline conditions with an adaptive selection time window specific for every day.

The algorithm is based on two basic assumptions. First, air masses measured at elevated stations represent well-mixed air, closest to baseline levels, within a certain time window of several hours during the day. For the elevated mountain stations discussed in this paper, this time interval is around midnight. Different diurnal patterns are apparent at each station, so the selection time window should be adjusted accordingly. Second, it is assumed that real baseline conditions are not subject to local influences and thus represent unperturbed lower free tropospheric air masses. This indicates that the variability of the measured CO₂ signal should be minimal within this selection time window. The methodological steps of ADVS are introduced in detail below in the two sections “starting selection” and “adaptive selection”.

2.2.1 Starting selection

For a given validated hourly dataset, ADVS starts data selection by finding a *start time window* for all days. The standardized selection procedure for the start time window results from site-specific parameters. This time interval is set as the most stable period from the diurnal variation. The step is referred to as *starting selection*. It begins by analyzing the mean diurnal cycle of the data input.

- Step 1: detrending is done by subtracting a 3-day average for each day, including the neighboring two days. It is the shortest possible time window to remove sudden changes in the time series related to the previous and posterior days while preserving the diurnal pattern.
- Step 2: the overall mean diurnal variation, \bar{d}_i ($i = 0$ to 23 h), is calculated from the complete set of detrended data.

- Step 3: the standard deviations s_{Δ_j} from the overall mean diurnal variation \bar{d}_i are calculated on a moving window Δ_j ($j = 6$ h). To be able to place a full set of 24 moving time windows over the overall mean diurnal variation, time windows across midnight (e.g., 6 h from 11 p.m. to 4 a.m. LT) are also included, that is, its first j hours are appended to the end of the 24 h in the overall mean diurnal variation. The time window with the smallest standard deviation is selected as the start time window.
- Result: the start time window $[i_{\text{start}}, \dots, i_{\text{end}}]$.

With the focus on elevated mountain stations, starting selection is purposely designed with the moving window Δ_j of 6 h, and the starting hour i_{start} to be between 6 p.m. and 5 a.m. LT for this study. For other stations with possibly different diurnal patterns, starting selection can be adjusted accordingly. For instance, at urban stations or stations completely within the continental PBL, the start time window can be chosen based on their best mixing conditions, which often occur in the afternoon with a shorter moving window, when the PBL reaches its maximum depth after “ingesting” free tropospheric air during its growth. Being aware that calculating the start time window from all data could differ from the start time windows calculated by season, the overall generated start time windows have been compared with seasonally generated start time windows for high altitude mountain stations (see Supplement Sect. S1.1). Because these differences were mostly small to moderate and this work aims at a methodical comparison under identical conditions, the start time windows are always derived from overall data.

2.2.2 Adaptive selection

The second component, *adaptive selection*, is designed to determine the most suitable time window for each day, based on the data variability. Through this method, the length of the start time window is expanded in both directions in time. Adaptive selection is performed on a daily basis, starting with the first day of the given dataset. The following steps only describe the *forward adaptive selection*. ADVS also runs the *backward adaptive selection* in an analogous manner but backwards in time.

- Step 1: the mean molar fraction \bar{x}_i , standard deviation s_i , and the proportion of missing values π_{missing} are calculated from data in the start time window $[i_{\text{start}}, \dots, i_{\text{end}}]$.
 - Step 2: if $s_i \leq 0.3$ ppm (CO₂) and $\pi_{\text{missing}} \leq 0.5$, ADVS continues to advance in time, examine whether the next data point x_f can be included in the selection time window W with $f = i_{\text{end}} + 1$. Otherwise, it is considered that the start time window does not fulfill the assumptions. In this case, no baseline data is selected for the present day and the algorithm proceeds to the next day.
 - Step 3: the absolute difference between x_f and \bar{x}_i is calculated, and the following threshold criterion is applied: $|x_f - \bar{x}_i| \leq \kappa \cdot s_i$, where κ is the threshold parameter. If this criterion holds, x_f is included in W and ADVS continues. Otherwise, ADVS stops for this day with only the start time window, and proceeds to the next day.
 - Step 4: mean \bar{x}_W and standard deviation s_W for the new selection time window W are calculated. If $s_W \leq 0.3$ ppm (CO₂), ADVS continues with the next data point x_f with $f = f + 1$. Otherwise, ADVS stops for this day with the previous selection time window and proceeds to the next day.
 - Step 5: the new absolute difference between x_f and \bar{x}_W is calculated, as well as the new threshold criteria. If condition $|x_f - \bar{x}_W| \leq \kappa \cdot s_W$ holds, x_f is included in W and ADVS goes back to Step 4. Otherwise, ADVS stops for this day and proceeds to the next day.
- When data selection for all days is finished, ADVS continues with backward adaptive selection. Afterwards, it proceeds to the result.
- Result: this is the final selection time window, which is a combination of W_{forward} and W_{backward} for the day in question.

The following limitations of the forward and backward expansions of the time window should be considered. ADVS always runs for no longer than 24 h including the start time window, i.e., $f \leq 24 \cdot \text{tr}$, where tr is the time resolution in data points per hour of the input data. This sometimes results in an overlap of “selected” and “unselected” data for two consecutive days. We always label the data as “selected” once it has been selected by ADVS. The threshold parameter κ is the controlling factor for the length of the selection time window. As κ increases, the length of the selection time window increases. A value of 2 was chosen heuristically for this study as a compromise between selecting as many data points as possible and achieving the least data variability. Similar values of sensitivity-controlling parameters in other data selection methods can be found (Thoning et al., 1989; Sirignano et al., 2010; Uglietti et al., 2011; Satar et al., 2016). In Step 2, values of 0.3 ppm and 0.5 indicate the threshold values for s_i and π_{missing} . We denote them as $s_{i,\text{threshold}}$ and $\pi_{\text{missing},\text{threshold}}$. Less remote stations at lower altitudes may require a larger value than 0.3 ppm because of different mixing conditions. When performing ADVS data selection at lower sites such as HPB and SSL, we recommend a higher $s_{i,\text{threshold}}$, such as 1.0 ppm. However, throughout this study we used the described parameter setting (0.3 ppm) for a methodical inter-comparison of selection methods at all stations. Potential influences of these parameter sizes ($s_{i,\text{threshold}}$ and tr) are discussed in Supplement Sect. S1.2 and S1.3.

2.3 Other statistical data selection methods for comparison

We compared ADVS with three statistical data selection methods. The first method named SI is based on “steady intervals” (Lowe et al., 1979; Stephens et al., 2013). Steady intervals, which are considered as baseline conditions, are defined by a standard deviation being lower than or equal to 0.3 ppm for six or more consecutive hours. Although this method has some similarity with ADVS, it treats all hours of the day equally without giving preference to hours where the variability is, on average, the smallest.

Second, we adopted a method applied by NOAA ESRL, which originated from Thoning et al. (1989). This selection routine has been applied specifically for measurements of background CO₂ levels at Mauna Loa. This method (referred to as THO) was applied as described on the website: http://www.esrl.noaa.gov/gmd/ccgg/about/co2_measurements.html. The first step of THO examines the within-hour variability by selecting hours with hourly standard deviation less than 0.3 ppm. For the hourly data used in this study, the within-hour variability is not applicable so that the first step is skipped. Second, it computes hourly averages and checks the hour-to-hour variability by retaining any two consecutive hourly values where the hour-to-hour difference is less than 0.25 ppm. The last step is based on the diurnal pattern (similar to ADVS), by excluding data from 11 a.m. to 7 p.m. LT due to transported air influenced by photosynthesis.

The last method compared is a moving average technique (MA). A moving time window of 30 days and a threshold criterion of two standard deviations from the moving averages were applied to discard outliers. Afterwards, new moving averages and new threshold criteria were calculated for data exclusion. This step is repeated until no more outliers were found. A more detailed description can be found in Uglietti et al. (2011) and Satar et al. (2016).

2.4 Seasonal-trend decomposition STL

To analyze the results from different data selection methods and compare them with the original validated datasets, we applied the seasonal-trend decomposition technique based on locally weighted regression smoothing (Loess), named STL (Cleveland, 1979; Cleveland et al., 1990). STL has been widely applied to measurements of atmospheric CO₂ and other trace gases (Cleveland et al., 1983; Carslaw, 2005; Brailsford et al., 2012; Hernández-Paniagua et al., 2015; Pickers and Manning, 2015). It decomposes a time series of interest into a trend component T , a seasonal component S , and a remainder component R , which allows detailed separate analyses of trend and seasonality. Two recursive procedures are included in the STL technique: an inner loop where seasonal and trend smoothing based on Loess are performed and updated in each pass, and an outer loop that computes

the robustness weights to reduce the influences of extreme values for the next run of the inner loop (Cleveland et al., 1990).

For this study, we used the implemented function *stl* in *R* (R Core Team, 2017). Owing to functional limitation of *stl*, full time coverage of monthly data is needed in order to reduce the risk of large time gaps or unequal spacing (Pickers and Manning, 2015). All data were first aggregated to monthly averages. Then, missing data were substituted by linear interpolation, using *R* function *na.approx* (Zeileis and Grothendieck, 2005). For the application of STL, two parameters need to be specified, which are the seasonal smoothing parameter $n_{(s)}$ (*s*-window in function *stl*) and the trend smoothing parameter $n_{(t)}$ (*t*-window in function *stl*). As $n_{(s)}$ and $n_{(t)}$ increase, the seasonal and trend components get smoother (Cleveland et al., 1990). For optimal compatibility in this study, the same parameters were chosen for all stations as $n_{(s)} = 7$ and $n_{(t)} = 23$, based on the recommendation of Cleveland et al. (1990). Another parameter combination of $n_{(s)} = 5$ and $n_{(t)} = 25$ was also tested according to Pickers and Manning (2015), but with no significant differences in results.

3 Results and discussion

3.1 Start time window

ADVS was applied to the validated hourly averages from all six stations with the parameter settings as described above. The detrended mean diurnal cycles were obtained together with the start time window for each station by starting selection (see Fig. 2, for conventional mean diurnal plots see Supplement Sect. S2). The observed differences in the start time windows, as well as in the widths of the confidence intervals (gray shades), reflect the characteristics of differently situated measurement sites and different sampling levels. The first subplot column (HPB50, HPB93, and HPB131), representing the three sampling heights at HPB, shows similar detrended diurnal patterns with similar start time windows. The slightly different start time window at HPB131 potentially indicates different dynamics of the atmospheric transport at higher elevation. The decreasing amplitude with increasing sampling height indicates that the higher the sampling inlet is above the ground, the less it is affected by the local surface fluxes. The three start time windows suggest that the most stable period at HPB occurs during the last few hours of a day, including midnight. However, in contrast to all other stations covering at least a full year, HPB data are only from September of 2015 to June of 2016. The results may not be fully comparable, but instead it shows that the data selection method is also applicable to data with time periods shorter than one year.

Regarding the second subplot column (SSL, SNB, and IZO), the start time windows can be found from midnight

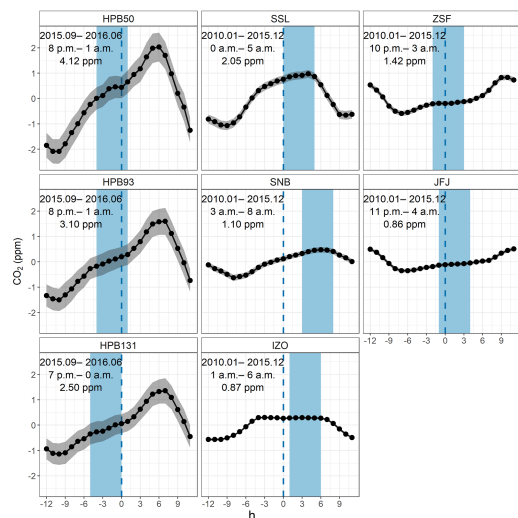


Figure 2. Detrended mean diurnal cycles of validated CO₂ datasets (black) with 95 % confidence intervals (gray) from six GAW stations (hours in LT). Measurements at HPB are differentiated by the sampling heights (e.g., HPB50 for 50 m a.g.l.). The covered time periods (top text), resulting start time windows (middle text, also in light blue shades), and mean diurnal amplitudes (bottom text) are shown in each subplot.

on or later in the morning. The start time window for SSL encompasses its diurnal maximum, indicating that data variability is considerably smaller in the early morning than in the afternoon because of its vicinity to the Black Forest region, which has strong influence due to local photosynthetic activity (Schmidt et al., 2003). A similar diurnal pattern can be found at SNB. The influence of CO₂ sources is not as prominent as the effect of distant CO₂ sinks, since it is situated at the isolated summit peak of Hoher Sonnblick surrounded only by mountains and glaciers, with a negligibly small number of tourists, thus anthropogenic activities are minimal. IZO is a special case, since it is located on a remote mountain plateau on the Island of Tenerife above the strong subtropical temperature inversion layer. Even though the start time window is limited to 6 h, IZO presents an ideal mean diurnal cycle for data selection from a potentially much longer time window.

In the right column of the figure, both ZSF and JFJ find their start time windows around midnight (including hours after midnight). ZSF shows higher diurnal CO₂ amplitude than JFJ, but the two sites show similar diurnal patterns. For the choice of the start time window from the mean diurnal variation, relatively close or even local anthropogenic sources may influence the CO₂ at these two stations, possibly due to touristic influences.

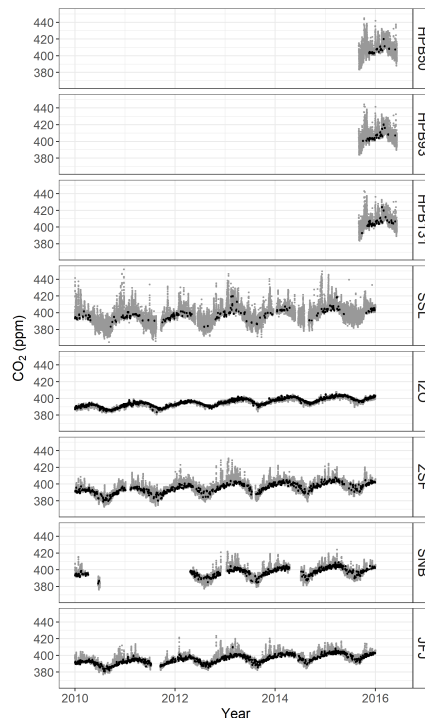


Figure 3. Time series plots of validated CO₂ datasets (gray), and selected datasets by ADVS (black) at six GAW stations.

3.2 Percentage of selected data

Starting from the initial start time windows, ADVS selected the baseline data for all stations (see Fig. 3). In addition, we calculated the percentages of the complete datasets selected by ADVS as baseline data, which are listed in the first column of Table 2. The higher the percentage the more well-mixed air is measured at the station, which is assumed to be a representation of lower free tropospheric conditions. This holds especially for IZO, where a larger percentage of 36.2 % was selected as baseline data. The sites with intermediate percentages are JFJ (22.1 %), SNB (19.3 %), and ZSF (14.8 %). For the three sampling heights at HPB, only 3.2 % (50 m), 4.8 % (93 m), and 6.2 % (131 m) of the data were selected by ADVS. Finally, a similarly low percentage was found for SSL (4.0 %), probably due to its higher data variability.

Table 2 clearly indicates that the percentage of baseline data increases with altitude for all methods, suggesting measurements at higher altitudes can capture progressively well-mixed and hence representative air. Based on this finding, a linear least squares regression was applied between the ab-

Table 2. Percentage of selected data in all data by different data selection methods. The bottom shows the linear regression coefficients of station (HPB is represented by HPB50; IZO is excluded) altitudes and the percentages of selected data at the significance level of 0.05 (***)

Station ID	ADVS	SI	THO	MA
HPB50	3.2	13.9	21.7	79.8
HPB93	4.8	18.5	25.0	79.4
HPB131	6.2	21.3	27.3	79.8
SSL	4.0	17.9	25.4	83.2
IZO	36.2	82.2	56.0	60.5
ZSF	14.8	47.1	40.8	79.0
SNB	19.3	58.7	44.2	76.9
JFJ	22.1	62.1	46.3	77.6
Linear regression coefficient (γ^2)	0.996***	0.992***	0.985***	0.645

solute altitudes and the percentages of selected data for continental stations. IZO is on a remote island and therefore not comparable. This approach reveals a significant positive linear trend (see coefficient in Table 2). The related figure of linear regression can be found in Supplement Sect. S3.1.

To examine the characteristic growth of the percentages of selected data by ADVS during the selection process, we additionally calculated percentages after completing both the starting selection and adaptive selection steps mentioned in Sect. 2.2 (see Supplement Sect. S3.2). All results of percentages show an order of stations similar to that above, and the percentages increase steadily step by step for all stations. The percentages of selected data by ADVS were then compared with those of the mentioned statistical data selection methods SI, THO, and MA (see Table 2, with the corresponding figure shown in Supplement Sect. S3.3).

Since the percentages of selected data indicate not only the amount of data declared as representative but also show the characteristics of the selection methods, this criterion is used for further assessment. All other methods except for MA result in higher percentages for higher altitude stations (IZO, ZSF, SNB, and JFJ) than for those of lower altitudes (HPB and SSL). ADVS always performs the strictest filtering in all cases. Based on the stepwise study (see Supplement Sect. S3.2), these low percentages are primarily due to the restrictive definition of the start time window requiring data with a standard deviation of less than 0.3 ppm. With adaptive selection, the percentages of selected data increase but remain lower than those of the other methods. SI and THO, in comparison, show differences between stations at high and low elevations. Compared with SI, THO is higher at stations at lower elevations, but lower at high ones. A major limitation of SI seems to be the requirement for consecutive hours, in our case of 6 h with 0.3 ppm standard deviation threshold, which might be too restrictive for stations at lower elevations. However, this criterion results in a fairly large percentage for

stations at high elevations. At ZSF, SNB, and JFJ, it results in the second largest, and even the largest in the case of IZO.

The highest percentages of selected data (approximately 80%) were obtained with MA at most stations except for IZO. However, IZO obtains the largest percentages from all other selection methods. This is probably caused by the very low variability of CO₂ at IZO, resulting in overly strict moving-average thresholds for the MA method. Thus, we conclude that MA does not work properly in the case of very well-mixed air (IZO). At all other stations, it is possible that MA declares too much data as representative. Therefore, MA was excluded from further analyses.

3.3 STL components

STL was applied to the validated datasets before and after baseline selection with SI, THO, and ADVS, except for HPB due to its limited length of time (less than one year). Depending on data availability, STL was performed on CO₂ data from 2012 to 2015 at SNB, while data inputs at SSL, IZO, ZSF, and JFJ cover the whole period from 2010 to 2015. Figure 4 gives an overview of the decomposition by STL. The following sections discuss the resulting components obtained by STL, namely the trend component, the seasonal component, and the remainder component.

3.3.1 Trend component

From the trend components, the mean annual growth rates were estimated by linear regression (see Table 3). Based on the 95% confidence intervals for the slope, positive trends i.e., increasing CO₂ concentrations are observed. Owing to the overlap of the confidence intervals, differences in the mean annual growth rates among VAL and selected datasets at the same station are all in good agreement. This indicates that the trend component is not significantly influenced by the statistical data selection method, which agrees well with the finding of Parrish et al. (2012) from a study of baseline ozone concentrations that there were no significant differences of the long-term changes between the baseline and unfiltered datasets. Moreover, the following fact is observed for all sites except for SSL. Compared to unselected data (VAL), the mean annual growth rates based on selected datasets are systematically higher approaching the growth rates at IZO. IZO can be considered as better representing the lower free tropospheric conditions and agrees well with the mean annual global CO₂ growth rates (2.31 ppm) during the same time period (2010–2015) based on data from <https://www.esrl.noaa.gov/gmd/ccgg/trends/global.html>. The exception at SSL is probably caused by stronger local influences as a result of its lower elevation. In addition, the confidence intervals of the mean annual growth rates are always smaller after data selection, which improves the precision of trends.

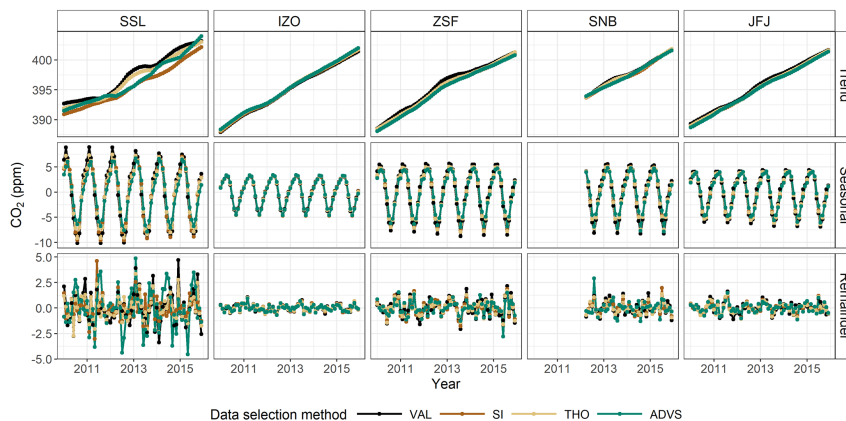


Figure 4. STL decomposition results from VAL (black), SI-selected (brown), THO-selected (yellow), and ADVS-selected (green) datasets at five GAW stations.

Table 3. Mean annual growth rates (ppm yr^{-1}) with 95 % confidence intervals from linear regression, applied on the trend components by STL over 2010 to 2015, except for SNB. Data at SNB were decomposed over 2012 to 2015 due to missing data from 2010 to 2011 and thus shown in italic font.

Station ID	VAL	SI	THO	ADVS
SSL	2.04 ± 0.09	1.89 ± 0.06	2.04 ± 0.06	2.03 ± 0.09
IZO	2.24 ± 0.03	2.26 ± 0.02	2.25 ± 0.02	2.25 ± 0.02
ZSF	2.13 ± 0.08	2.16 ± 0.05	2.17 ± 0.06	2.19 ± 0.06
<i>SNB</i>	<i>2.02 ± 0.07</i>	<i>2.06 ± 0.06</i>	<i>2.06 ± 0.06</i>	<i>2.08 ± 0.04</i>
JFJ	2.13 ± 0.03	2.15 ± 0.02	2.14 ± 0.02	2.14 ± 0.02

3.3.2 Seasonal component

The resulting seasonal components show systematic differences between VAL and selected datasets. The mean monthly variations were calculated on a monthly scale over the entire period from the analyzed data. Figure 5a and b present the results at stations ZSF and IZO. At most stations (except for IZO), the seasonal amplitudes have been substantially reduced compared to VAL (see also Fig. 4). At ZSF, the averaged peak-to-peak seasonal amplitude, defined as mean seasonal maximum minus seasonal minimum, drops the most by 18.9 % from VAL with the ADVS selected dataset. An explanation of this reduction is CO_2 signal exclusion from local sources and sinks by data selection. When taking a closer look at the monthly averages, lower CO_2 values are found in the selected datasets in the winter months from October to April, indicating that the CO_2 concentrations estimated by VAL are above the background levels because of more dominant anthropogenic activities and no active vegetation.

Higher values in the summer months from May to September explain underestimation of VAL due to intensified upward transport of photosynthetic signatures resulting from vegetation. Similar patterns can be found at stations SSL, SNB, and JFJ (see Supplement Sect. S4). IZO always shows the smallest seasonal amplitude and there is almost no difference between VAL and selected datasets. Based on this consideration, it is very likely that the lower free troposphere will react with a delay to CO_2 concentration changes of effective sources and sinks on the ground, acting like an atmospheric memory.

A time delay of one month in the mean seasonal maximum is shown in Fig. 5a at ZSF with selected datasets by SI and ADVS (March), compared with the maximum from the validated data (February). A similar time shift can also be found by other selection methods at stations SSL (one-month delay from February to March by SI and ADVS) and JFJ (two-month delay from February to April by SI, THO, and ADVS). As for station IZO (April) in Fig. 5b and station SNB (March), the seasonal maxima stay the same. The magnitude of these delays may be related to mixing in the lower free troposphere. Rapid changes are usually observed close to sources and sinks, e.g., from anthropogenic and biogenic activities. Thus, the higher the station is above the boundary layer, the later the maxima during the winter can be observed because of the late response due to inhibited mixing. However, this delay does not occur for the minima during the summer because of the very effective upward transport and more favorable mixing conditions at that time of year. Consequently, no change in the seasonal minima is observed at all measurement sites, which is taken as an indicator of enhanced thickness of the mixing layer as good mixing conditions. Taking ZSF as an example, Birmili et al. (2009) observed low concentrations of particle numbers in winter and

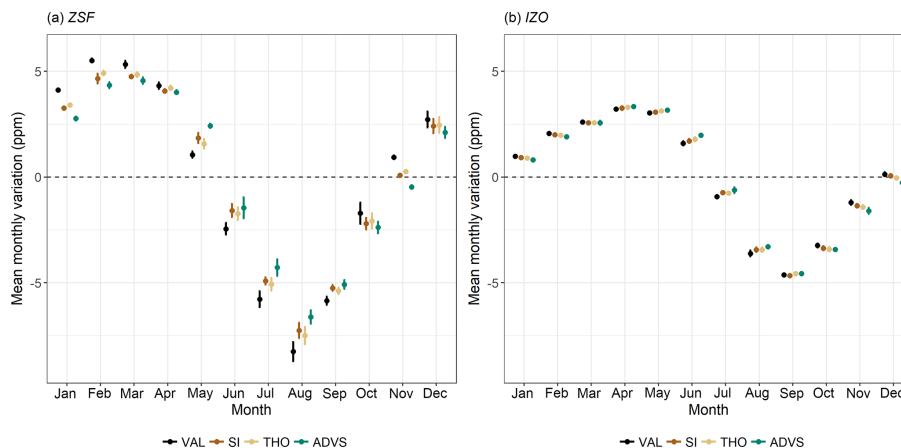


Figure 5. Mean monthly variation of the seasonal component decomposed by STL at (a) ZSF and (b) IZO over the whole period. For a better visualization of the results of selection methods, dots have been separated horizontally and equidistantly. The 95 % confidence intervals are shown as error bars.

found it representative for the free tropospheric air by analyzing the annual and diurnal cycles. From spring onwards, the PBL rises with increasing temperatures. The intense vertical atmospheric exchange during summer months results in a daily air mass transport from the boundary layer to reach ZSF due to thermal convection (Reiter et al., 1986; Birmili et al., 2009). Thus there are optimal transport and mixing conditions. Therefore after data selection, the timing of seasonal peaks corresponds better among the stations.

3.3.3 Remainder component

The remainder component resembles random noise from local influences in its structure, being different from site to site and statistically uncorrelated with the general signal of CO₂ concentrations in the lower free troposphere (Thoning et al., 1989). The standard deviation of the remainder component is taken here as a measure for external influences (see Fig. 4). Table 4 shows the calculated standard deviations from the remainder components at each station. Comparable results are derived from all selected datasets. SSL, as the lowest altitude station, exhibits the largest variation. IZO with the smallest standard deviations in the remainder component proves to be the station least influenced by its surrounding environment. The three alpine measuring stations (ZSF, SNB, and JFJ) exhibit intermediate variability. From this perspective, STL performs well in showing the site characteristics. Consequently, the noise of the remainder components, given in Table 4, decreases with increasing altitude of the continental mountain stations, which is in inverse relation to the percentages of selected data (Table 2). IZO was excluded in both regressions against altitude because of its maritime character.

Table 4. Standard deviations of the remainder components by STL over 2010 to 2015, except for SNB. Data at SNB were decomposed over 2012 to 2015 due to missing data from 2010 to 2011 and thus shown in italic font.

Station ID	VAL	SI	THO	ADVS
SSL	1.61	1.16	1.26	1.99
IZO	0.34	0.33	0.30	0.30
ZSF	0.89	0.75	0.72	0.73
SNB	<i>0.66</i>	<i>0.56</i>	<i>0.55</i>	<i>0.70</i>
JFJ	0.56	0.45	0.48	0.47

3.4 Correlation analysis

As mentioned above, data selection is defined here as an approach of extracting a group of data to be the best representative for the lower free troposphere. Consequently, the selected CO₂ datasets should have properties that are well correlated between the sites. For evaluating this hypothesis, we took the combination of the trend and seasonal components from STL and examined the correlations between each pair of stations in a Pearson correlation matrix (see Fig. 6a). The trend and seasonal components of all VAL and selected datasets were first compiled, and then Pearson's correlation coefficients were calculated assuming normal distribution of data examined by the Anderson–Darling test ($P < 0.05$). The correlation matrices are shown for each data selection method individually, in order to enable a comparison between ADVS and other methods. Data used for correlation were chosen only when available at all stations (2012–2015). In general, most pairs show higher correlation coefficients

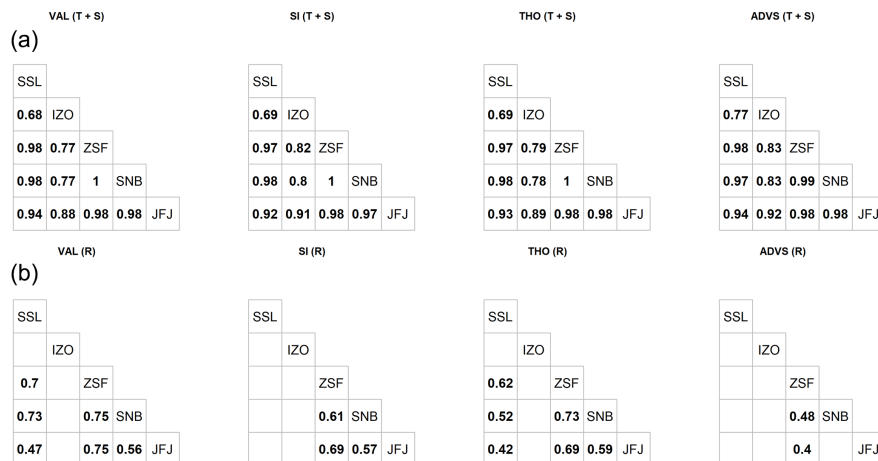


Figure 6. Pearson's correlation matrices of combinations of trend and seasonal components ($T+S$, **a**), and only remainder components (R , **b**) at stations SSL, IZO, ZSF, SNB, and JFJ by different selection methods. Correlations with no significant coefficients at the 0.05 significance level were left blank.

with selected data irrespective of the selection method, especially between the three Alpine stations (ZSF, SNB, and JFJ). This evaluation shows a similar result to the method presented by Sepúlveda et al. (2014) for identifying baseline conditions based on the correlation between distant measuring stations. Pairs including IZO after data selection by ADVS show a notable increase in the correlation coefficients, meaning better coherence between the reference station IZO and the others.

Conversely, when selecting representative data more effectively, the results should contain less local and regional influences. Therefore, we compared the remainder components derived from STL pairwise to check whether the Pearson correlation coefficients decreased after data selection (see Fig. 6b). The number of insignificant correlations between the station pairings is the greatest for ADVS. For the only two coefficients significant at the 0.05 significance level (ZSF-SNB and ZSF-JFJ), they drop largely from 0.75 to 0.48, and from 0.75 to 0.40, respectively, which cannot be observed by the other selection methods. This means that by ADVS the combination of trend and seasonal components correlate best and the remaining unselected data have the lowest correlation among the methods. If these two criteria are used to separate the representative part of the data from the unrepresentative part, the ADVS method produces the best results.

4 Conclusions and outlook

We presented the novel statistical ADVS method for selecting representative baseline data for CO₂ measurements at elevated GAW mountain stations. For assessment of the

data selection procedure, we applied the method to six CO₂ datasets measured at GAW mountain stations in the European Alps. The ADVS resulted in an increasing number of percentages of selected data representing the background conditions with growing altitude of continental measurement sites, which is reasonable due to the underlying atmospheric dynamics. For comparison, three well-known statistical data selection methods were applied to the same datasets and most methods yielded similar increasing percentages with growing altitude. Among all the methods, ADVS is the most restrictive in terms of the number of selected data in the overall datasets.

In addition, we applied the time series decomposition method STL to all datasets before and after data selection. All statistical data selection methods resulted in the same annual trend within the 95% confidence interval of the datasets before selection, while the seasonal signal varied substantially with smaller seasonal amplitudes and delayed occurrences of seasonal maxima. We also presented an additional assessment of ADVS compared with the other statistical data selection methods based on correlation analysis. For the combination of trend and seasonal components by STL, higher correlation coefficients between stations were found with ADVS data selection than SI and THO. Inversely, ADVS resulted in lower correlation coefficients in the remainder components than the other methods. Both indicate a better performance of selecting baseline data by ADVS.

The presented method is useful for data selection of atmospheric CO₂ data representative of the lower free troposphere. It requires only data from a single measurement site, is easily adjustable to the local conditions, and runs

automatically. The method can also be applied to historical datasets. The results provide evidence that the proposed ADVS method confers the possibility of selecting data that are representative of CO₂ concentrations of a larger area of the lower free troposphere. This is an elementary prerequisite for application of the method to a larger number of different stations and an essential step towards generalization. It directly supports the objective of GAW to extrapolate from a set of point measurements from single stations to a larger representative area or region in the lower free troposphere (WMO, 2017). In future, there is a need to test whether such results could be used for additional applications, such as ground calibration of satellite measurements. Finally, it would be very interesting to test as a next step whether this presented method is applicable to stations in other regions and on other continents. Moreover, the issue of whether and how to include coastal stations in a systematic and practically generalizable approach for selecting representative data at GAW stations will be a particular concern.

Data availability. Hourly CO₂ data can be downloaded from WMO's World Data Centre for Greenhouse Gases (<http://ds.data.jma.go.jp/gmd/wdccc/cgi-bin/wdccc/catalogue.cgi>; last access: 15 March 2018), data with higher resolution can be requested from the station data providers.

The Supplement related to this article is available online at <https://doi.org/10.5194/amt-11-1501-2018-supplement>.

Competing interests. The authors declare that they have no conflict of interest.

Acknowledgements. This work was supported by a scholarship from China Scholarship Council (CSC) under grant CSC No. 201508080110. This work was supported by a MICMoR Fellowship through KIT/IMK-IFU to Ye Yuan. This work was supported by the German Research Foundation (DFG) and the Technical University of Munich (TUM) in the framework of the Open Access Publishing Program. The CO₂ measurements at Zugspitze and Schauinsland were supported by the German Environment Agency (UBA). We thank Markus Wallasch for providing CO₂ data obtained at Schauinsland and Ralf Sohmer for technical support. The CO₂ measurements at Hohenpeissenberg were conducted by the German Meteorological Service within the ICOS Atmospheric Station Network. The CO₂ measurements at Jungfraujoch were supported by the Swiss Federal Office for the Environment, ICOS-Switzerland, and the International Foundation High Alpine Research Stations Jungfraujoch and Gornergrat. Martin Steinbacher acknowledges funding from the GAW Quality Assurance/Science Activity Centre Switzerland (QA/SAC-CH), which is supported by MeteoSwiss and Empa. The Izaña (IZO) CO₂ measurements were performed within the GAW Program

at the Izaña Atmospheric Research Center, financed by AEMET. Finally, we also thank Wolfgang Spangl from the Austrian Environment Agency (UBA-At) for providing CO₂ data obtained at Sonnblick.

This work was supported by the German Research Foundation (DFG) and the Technische Universität München within the funding programme Open Access Publishing.

Edited by: Dominik Brunner

Reviewed by: Jooil Kim and one anonymous referee

References

- Bacastow, R. B., Keeling, C. D., and Whorf, T. P.: Seasonal Amplitude Increase in Atmospheric CO₂ Concentration at Mauna Loa, Hawaii, 1959–1982, *J. Geophys. Res.*, 90, 10529–10540, <https://doi.org/10.1029/JD090iD06p10529>, 1985.
- Balzani Lööb, J. M., Henne, S., Legreid, G., Staehelin, J., Reimann, S., Prévôt, A. S. H., Steinbacher, M., and Vollmer, M. K.: Estimation of background concentrations of trace gases at the Swiss Alpine site Jungfraujoch (3580 m a.s.l.), *J. Geophys. Res.*, 113, D22305, <https://doi.org/10.1029/2007JD009751>, 2008.
- Birmili, W., Ries, L., Sohmer, R., Anastou, A., Sonntag, A., König, K., and Levin, I.: Feine und ultrafeine Aerosolpartikeln an der GAW-Station Schneefernerhaus/Zugspitze, *Gefährst. Reinhalt. L.*, 69, 31–35, 2009.
- Brailsford, G. W., Stephens, B. B., Gomez, A. J., Riedel, K., Mikaloff Fletcher, S. E., Nichol, S. E., and Manning, M. R.: Long-term continuous atmospheric CO₂ measurements at Baring Head, New Zealand, *Atmos. Meas. Tech.*, 5, 3109–3117, <https://doi.org/10.5194/amt-5-3109-2012>, 2012.
- Brooks, B.-G. J., Desai, A. R., Stephens, B. B., Bowling, D. R., Burns, S. P., Watt, A. S., Heck, S. L., and Sweeney, C.: Assessing filtering of mountaintop CO₂ mole fractions for application to inverse models of biosphere-atmosphere carbon exchange, *Atmos. Chem. Phys.*, 12, 2099–2115, <https://doi.org/10.5194/acp-12-2099-2012>, 2012.
- Calvert, J. G.: Glossary of atmospheric chemistry terms, *Pure Appl. Chem.*, 62, 2167–2219, <https://doi.org/10.1351/pac199062112167>, 1990.
- Carnuth, W. and Trickl, T.: Transport studies with the IFU three-wavelength aerosol lidar during the VOTALP Mesolcina experiment, *Atmos. Environ.*, 34, 1425–1434, [https://doi.org/10.1016/S1352-2310\(99\)00423-9](https://doi.org/10.1016/S1352-2310(99)00423-9), 2000.
- Carnuth, W., Kempfer, U., and Trickl, T.: Highlights of the tropospheric lidar studies at IFU within the TOR project, *Tellus B*, 54, 163–185, <https://doi.org/10.1034/j.1600-0889.2002.00245.x>, 2002.
- Carlsaw, D. C.: On the changing seasonal cycles and trends of ozone at Mace Head, Ireland, *Atmos. Chem. Phys.*, 5, 3441–3450, <https://doi.org/10.5194/acp-5-3441-2005>, 2005.
- Chambers, S. D., Williams, A. G., Conen, F., Griffiths, A. D., Reimann, S., Steinbacher, M., Krummel, P. B., Steele, L. P., van der Schoot, M. V., Galbally, I. E., Molloy, S. B., and Barnes, J. E.: Towards a Universal “Baseline” Characterisation of Air Masses for High- and Low-Altitude Observing Sta-

- tions Using Radon-222, *Aerosol Air Qual. Res.*, 16, 885–899, <https://doi.org/10.4209/aaqr.2015.06.0391>, 2016.
- Cleveland, R. B., Cleveland, W. S., McRae, J. E., and Terpenning, I.: STL: A seasonal-trend decomposition procedure based on Loess, *J. Off. Stat.*, 6, 3–73, 1990.
- Cleveland, W. S.: Robust locally weighted regression and smoothing scatterplots, *J. Am. Stat. Assoc.*, 74, 829–836, <https://doi.org/10.1080/01621459.1979.10481038>, 1979.
- Cleveland, W. S., Freeny, A. E., and Graedel, T. E.: The Seasonal Component of Atmospheric CO₂: Information From New Approaches to the Decomposition of Seasonal Time Series, *J. Geophys. Res.*, 88, 10934–10946, <https://doi.org/10.1029/JC088iC15p10934>, 1983.
- Cui, J., Pandey Deolal, S., Sprenger, M., Henne, S., Staehelin, J., Steinbacher, M., and Nédélec, P.: Free tropospheric ozone changes over Europe as observed at Jungfraujoch (1990–2008): An analysis based on backward trajectories, *J. Geophys. Res.*, 116, D10304, <https://doi.org/10.1029/2010JD015154>, 2011.
- Elliott, W. P. (Ed.): The Statistical treatment of CO₂ data records, NOAA Technical Memorandum ERL ARL, 173, U.S. Dept. of Commerce, National Oceanic and Atmospheric Administration, Environmental Research Laboratories, Silver Spring, Md., USA, 131 pp., 1989.
- Fang, S. X., Tans, P. P., Steinbacher, M., Zhou, L. X., and Luan, T.: Comparison of the regional CO₂ mole fraction filtering approaches at a WMO/GAW regional station in China, *Atmos. Meas. Tech.*, 8, 5301–5313, <https://doi.org/10.5194/amt-8-5301-2015>, 2015.
- Ferrer, J., Rüttimann, R., Schneiter, D., Fischer, A., Buchmann, B., and Hofer, P.: Variability of trace gases at the high-Alpine site Jungfraujoch caused by meteorological transport processes, *J. Geophys. Res.*, 105, 12241–12251, <https://doi.org/10.1029/1999JD901178>, 2000.
- Gilge, S., Plass-Duelmer, C., Fricke, W., Kaiser, A., Ries, L., Buchmann, B., and Steinbacher, M.: Ozone, carbon monoxide and nitrogen oxides time series at four alpine GAW mountain stations in central Europe, *Atmos. Chem. Phys.*, 10, 12295–12316, <https://doi.org/10.5194/acp-10-12295-2010>, 2010.
- Gomez-Pelaez, A. J., Ramos, R., Cuevas, E., and Gomez-Trueba, V.: 25 years of continuous CO₂ and CH₄ measurements at Izaña Global GAW mountain station: annual cycles and interannual trends, in: Proceedings of the Symposium on Atmospheric Chemistry and Physics at Mountain Sites (ACP Symposium 2010), 8–10 June 2010, Interlaken, Switzerland, 157–159, 2010.
- Gomez-Pelaez, A. J., Ramos, R., Gomez-Trueba, V., Novelli, P. C., and Campo-Hernandez, R.: A statistical approach to quantify uncertainty in carbon monoxide measurements at the Izaña global GAW station: 2008–2011, *Atmos. Meas. Tech.*, 6, 787–799, <https://doi.org/10.5194/amt-6-787-2013>, 2013.
- Henne, S., Brunner, D., Folini, D., Solberg, S., Klausen, J., and Buchmann, B.: Assessment of parameters describing representativeness of air quality in-situ measurement sites, *Atmos. Chem. Phys.*, 10, 3561–3581, <https://doi.org/10.5194/acp-10-3561-2010>, 2010.
- Hernández-Paniagua, I. Y., Lowry, D., Clemittshaw, K. C., Fisher, R. E., France, J. L., Lanoisellé, M., Ramonet, M., and Nisbet, E. G.: Diurnal, seasonal, and annual trends in atmospheric CO₂ at southwest London during 2000–2012: Wind sector analysis and comparison with Mace Head, Ireland, *Atmos. Environ.*, 105, 138–147, <https://doi.org/10.1016/j.atmosenv.2015.01.021>, 2015.
- Herrmann, E., Weingartner, E., Henne, S., Vuilleumier, L., Bukowiecki, N., Steinbacher, Coen, F., Collaud Conen, M., Hammer, E., Jurányi, Z., Baltensperger, U., and Gysel, M.: Analysis of long-term aerosol size distribution data from Jungfraujoch with emphasis on free tropospheric conditions, cloud influence, and air mass transport, *J. Geophys. Res.-Atmos.*, 120, 9459–9480, <https://doi.org/10.1002/2015JD023660>, 2015.
- Kaiser, A., Scheifinger, H., Spangl, W., Weiss, A., Gilge, S., Fricke, W., Ries, L., Cemas, D., and Jesenovec, B.: Transport of nitrogen oxides, carbon monoxide and ozone to the Alpine Global Atmosphere Watch stations Jungfraujoch (Switzerland), Zugspitze and Hohenpeissenberg (Germany), Sonnblick (Austria) and Mt. Kravac (Slovenia), *Atmos. Environ.*, 41, 9273–9287, <https://doi.org/10.1016/j.atmosenv.2007.09.027>, 2007.
- Keeling, C. D.: The Concentration and Isotopic Abundances of Carbon Dioxide in the Atmosphere, *Tellus*, 12, 200–203, <https://doi.org/10.1111/j.2153-3490.1960.tb01300.x>, 1960.
- Locher, R. and Ruckstuhl, A.: IDPmisc: Utilities of Institute of Data Analyses and Process Design, available at: <https://CRAN.R-project.org/package=IDPmisc> (last access: 28 August 2017), 2012.
- Lowe, D. C., Guenther, P. R., and Keeling, C. D.: The concentration of atmospheric carbon dioxide at Baring Head, New Zealand, *Tellus*, 31, 58–67, <https://doi.org/10.1111/j.2153-3490.1979.tb00882.x>, 1979.
- Massen, F. and Beck, E.-G.: Accurate Estimation of CO₂ Background Level from Near Ground Measurements at Non-Mixed Environments, in: The Economic, Social and Political Elements of Climate Change, edited by: Leal Filho, W., Climate Change Management, Springer Berlin Heidelberg, Berlin, Heidelberg, Germany, 509–522, 2011.
- Pales, J. C. and Keeling, C. D.: The Concentration of Atmospheric Carbon Dioxide in Hawaii, *J. Geophys. Res.*, 70, 6053–6076, <https://doi.org/10.1029/JZ070i024p06053>, 1965.
- Parrish, D. D., Law, K. S., Staehelin, J., Derwent, R., Cooper, O. R., Tanimoto, H., Volz-Thomas, A., Gilge, S., Scheel, H.-E., Steinbacher, M., and Chan, E.: Long-term changes in lower tropospheric baseline ozone concentrations at northern mid-latitudes, *Atmos. Chem. Phys.*, 12, 11485–11504, <https://doi.org/10.5194/acp-12-11485-2012>, 2012.
- Peterson, J. T., Komhyr, W. D., Harris, T. B., and Waterman, L. S.: Atmospheric carbon dioxide measurements at Barrow, Alaska, 1973–1979, *Tellus*, 34, 166–175, <https://doi.org/10.1111/j.2153-3490.1982.tb01804.x>, 1982.
- Pickers, P. A. and Manning, A. C.: Investigating bias in the application of curve fitting programs to atmospheric time series, *Atmos. Meas. Tech.*, 8, 1469–1489, <https://doi.org/10.5194/amt-8-1469-2015>, 2015.
- R Core Team: R: A Language and Environment for Statistical Computing, Vienna, Austria, available at: <https://www.R-project.org/>, last access: 28 August 2017.
- Reiter, R., Sladkovic, R., and Kanter, H.-J.: Concentration of trace gases in the lower troposphere, simultaneously recorded at neighboring mountain stations, *Meteorol. Atmos. Phys.*, 35, 187–200, <https://doi.org/10.1007/BF01041811>, 1986.
- Risius, S., Xu, H., Di Lorenzo, F., Xi, H., Siebert, H., Shaw, R. A., and Bodenschatz, E.: Schneefernerhaus as a mountain research

- station for clouds and turbulence, *Atmos. Meas. Tech.*, 8, 3209–3218, <https://doi.org/10.5194/amt-8-3209-2015>, 2015.
- Ruckstuhl, A. F., Henne, S., Reimann, S., Steinbacher, M., Vollmer, M. K., O'Doherty, S., Buchmann, B., and Hueglin, C.: Robust extraction of baseline signal of atmospheric trace species using local regression, *Atmos. Meas. Tech.*, 5, 2613–2624, <https://doi.org/10.5194/amt-5-2613-2012>, 2012.
- Satar, E., Berhanu, T. A., Brunner, D., Henne, S., and Leuenberger, M.: Continuous CO₂/CH₄/CO measurements (2012–2014) at Beromünster tall tower station in Switzerland, *Biogeosciences*, 13, 2623–2635, <https://doi.org/10.5194/bg-13-2623-2016>, 2016.
- Schibig, M. F., Steinbacher, M., Buchmann, B., van der Laan-Luijkx, I. T., van der Laan, S., Ranjan, S., and Leuenberger, M. C.: Comparison of continuous in situ CO₂ observations at Jungfraujoch using two different measurement techniques, *Atmos. Meas. Tech.*, 8, 57–68, <https://doi.org/10.5194/amt-8-57-2015>, 2015.
- Schmidt, M., Graul, R., Sartorius, H., and Levin, I.: The Schauinsland CO₂ record: 30 years of continental observations and their implications for the variability of the European CO₂ budget, *J. Geophys. Res.-Atmos.*, 108, 4619, <https://doi.org/10.1029/2002JD003085>, 2003.
- Sepúlveda, E., Schneider, M., Hase, F., Barthlott, S., Dubravica, D., García, O. E., Gomez-Pelaez, A., González, Y., Guerra, J. C., Gisi, M., Kohlhepp, R., Dohe, S., Blumenstock, T., Strong, K., Weaver, D., Palm, M., Sadeghi, A., Deutscher, N. M., Warneke, T., Notholt, J., Jones, N., Griffith, D. W. T., Smale, D., Brailsford, G. W., Robinson, J., Meinhardt, F., Steinbacher, M., Aalto, T., and Worthy, D.: Tropospheric CH₄ signals as observed by NDACC FTIR at globally distributed sites and comparison to GAW surface in situ measurements, *Atmos. Meas. Tech.*, 7, 2337–2360, <https://doi.org/10.5194/amt-7-2337-2014>, 2014.
- Sirignano, C., Neubert, R. E. M., Rödenbeck, C., and Meijer, H. A. J.: Atmospheric oxygen and carbon dioxide observations from two European coastal stations 2000–2005: continental influence, trend changes and APO climatology, *Atmos. Chem. Phys.*, 10, 1599–1615, <https://doi.org/10.5194/acp-10-1599-2010>, 2010.
- Stephens, B. B., Brailsford, G. W., Gomez, A. J., Riedel, K., Mikaloff Fletcher, S. E., Nichol, S., and Manning, M.: Analysis of a 39-year continuous atmospheric CO₂ record from Baring Head, New Zealand, *Biogeosciences*, 10, 2683–2697, <https://doi.org/10.5194/bg-10-2683-2013>, 2013.
- Thoning, K. W., Tans, P. P., and Komhyr, W. D.: Atmospheric Carbon Dioxide at Mauna Loa Observatory: 2. Analysis of the NOAA GMCC Data, 1974–1985, *J. Geophys. Res.*, 94, 8549–8565, <https://doi.org/10.1029/JD094iD06p08549>, 1989.
- Uglietti, C., Leuenberger, M., and Brunner, D.: European source and sink areas of CO₂ retrieved from Lagrangian transport model interpretation of combined O₂ and CO₂ measurements at the high alpine research station Jungfraujoch, *Atmos. Chem. Phys.*, 11, 8017–8036, <https://doi.org/10.5194/acp-11-8017-2011>, 2011.
- WMO: WMO Global Atmosphere Watch (GAW) Implementation Plan: 2016–2023, Geneva, Switzerland, 81 pp., 2017.
- Zeileis, A. and Grothendieck, G.: zoo: S3 Infrastructure for Regular and Irregular Time Series, *J. Stat. Soft.*, 14, 1–27, <https://doi.org/10.18637/jss.v014.i06>, 2005.
- Zellweger, C., Forrer, J., Hofer, P., Nyeki, S., Schwarzenbach, B., Weingartner, E., Ammann, M., and Baltensperger, U.: Partitioning of reactive nitrogen (NO_y) and dependence on meteorological conditions in the lower free troposphere, *Atmos. Chem. Phys.*, 3, 779–796, <https://doi.org/10.5194/acp-3-779-2003>, 2003.



On the diurnal, weekly, and seasonal cycles and annual trends in atmospheric CO₂ at Mount Zugspitze, Germany, during 1981–2016

Ye Yuan¹, Ludwig Ries², Hannes Petermeier³, Thomas Trickl⁴, Michael Leuchner^{1,5}, Cédric Couret², Ralf Sohmer², Frank Meinhardt⁶, and Annette Menzel^{1,7}

¹Department of Ecology and Ecosystem Management, Technical University of Munich (TUM), Freising, Germany

²German Environment Agency (UBA), Zugspitze, Germany

³Department of Mathematics, Technical University of Munich (TUM), Garching, Germany

⁴Institute of Meteorology and Climate Research, Atmospheric Environmental Research (IMK-IFU),

Karlsruhe Institute of Technology (KIT), Garmisch-Partenkirchen, Germany

⁵Springer Nature B.V., Dordrecht, the Netherlands

⁶German Environment Agency (UBA), Schauinsland, Germany

⁷Institute for Advanced Study, Technical University of Munich (TUM), Garching, Germany

Correspondence: Ye Yuan (yuan@wzw.tum.de)

Received: 14 August 2018 – Discussion started: 30 August 2018

Revised: 19 December 2018 – Accepted: 10 January 2019 – Published: 25 January 2019

Abstract. A continuous, 36-year measurement composite of atmospheric carbon dioxide (CO₂) at three measurement locations on Mount Zugspitze, Germany, was studied. For a comprehensive site characterization of Mount Zugspitze, analyses of CO₂ weekly periodicity and diurnal cycle were performed to provide evidence for local sources and sinks, showing clear weekday to weekend differences, with dominantly higher CO₂ levels during the daytime on weekdays. A case study of atmospheric trace gases (CO and NO) and the passenger numbers to the summit indicate that CO₂ sources close by did not result from tourist activities but instead obviously from anthropogenic pollution in the near vicinity. Such analysis of local effects is an indispensable requirement for selecting representative data at orographic complex measurement sites. The CO₂ trend and seasonality were then analyzed by background data selection and decomposition of the long-term time series into trend and seasonal components. The mean CO₂ annual growth rate over the 36-year period at Zugspitze is 1.8 ± 0.4 ppm yr⁻¹, which is in good agreement with Mauna Loa station and global means. The peak-to-trough amplitude of the mean CO₂ seasonal cycle is 12.4 ± 0.6 ppm at Mount Zugspitze (after data selection: 10.5 ± 0.5 ppm), which is much lower than at nearby measurement sites at Mount Wank (15.9 ± 1.5 ppm) and

Schauinsland (15.9 ± 1.0 ppm), but following a similar seasonal pattern.

1 Introduction

Long-term records of atmospheric carbon dioxide (CO₂) improve our understanding of the global carbon cycle, as well as long- and short-term changes, especially at remote background locations. The longest continuous measurements of atmospheric CO₂ started in 1958 at Mauna Loa, Hawaii, initiated by investigators of the Scripps Institution of Oceanography (Pales and Keeling, 1965). The measurements were performed on the north slope of the Mauna Loa volcano at an elevation of 3397 m above sea level (a.s.l.), thus at long distances from CO₂ sources and sinks. Later, additional measurement sites were established for background studies of global atmospheric CO₂, such as the South Pole (Keeling et al., 1976), Cape Grim, Australia (Beardmore and Pearman, 1987), Mace Head, Ireland (Bousquet et al., 1996), and Baring Head, New Zealand (Stephens et al., 2013). Along with sites located in Antarctica or along coastal/island regions, continental mountain stations offer excellent options to observe background atmospheric levels due to high elevations that are less affected by local influences, for example,

Mount Waliguan, China (Zhang et al., 2013), Mount Cimone, Italy (Ciattaglia, 1983), Jungfrauoch, Switzerland, and Puy de Dôme, France (Sturm et al., 2005).

Although mountainous sites experience less impact from local pollution and represent an improved approach to background conditions compared with stations at lower elevations, we cannot fully dismiss the influence of local to regional emissions. This influence largely depends on air-mass transport and mixing within the moving boundary layer height. Lidar measurements show that air from the boundary layer is orographically lifted to approximately 1–1.5 km above typical summit heights during daytime in the warm season (Carnuth and Trickl, 2000; Carnuth et al., 2002). A 14-year record of atmospheric CO₂ at Mount Waliguan (3816 m a.s.l.), China, reveals significant diurnal cycles and depleted CO₂ levels during summer that are mainly driven by biological and local influences from adjacent regions, although the magnitude and contribution of these influences are smaller than those at other continental or urban sites (Zhang et al., 2013). At the Mt. Bachelor Observatory (2763 m a.s.l.), USA, atmospheric CO₂ variations were studied in the free troposphere and boundary layer separately, where wildfire emissions were observed to drive CO₂ enhancement at times (McClure et al., 2016). However, it still remains unclear to exactly what extent elevated mountain sites are influenced by local activities and how to characterize better local sources and sinks at such stations. It is difficult to make quantitative conclusions on the anthropogenic and biogenic contributions to these measurements (Le Queré et al., 2009). Analyzing weekly periodicity may be a potential indicator since periodicity represents anthropogenic activity patterns during 1 week (7 days) without the influence of natural causes (Cerveny and Coakley, 2002). From the perspective of modeling and satellite observational systems, studies have shown that the weekly variability has implications on the quantification and verification of anthropogenic CO₂ emissions, as well as diurnal variability (e.g., Nassar et al., 2013; Liu et al., 2017). Regarding in situ measurements, results from Ueyama and Ando (2016) clearly indicate the presence of elevated weekday CO₂ emissions compared with weekend and/or holiday CO₂ emissions at two urban sites in Sakai, Japan. Cerveny and Coakley (2002) detected significantly lower CO₂ concentrations on weekends than on weekdays at Mauna Loa, which was assumed to result from anthropogenic emissions from Hawaii and nearby sources.

In this study, we present a composite 36-year record of atmospheric CO₂ measurements (1981–2016) at Mount Zugspitze, Germany (2962 m a.s.l.). The objective of this study is to achieve an improved measurement site characterization with respect to historical CO₂ data in terms of diurnal and weekly cycles, and to produce a consistent overall analysis of CO₂ trend and seasonality. The CO₂ measurements were performed at three locations on Mount Zugspitze: at a pedestrian tunnel (ZPT), at the summit (ZUG), and at the Schneefernerhaus (ZSF) on the southern face of the moun-

tain. In addition, CO₂ measurements were taken at the nearby lower mountain station, Wank Peak (WNK), but for a shorter time period. Short-term variations of weekly CO₂ periodicities and diurnal cycles were evaluated for Mount Zugspitze. In addition, a case study combining atmospheric CO and NO measurements and records of passenger numbers was used to examine weekday–weekend influences. Then the results for the CO₂ annual growth rates and seasonal amplitudes were studied separately via seasonal-trend decomposition and compared with CO₂ data for the comparable time period (1981–2016) at the Global Atmospheric Watch (GAW) regional observatory Schauinsland, Germany (SSL), and the GAW global observatory Mauna Loa, Hawaii (MLO), as well as the global CO₂ means calculated by the NOAA/ESRL and the World Data Centre for Greenhouse Gases (WDCGG).

2 Experimental methods and data

2.1 Measurement locations

Mount Zugspitze is located approximately 90 km southwest of Munich, Germany. The nearest major town is Garmisch-Partenkirchen (GAP; 708 m a.s.l.). Measurements of CO₂ were first performed between 1981 and 1997 at a southward-facing balcony in a pedestrian tunnel (ZPT; 47°25' N, 10°59' E; 2710 m a.s.l.) situated about 250 m below the summit of Mount Zugspitze, which joined the ancient summit station of the first Austrian cable car to the Schneefernerhaus (Reiter et al., 1986). The Schneefernerhaus was a hotel until 1992 when it was rebuilt into an environmental research station. From 1995 until 2001, a new set of measurements were made at a sheltered laboratory on the terrace of the summit (ZUG; 47°25' N, 10°59' E; 2962 m a.s.l.). These two measurement periods were performed by the Fraunhofer Institute for Atmospheric Environment Research (IMK-IFU), and, since 1995 these measurements have been carried out on behalf of the German Environmental Agency (UBA). Since 2001, to continue contributing to the GAW program, CO₂ measurements have been performed at the Environmental Research Station Schneefernerhaus (ZSF; 47°25' N, 10°59' E; 2656 m a.s.l.). Approximately 100 m below the Schneefernerhaus, the glacier plateau Zugspitzplatt can be reached from the valley via cable cars or cogwheel trains. The Zugspitzplatt descends eastward via a moderate to steep slope across the Knorrhütte towards the Reintalangerhütte as shown in Fig. 1 (Gantner et al., 2003).

2.2 Instrumental setup and data processing

CO₂ mole fractions were processed separately because of different measurement locations and time periods at Mount Zugspitze as described above. Information on the first time period (ZPT) was collected based on personal communication with corresponding staff, logbooks, and literature research (Reiter et al., 1986). The CO₂ measurement at ZPT

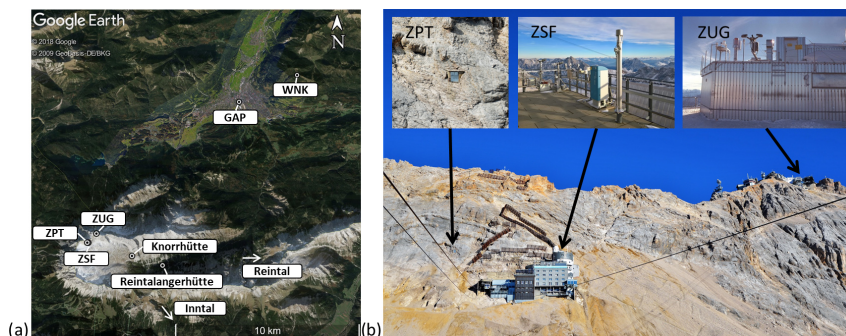


Figure 1. (a) Map showing the study area (GAP – Garmisch-Partenkirchen; WNK – Mount Wank; ZPT – pedestrian tunnel at Mount Zugspitze; ZUG – Zugspitze summit; ZSF – Zugspitze Schneefernerhaus). (b) A photograph showing the locations (ZPT, ZSF, and ZUG) on Mount Zugspitze at which atmospheric CO₂ measurements were performed.

was continuously performed with different instrument models used consecutively (i.e., the URAS-2, 2T, and 3G) employing the nondispersive infrared (NDIR) technique. The measured values were corrected by simultaneously measured air pressure with a hermetically sealed nitrogen-filled gas cuvette due to no flowing reference gas being used. Two commercially available working standards (310 and 380 ppm of CO₂ in N₂) were used for calibration every day at different times. The CO₂ concentration in this gas bottle was compared in short intervals with a reference standard provided by UBA which was adjusted to the Keeling standard reference scale.

At ZUG the sampling line consisted of a stainless steel tube with an inner core of borosilicate glass and a cylindrical stainless steel top cup to prevent intake of precipitation. The inlet was mounted on a small mast (approximately 4 m high) on the top of the laboratory building, which is situated on the Zugspitze summit platform (see Fig. 1b). Inside the laboratory a turbine with a fast real-time fine control ensured a constant sample inflow of 500 L min⁻¹ of in situ air. The borosilicate glass tube (about 10 cm diameter) continued inside the laboratory, providing a number of outlets from which the instruments could get the sample air for their own analyses. The measurement and calibration were performed with a URAS-3G device and an Ansyco mixing box. The mixing controller allowed automatic switching for up to four calibration gases and sampling air by a self-written calibration routine using Testpoint software. The linear two-point calibration enveloping the actual ambient values with low and high CO₂ concentrations was taken every 25th hour. Every 6 months the working standards were checked and readjusted, when required, according to the standard reference scale using intercomparison measurements with the station standards.

At ZSF the same construction principle was applied for atmospheric sampling. There, the mast height is about 2.5 m

above the pavement of the research terrace on the fifth floor at an altitude of 2670 m a.s.l. Measurements of CO₂ at Schneefernerhaus continued thereafter until the present with a modified HP 6890 using a gas chromatograph (GC), with an intermediate upgrade in 2008 (Bader, 2001; Hammer et al., 2008; Müller, 2009). In 2012 and 2013, because of an instrumental failure of the GC, CO₂ data were recorded with a cavity ring-down spectrometer (CRDS; Picarro EnviroSense 3000i) connected to the same air inlet, which had been installed in parallel since 2011. The GC calibrations were carried out at 15 min intervals using working standards (near-ambient), which had been calibrated with station standards from the GAW Central Calibration Laboratory (CCL) operated by the NOAA/ESRL Global Monitoring Division. The GC data acquisition system (see Supplement Fig. S1) produced a calibration value every 15 min and two values from the sampled air based on one chromatogram every 5 min. For continuous quality assurance the GC was checked daily for flows, retention times, gas pressures, and the structure of chromatograms. Calibration factors and metadata were used to convert raw data into the final data product. Invalid and unrepresentative data due to local influences were flagged according to a logged list of local pollution from working activities in the research station. The measurement quality was controlled by comparison with simultaneous measurements of identical gas (CRDS) or with measurements of other trace substances and meteorological data, and additional support from station logbooks and checklists. The data were flagged according to quality control results. In principle, the acquisition system stores all measured data (flagged or not) and never discards them. Drifts in the working standards were controlled by a second target (measured approximately 25 times per day) and a regular 2-month intercomparison between the working standard and NOAA station standards, performing corrections as needed. Calibration for CRDS was performed automatically, with three different concentrations

every 12 h. Until 2013 the calibrations were performed automatically every 24 h with one concentration, very close to the ambient value. Every 2 months the concentrations were rechecked according to the station reference standards.

Additional atmospheric CO₂ measurements throughout the GAP area were performed between 1978 and 1996 at Mount Wank summit (WNK; 47°31′ N, 11°09′ E; 1780 m a.s.l.) using a URAS-2T instrument. Wank Observatory is located in an alpine grassland just above the tree line (Reiter et al., 1986; Slemr and Scheel, 1998). Detailed information on the CO₂ measurements at Schauinsland (SSL; 47°55′ N, 7°54′ E; 1205 m a.s.l.) and Mauna Loa, Hawaii (MLO; 19°28′ N, 155°35′ W; 3397 m a.s.l.), which we use to compare the results of this study with, can be found in Schmidt et al. (2003) for SSL and Thoning et al. (1989) for MLO. The CO₂ data from these measurement sites and from Mount Zugspitze locations were considered as validated data set (Level 2: calibrated, screened, and artefacts and outliers removed), without any further data processing prior to the selection of representative data. The different instruments and calibration scales used at each location are summarized in Table 1.

2.3 Offset adjustment

According to NOAA CMDL (http://ds.data.jma.go.jp/wcc/co2/co2_scale.html; last access: 23 January 2019), no significant offsets are documented between the calibration scales WMO X74 and WMO X85 and the current WMO mole fraction scale. However, for the 3-year parallel CO₂ measurements at ZPT and ZUG (1995–1997), clear offsets of -5.8 ± 0.4 ppm (CO_{2,ZPT} minus CO_{2,ZUG}, 1 SD) were observed. The major reason for this bias is assumed to be the pressure-broadening effect in the gas analyzers used and the different gas mixtures used in the standards (Table 1), CO₂/N₂ vs. CO₂/air, the so-called “carrier gas correction” (CGC) (Bischof, 1975; Pearman and Garratt, 1975). It is known from previous studies that the measured CO₂ concentration, when using CO₂/N₂ mixtures as reference, is usually underestimated by several parts per million for the URAS instruments, and such offsets vary from different types of analyzers (Pearman, 1977; Manning and Pohl, 1986). The carrier gas effect varies even between the same type of analyzer as well as with replacement of parts of the analyzer (Griffith et al., 1982; Kirk Thoning, personal communication, 1 August 2018). Since we have insufficient information to determine a physically derived correction to the ZPT CO₂ data, an offset adjustment was made for further analyses based on the offsets in data computed in the overlapping years. A single correction factor

$$G = 0.956 + 0.00017 \cdot C_{ZPT} \quad (1)$$

was applied to the ZPT data, where C_{ZPT} denotes the CO₂ concentrations at ZPT. Because of the same calibration mixtures, an additional adjustment was applied to the CO₂ con-

centrations at WNK by calculating the CO₂ differences between ZPT and WNK. A detailed description on the offset adjustment of CGC with potential errors is given in the Supplement. Two similar CGCs by Manning and Pohl (1986) at Baring Head, New Zealand, and Cundari et al. (1990) at Mt. Cimone, Italy, were comparable in magnitude to our offset adjustment.

On the other hand, there were 9 consecutive months, from April to December 2001, of parallel atmospheric CO₂ measurements at both ZUG and ZSF, based on which an inter-comparison between the two series was made. The offset between these two records attained an average of 0.1 ± 0.4 ppm (CO_{2,ZUG} minus CO_{2,ZSF}, 1 SD), which fulfills the requirement of the GAW data quality objective (DQO; ± 0.1 ppm) for atmospheric CO₂ in the Northern Hemisphere. Therefore, no adjustments regarding this offset were applied to the data sets.

In this study, we took CO₂ measurements during the corresponding time intervals at ZPT (1981–1994), ZUG (1995–2001), and ZSF (2002–2016) to assemble a composite time series for Mount Zugspitze over 36 years. Nevertheless, we always treat measurements from each location separately for further analyses. At WNK, as well as at SSL and MLO, we used measured CO₂ data starting from 1981 for time consistency with measurements at Mount Zugspitze.

2.4 ADVS data selection

Adaptive diurnal minimum variation selection (ADVS), a recently published, novel statistical data selection strategy, was used to ensure that the data were clean and consistent with respect to the state of a locally unaffected lower free troposphere at the measurement sites (Yuan et al., 2018). ADVS, which was originally designed to characterize mountainous sites, selects data based on diurnal patterns, with the aim of selecting optimal data that can be considered representative of the lower free troposphere. To achieve this, variations in the mean diurnal CO₂ were first evaluated and a time window was selected based on minimal data variability around midnight, at which point data selection began. The data outside the starting time window were examined on a daily basis both forward and backward in time for the day under consideration, by applying an adaptive threshold criterion. The selected data represent background CO₂ levels at the different measurement sites.

ADVS data selection was applied to all CO₂ records based on the same threshold parameters, followed by examining the starting time window and calculating the percentages of the ADVS-selected data. Figure 2a shows the CO₂ time series before and after ADVS data selection. We also evaluated the starting time windows resulting from ADVS data selection with the detrended mean diurnal cycles as described in Yuan et al. (2018) for each measurement site in Fig. 2b. The number of ADVS-selected data is summarized as percentage per

Table 1. Detailed description of atmospheric CO₂ measurement techniques (NDIR is the nondispersive infrared, GC is gas chromatography, and CRDS is cavity ring-down spectroscopy). At ZSF, CO₂ data from GC measurements were not available from 2012 to 2013 due to an instrumental failure; thus data from CRDS measurements were used in these 2 years for this study. However, CRDS measurements were performed in parallel from the same air inlet from 2011.

ID	Time period	Instrument (analytical method)	Scale	Calibration gas
ZPT	1981–1997	1981–1984: Hartmann & Braun URAS 2 (NDIR) 1985–1988: Hartmann & Braun URAS 2T (NDIR) 1989–1997: Hartmann & Braun URAS 3G (NDIR)	WMO X74 scale	CO ₂ in N ₂
ZUG	1995–2001	Hartmann & Braun URAS 3G (NDIR)	WMO X85 scale	CO ₂ in natural air
ZSF	2001–2016	2001–2016: Hewlett Packard Modified HP 6890 Chem. station (GC) 2012–2013: Picarro EnviroSense 3000i (CRDS)	WMO X2007 scale	CO ₂ in natural air
WNK	1981–1996	Hartmann & Braun URAS 2T (NDIR)	WMO X74 scale	CO ₂ in N ₂

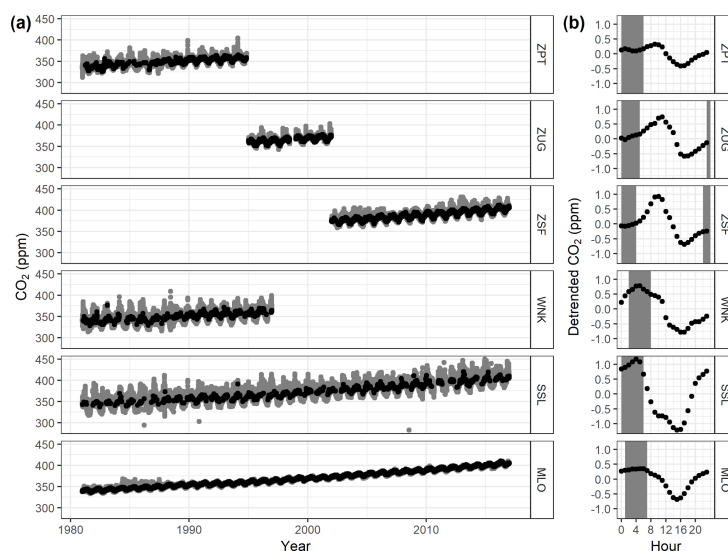


Figure 2. (a) Time series plot of 30-min averaged CO₂ concentrations measured at Mount Zugspitze (ZPT, ZUG, and ZSF) and Wank (WNK), and hourly averaged CO₂ concentrations measured at Schauinsland (SSL) and Mauna Loa (MLO) with ADVS selection. Grey and black colors are used for the unselected and selected results. (b) Detrended mean diurnal cycles with starting time windows (in grey) for ADVS data selection.

hour in the total number of all CO₂ data in Fig. 3. A detailed description and discussion is given in Sect. 3.1.

2.5 Mean symmetrized residual

Weekly periodicity was calculated using the mean symmetrized residual (MSR) method, which was originally applied to atmospheric CO₂ data (Cerveny and Coakley, 2002). The MSR method focuses on variations in mean values for the days of the week. Daily deviations from the 7-day (consecutive) averages are calculated without ADVS selection to account for the most likely emission cycles. Then, the MSR values are derived by averaging the differences for each sin-

gle day. Additionally, only the MSR values with no data gaps in all the seven differences are considered as valid. Finally, all the MSR values are aggregated into overall mean values for each day of the week. In addition, the MSR values are standardized so that the sum of all the seven values is equal to 0 (Cerveny and Coakley, 2002).

2.6 STL decomposition

The seasonal-trend decomposition technique (STL) was applied to decompose the CO₂ time series into trend, seasonal, and remainder components individually (Cleveland et al., 1983, 1990), which, in previous studies, has been

a commonly applied method (e.g., Stephens et al., 2013; Hernández-Paniagua et al., 2015). Locally weighted polynomial regressions were iteratively fitted to all monthly values in both an outer and an inner loop. According to Cleveland et al. (1990) and Pickers and Manning (2015), we set the trend and seasonal smoothing parameters to 25 and 5, respectively. The CO₂ time series at each site or location were aggregated into monthly averages and, then, decomposed using STL. Missing monthly values were substituted using spline interpolation.

To study the trend and seasonality, we firstly intended to apply STL decomposition to the ADVS-selected time series. However, due to multiple occurrences of consecutively missing values in the ADVS-selected monthly averages, especially for measurement sites at lower elevations (WNK and SSL), it was more practical to use the original CO₂ time series without ADVS data selection for STL decomposition, to preserve time series continuity (Pickers and Manning, 2015). There is one missing 6-month time interval at ZUG in 1998 (July to December). Thus STL was performed separately for the time periods before (January 1995–June 1998) and after (January 1999–December 2001) the gap. Nevertheless, we still applied STL decomposition to the ADVS-selected data sets from Mount Zugspitze and Mauna Loa, since these selected time series were applicable. At ZPT, due to larger time gaps of missing data at the beginning (1981 and 1982) of the ADVS-selected data set, the ADVS-selected and STL-decomposed results were only studied starting from 1983. Individual figures of each STL-decomposed component at all stations can be found in the Supplement.

For annual growth rates we did not include the WNK time series due to shorter time periods of available data. Monthly trend components were first aggregated into annual mean values. Then, the annual CO₂ growth rates were calculated as the difference between the CO₂ value of the current year and the value from the previous year (Jones and Cox, 2005). The mean seasonal cycle was aggregated directly from the monthly seasonal components by month. To observe potential deviations on the regional and global scale, we compared the trend and seasonality derived from the STL-decomposed components at Zugspitze with other measurement sites. We included the globally averaged marine surface monthly mean data from NOAA (<https://www.esrl.noaa.gov/gmd/ccgg/trends/>; last access: 23 January 2019) and data for the global mean mole fractions from WDCGG (WMO Greenhouse Gas Bulletin, 2018) as references, and processed these data based on the identical STL decomposition routine. All the statistical analyses described above (including ADVS, MSR, and STL) were performed in the R environment (R Core Team, 2018).

3 Results and discussion

3.1 ADVS selection and diurnal variation

The resulting ADVS-selected CO₂ data showed a clear linkage of the percentage of selected data and the altitude of the measurement site. Among the continental stations, the percentage increased with altitude. A lower percentage indicates higher data variability due to lower elevation and proximity to local sources and sinks. At Schauinsland, the percentage of CO₂ data by the ADVS selection was 6.3 %, while the percentages at Mount Zugspitze reached 9.9 % (ZPT), 19.5 % (ZUG), and 13.6 % (ZSF), respectively. A moderate percentage of 6.3 % was also derived at Mount Wank. However, regarding the elevated mountain station Mauna Loa on the island of Hawaii, a much higher percentage (40.0 %) of CO₂ data was selected using ADVS as being representative of its background concentration, mainly due to the very limited nearby anthropogenic sources as well as mostly clean, well-mixed air arriving there. A similar result for an island mountain station can be found in Yuan et al. (2018), in which a percentage of 36.2 % was computed for the CO₂ measurements at Izaña station on the island of Tenerife (28° 19' N, 16° 30' E; 2373 m.a.s.l.). This can also be explained by the detrended mean diurnal cycles shown in Figs. 2b and 3. The mean diurnal cycle at MLO only exhibits a clear trough during daytime, especially starting from 12:00 local time (LT), which is believed to be influenced by the vegetation activity (photosynthesis) in the surroundings. The same effect can be seen at WNK and SSL, but with larger magnitudes and earlier occurrences of the minima because of their lower locations closer to CO₂ sinks. In contrast, at these two sites the CO₂ maxima in the diurnal cycles were not as clearly noticeable as at Mount Zugspitze due to anthropogenic sources and high biogenic respiration. At the three locations on Mount Zugspitze, the CO₂ peaks in the mean diurnal cycles are driven by the late-morning convective upslope wind, which was relatively obvious at both ZUG and ZSF. However, from the perspective of data selection, a significantly higher percentage of CO₂ data was selected at ZSF compared with ZPT, although there is only a small difference in altitude of around only 70 m. This proves that ZSF is capable of capturing more background conditions than ZPT during the day. Nevertheless, based on the starting time window computed for ADVS selection, we found that, in general, most stations exhibited similar starting time windows beginning around midnight, and the ADVS data selection was applied systematically by including more data around these hours (see Fig. 3), which confirmed our assumption of background conditions during midnight for the ADVS data selection (Yuan et al., 2018).

3.2 Weekly periodicity

For a better characterization of the differences among the measurement locations at Mount Zugspitze, the mean CO₂

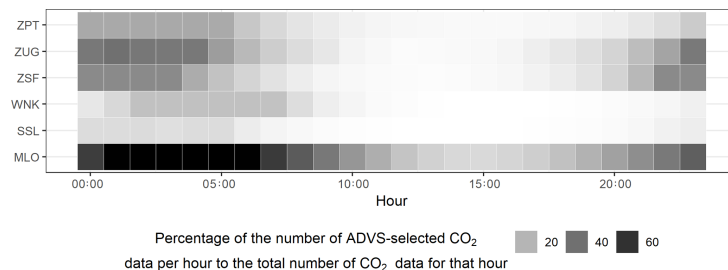


Figure 3. Frequency of the percentages of the number of ADVS-selected CO₂ data for each hour (0 to 23) in the total number of CO₂ data for that hour as shown in greyscale.

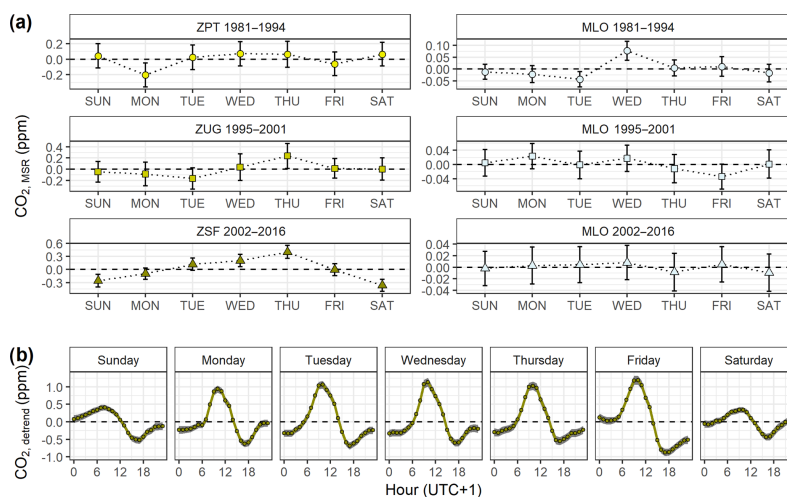


Figure 4. (a) Mean MSR CO₂ values at Mount Zugspitze and MLO as a function of the day of the week. Mean MSR values are adjusted such that they sum to 0. (b) Detrended mean CO₂ diurnal cycles at ZSF by day of the week from 2002 to 2016. Uncertainties at the 95% confidence interval are shown by the shaded areas.

weekly cycles were analyzed as a function of mean MSR values (see Fig. 4a). The mean MSR values at the MLO for the corresponding time intervals were also calculated. Most weekly cycles exhibited no clear peaks or patterns for both sites. However, the magnitude of MSR data variability is mostly higher at Zugspitze, with a maximum on Thursdays. The only significant weekday–weekend difference is observed at ZSF in terms of the 95% confidence interval, which shows weekly maxima and weekly minima on Thursday and Saturday, respectively (peak-to-trough difference: 0.76 ppm). Gilge et al. (2010) observed similar phenomena when studying O₃ and NO₂ concentrations at Alpine mountain stations, including Zugspitze. Clear weekly cycles, with enhanced O₃ levels on working days, were observed at ZSF in summer, with weekly maxima and minima on Thursdays and Sundays, respectively. For NO₂, maximum mixing ratios

on working days and minimum ratios on Sundays at neighboring stations were observed, generally suggesting an anthropogenic impact at all elevations.

We obtained more insights into the weekly CO₂ cycle at Mount Zugspitze by comparing the mean diurnal cycles of weekdays and weekends (see Fig. 4b). Detrended mean diurnal cycles at ZSF, from Sunday to Saturday, were calculated by subtracting the daily averages from the daily data between 2002 and 2016. In the morning around 09:00 to 10:00 LT the CO₂ levels at ZSF are higher on weekdays than weekends, while CO₂ diurnal patterns during the rest of the week are relatively stable. Such weekly cycles are not observable at ZPT and ZUG, nor at WNK and SSL (see Fig. S18). At ZPT, there are fewer variations in the diurnal cycle compared to ZSF, indicating that this location does not receive the effect of regular local anthropogenic working activities and hence it

is more representative of lower free tropospheric conditions regarding this aspect. The weekday–weekend differences at ZSF are possibly due to local working patterns, whereas the absence of this pattern at lower sites may indicate influences from a more regional reservoir. In fact, ZSF is closed on the weekends and, thus, is influenced by less immediate anthropogenic activities.

3.3 Case study on atmospheric CO and NO and passenger numbers at Zugspitze

To study the potential sources and sinks for such weekday–weekend differences in the CO₂ diurnal cycles at ZSF further, we analyzed atmospheric CO and NO data at ZSF and the daily combined number of cable car and train passengers to Zugspitzplatt and to the Zugspitze summit in 2016. Atmospheric CO and NO are known to be good indicators of local anthropogenic influences due to highly variable short-term signals and are thus helpful to identify potential CO₂ sources (Tsutsumi et al., 2006; Sirignano et al., 2010; Wang et al., 2010; Liu et al., 2016). In this study, we used atmospheric NO due to its short lifetime based on rapid atmospheric NO₂ formation with resulting altitude-dependent O₃ surplus, indicating the presence of sources at closer distances. The CO and NO data shown in Fig. 5 include data that were flagged during data processing because for the delivery to GAW World Data Centres the logged and recognized work-dependent concentration peaks are flagged. A clear weekday–weekend difference is observed for both CO and NO. Only weekdays are characterized by multiple short-term atmospheric CO events and higher atmospheric NO peaks during the daytime (mostly around 09:00 LT), which fits perfectly with daytime peaks in CO₂ diurnal cycles. A general fluctuating pattern in NO throughout the week is thought to originate from heating of the Zugspitzplatt and changing work with combustion engines. On the other hand, the daily number of passengers at Zugspitze (see Fig. 5c) shows a clear weekday–weekend pattern, with a higher number of passengers on the weekends. However, increased numbers of passengers on the weekends do not correspond to higher levels of CO and CO₂, indicating that measured CO₂ levels are not significantly influenced by tourist activities nearby. Instead, it is more likely that anthropogenic working activities are the main driver of weekly periodicity.

3.4 Trend

Based on the STL-decomposed results, the mean annual growth rate of the 36-year composite record at Mount Zugspitze from the three measurement locations is 1.8 ± 0.4 ppm yr⁻¹, which is consistent with the SSL (1.8 ± 0.4 ppm yr⁻¹), MLO (1.8 ± 0.2 ppm yr⁻¹), and global means (NOAA: 1.8 ± 0.2 ppm yr⁻¹; WDCGG: 1.8 ± 0.2 ppm yr⁻¹). The mean annual growth rates from the ADVS-selected data sets at Mount Zugspitze and Mauna Loa also result in the

identical value of 1.8 ppm yr⁻¹. Then, we divided the entire time period (1981–2016) into three time blocks, corresponding to the different locations at Mount Zugspitze, in order to observe potential differences with respect to other sites separately (see Table 2). The results show good agreement of each location on Mount Zugspitze with other measurement sites (also for the ADVS-selected results) as well as a clearly increasing trend of the annual growth rates over these three time blocks. Only the mean annual growth rate between 1995 and 2001 at ZUG is obviously lower than at the other sites. This can be explained by the missing monthly values in 1998, and thus in turn the annual growth rates of 1998 and 1999 were left out for the average. However, the annual growth rates of these 2 years reached anomalous peaks at most sites (see details later in Sect. 3.6). Möller (2017) also mentioned that 1981 to 1992 growth rates at both German stations and MLO were identical.

3.5 Seasonality

For the overall seasonality, Fig. 6 presents the mean seasonal cycles for the STL-decomposed seasonal components. We observed similar patterns in the SSL and WNK seasonal cycles, with mean peak-to-trough amplitudes of 15.9 ± 1.0 and 15.9 ± 1.5 ppm, respectively. The composite data set at Mount Zugspitze results in a lower amplitude (12.4 ± 0.6 ppm), but still exhibits a similar seasonality influenced by active biogenic processes (mainly photosynthesis) in summer compared with SSL and WNK (Dettinger and Ghil, 1998). As vegetation grows with rising temperatures (approaching summer), CO₂ levels decrease due to more and more intense photosynthetic activities till a minimum in August. In addition, with rising temperatures, locally influenced air masses reach Mount Zugspitze more often due to “Alpine pumping” (Carnuth et al., 2002; Winkler et al., 2006). As such, air sampled in summer is more frequently mixed with air from lower levels, which is characterized by lower CO₂ concentrations, intensifying the August minimum. Anthropogenic activities and plant respiration dominate the increases in concentration in the winter (January to April). This influence appears to be stronger at SSL and WNK than at Mount Zugspitze. Lower levels of CO₂ and a 1-month delay, from February to March, of the seasonal maximum at Mount Zugspitze are in agreement with the expectation of thermally driven orographic processes that drive the upward transport of CO₂ from local sources, as well as limited human access to Mount Zugspitze and the prevailing absence of biogenic activities at such high elevations. Regarding the resulting seasonal cycles based on ADVS-selected Zugspitze data sets, similar patterns were observed but with a lower amplitude (10.5 ± 0.5 ppm) as well as a 2-month shift of the seasonal maximum to April.

The Mauna Loa CO₂ record is characterized by a seasonal maximum in May and a minimum in September, with a peak-to-trough amplitude of 6.8 ± 0.1 ppm, which agrees with observations from Dettinger and Ghil (1998) and Lint-

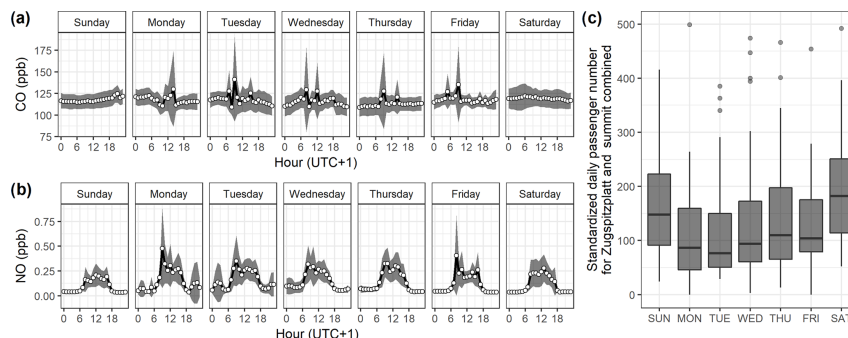


Figure 5. Mean diurnal plots at ZSF during 2016 by day of the week for (a) CO and (b) NO, and (c) the standardized daily passenger number at the Zugspitzplatt and Zugspitze summit combined.

Table 2. Mean annual CO₂ growth rates in ppm yr⁻¹ at the 95 % confidence interval based on three time blocks for all measurement sites/locations studied (SSL – Schauinsland; WNK – Mount Wank; ZPT – pedestrian tunnel at Mount Zugspitze; ZUG – Zugspitze summit; ZSF – Zugspitze Schneefernerhaus; MLO – Mauna Loa; WDCGG and NOAA – global means). ADVS means the data were selected using the ADVS method. This comparison refers to data from all years including the corresponding time period for all stations. Measurement sites or locations where data are not available for calculating the corresponding time blocks are shown by “–”.

Time block	SSL	WNK	ZPT	ZPT ADVS	ZUG	ZUG ADVS	ZSF	ZSF ADVS	MLO	MLO ADVS	WDCGG	NOAA
1981–1994	1.5 ± 0.5	1.4 ± 1.1	1.5 ± 0.8	1.5 ± 1.4	–	–	–	–	1.4 ± 0.3	1.4 ± 0.3	1.4 ± 0.4	1.4 ± 0.3
1995–2001	1.7 ± 1.1	–	–	–	1.3 ± 0.8	1.5 ± 0.5	–	–	1.8 ± 0.5	1.8 ± 0.5	1.8 ± 0.4	1.7 ± 0.5
2002–2016	2.2 ± 0.7	–	–	–	–	–	2.2 ± 0.4	2.2 ± 0.4	2.2 ± 0.2	2.2 ± 0.2	2.2 ± 0.2	2.2 ± 0.2

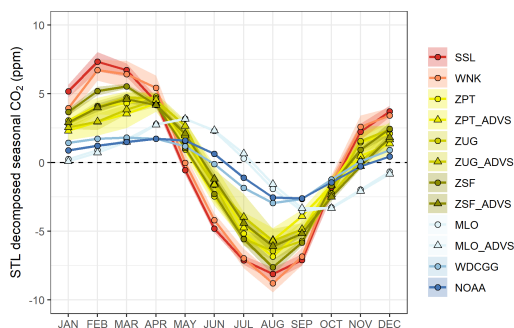


Figure 6. Mean CO₂ seasonal cycles from the STL seasonal component at each measurement site or location. Uncertainties at the 95 % confidence interval are shown by the shaded areas with corresponding colors.

ner et al. (2006). The ADVS-selected results for MLO also show a similar pattern, with a lower amplitude of 6.6 ± 0.1 ppm. Global means exhibited the lowest seasonal amplitudes, 4.4 ± 0.1 ppm (NOAA) and 4.8 ± 0.0 ppm (WDCGG). Compared with WDCGG, the NOAA global mean better fits the seasonal cycle of MLO supporting the presence of a typ-

ical marine boundary layer (MBL) condition for the levels of background CO₂ in the atmosphere. On the other hand, the WDCGG global mean includes continental characteristics for its calculation, thus exhibiting a slightly more continental signature which can be equally seen in the seasonal cycles at continental sites, such as Mount Zugspitze. April and October appear to be the important months that indicate the switch of either CO₂ source to sinks or vice versa for the continent.

We then examine in more detail the seasonal cycles at ZPT, ZUG, and ZSF. Despite the close proximity, there are differences in their seasonal amplitudes (ZPT: 11.9 ± 1.2 ppm; ZUG: 11.2 ± 1.0 ppm; ZSF: 13.3 ± 0.7 ppm). Good agreement is shown between CO₂ seasonal cycles from April to June and from October to December. However, significantly higher levels of CO₂ were evident at ZSF from January to March as well as lower levels from July to September. After data selection with lower seasonal amplitudes of 10.3 ± 1.3 (ZPT_ADVS), 10.3 ± 1.2 (ZUG_ADVS), and 10.9 ± 0.6 ppm (ZSF_ADVS), similar differences of the CO₂ levels in the seasonal cycles could be observed. These results indicate that factors such as elevation and measurement surroundings strongly determine the air-mass composition via local vertical transport. The amount of air-mass transport via orographic lifting affects the three locations differently. The

lower elevation station, ZSF, apparently captures more mixed air masses due to a daytime up-valley flow along the Reintal (Gantner et al., 2003) as well as a slightly southeastern flow from the Inntal (see Fig. 1) that is less frequent for the higher locations (ZPT or ZUG). In addition, comparably postponed seasonal maxima at ZUG and ZPT from March to April show delayed onset of convective upwind air-mass transport and changing planetary boundary layer (PBL) compositions. On the other hand, these differences in the seasonal amplitudes (even though not significant at the 95 % confidence interval) might be influenced by a potential trend in the seasonal amplitude over time. Such increasing trends of the seasonal CO₂ amplitudes (i.e., +0.32 % yr⁻¹ at Mauna Loa and +0.60 % yr⁻¹ at Utqiagvik, formerly Barrow, Alaska) were studied in Graven et al. (2013), indicating an enhanced interaction between the biospheric and atmospheric CO₂ across the Northern Hemisphere.

3.6 Interannual variation

To study the interannual variability, we focused on the percentages of ADVS selection, the growth rates, and the seasonal amplitudes. The annual percentages from ADVS data selection are shown for years without missing monthly averages (see Fig. 7a). An exceptionally high percentage at Zugspitze in 2000 resulted from careful and intensive filtering of the original CO₂ data. The total number of original validated 30 min data points in 2000 is only 4634, while the number of data for other years ranges from 8754 to 15 339 (except for 1998, with only 6-month data, the total number of 30 min CO₂ data is 6441). As described in the previous section, the annual growth rates are plotted in Fig. 7b. The annual CO₂ seasonal amplitudes are calculated as the difference between the yearly maximum and minimum monthly CO₂ values from the STL-decomposed seasonal components (see Fig. 7c).

Focusing on the annual percentages from ADVS-selected representative data after 1990, we calculated the mean annual percentages at Mount Zugspitze locations, for the time periods between 1990 and 2001 (2000 was not included for ZUG) and 2002 and 2016. We observe significantly higher percentages at ZPT and ZUG (18.5 ± 2.4 %) than at ZSF (13.6 ± 1.1 %) at the 95 % confidence interval. These percentages are different from SSL (4.2 ± 0.5 % vs. 4.2 ± 0.6 %) and MLO (43.5 ± 1.4 % vs. 42.1 ± 1.6 %). A likely explanation is that there are systematically different air-mass transport characteristics reaching each of these locations. Higher percentages at ZPT and ZUG indicate that these locations are capable of capturing more air masses that have traveled over long distances along the mountains. These air masses trap air that ascends from many Alpine valleys, but also from remote source regions up to the intercontinental scale (Trickl et al., 2003; Huntrieser et al., 2005). On the other hand, ZSF is dominated by mixing air masses that have traveled along the Zugspitzplatt area, which contain higher levels of

CO₂ due to daily, local anthropogenic sources during winter and convective upwind transport during seasons without snow cover that are characterized by lower concentrations of CO₂ at lower altitudes. Such patterns in the data are also evident in the annual growth rates and seasonal amplitudes. The overall patterns at Mount Zugspitze agree with SSL and WNK. However, SSL and WNK exhibit more variation in the annual growth rates and higher seasonal amplitude levels (see Fig. 7b and c). In addition, slightly higher seasonal amplitudes for the WDCGG global mean compared with the NOAA one can be explained by the WDCGG global mean calculation method, which includes more continental stations (WMO Greenhouse Gas Bulletin, 2018).

Anomalies in the annual growth rates are frequently observed, which are possibly explained by climatic influences such as the El Niño–Southern Oscillation (ENSO), volcanic activity, and extreme weather conditions (Keeling et al., 1995; Jones and Cox, 2001; Francey et al., 2010; Keenan et al., 2016). One of the largest positive annual growth rate anomalies occurred in 1998 and is clearly seen in all the records (aside from ZUG with missing values), which is attributed to a strong El Niño event (Watanabe et al., 2000; Jones and Cox, 2005). Similar signals are found in 1988, especially at MLO and in global means. Such anomalies are more clearly observed in the global and seaside time series. Regarding continental sites, interannual signals may be hidden by more intense land influences rather than global effects. Moreover, positive consecutive anomalies between 2002 and 2003 are clearly observed at ZSF and SSL, which are potentially due to anomalous climatic conditions, such as the dry European summer in 2003 that led to an increasing number of forest fires. These events are also observable in the MLO and global means but at a smaller scale (Jones and Cox, 2005). At all German sites, clear negative anomalies, due to violent eruptions of the El Chichón and Mt. Pinatubo volcanoes and the subsequent volcanic-induced surface cooling effect are observed after stratospheric aerosol maxima above Garmisch-Partenkirchen in 1983 and 1992, respectively (Lucht et al., 2002; Frölicher et al., 2011, 2013; Trickl et al., 2013). This effect is only slightly visible in the MLO and global means despite the fact that volcanic aerosols spread over the entire globe.

However, the reasons for some anomalies are still unclear. These include the negative anomalies during 1985 and 1986 at all German sites. Certain anomalies in the annual percentages and seasonal amplitudes also derive from extremely low ADVS selection percentages beginning in 1984 and continuing until 1990, with peaks in seasonal amplitudes between 1985 and 1986. This is the reason why we calculated the mean annual ADVS selection percentage beginning at 1990. We assume that local influences mask similar physical mechanisms at the sites. However, annual percentages at the MLO also have similar characteristics. Therefore, it is still unclear what triggers such distinct interannual data variability across measurement sites. Another clear negative annual

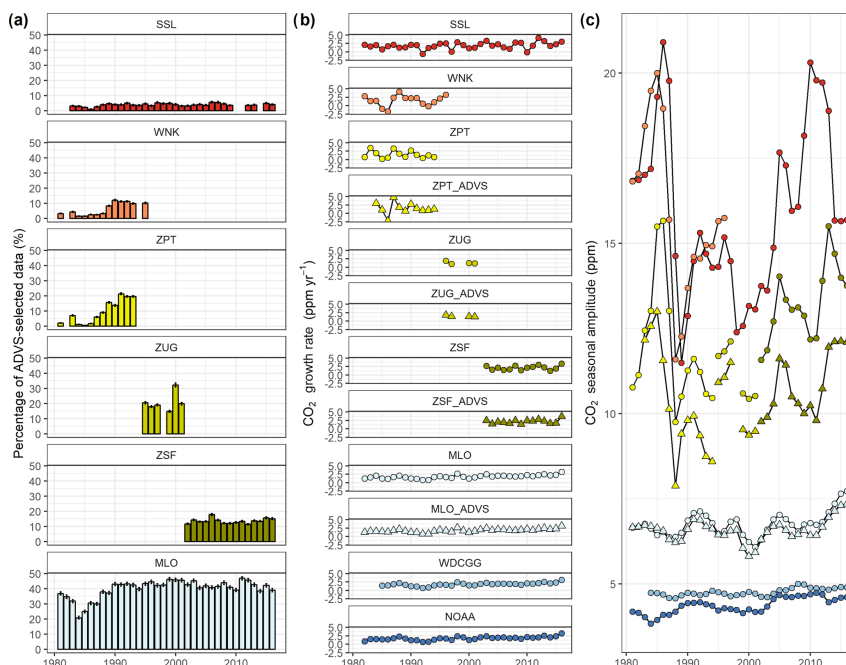


Figure 7. (a) Annual ADVS-selected percentages. (b) Annual CO₂ growth rates and global means from the NOAA and the WDCGG. The calculated growth rates are shown at the beginning of the year. Since the time period starts in 1981, the values of growth rates start in 1982. WDCGG data are only available starting in 1984. (c) Annual CO₂ seasonal amplitudes.

growth rate anomaly occurred in 2014 across all sites. Such anomalies still require further investigation, but are beyond the scope of this study.

4 Conclusions

In this study, we presented a time series analysis of a 36-year composite CO₂ measurement record at Mount Zugspitze in Germany, together with a thorough study of the weekly periodicity combined with diurnal cycles. Even though it is challenging to quantify local sources and sinks, this study shows that it is possible to gain information on variation in this regard. Compared with the GAW regional observatories at Schauinsland and Wank Peak, as well as the GAW global observatory at Mauna Loa, Mount Zugspitze proves to be a highly suitable site for monitoring the background levels of air components using proper data selection procedures. The long-term trend at Zugspitze agrees well with that at Mauna Loa and global means. The seasonality and short-term variations show similar patterns, but are considerably less influenced by local to regional mechanisms than the lower elevation stations at Schauinsland and Wank Peak. Interannual variations also correlate well with anomalous global events.

However, several anomalies still exist across most stations that lack clear explanations. These anomalies require further investigation, possibly by analyzing correlations between extreme events and historical meteorological or hydrological data. Finally, we conclude that, at Zugspitze, we cannot neglect local to regional influences. Regarding the seasonal amplitude, Mount Zugspitze is significantly more influenced by biogenic activity, mostly in the summer, compared with Mauna Loa and global means. On the other hand, the weekly periodicity analysis provides a clear picture of local CO₂ sources that potentially result from human working activities, especially at ZSF. Overall, this study provides detailed insights into long-term atmospheric CO₂ measurements, as well as site characteristics at Mount Zugspitze. We propose the application of this type of analysis as a systematic tool for the physical and quantitative classification of stations with respect to their lower free tropospheric representativeness. As an additional component in this analysis, weekly periodicity can be used to analyze anthropogenic influences. The systematic application of this approach to larger continental or global regions can serve as a basis for more quantitative analyses of global greenhouse gases trends such as CO₂. Based on the physical foundation of the methodology pre-

sented here, we suggest that these techniques can be applied to other greenhouse gases such as SF₆, CH₄, and aerosols.

Data availability. NOAA global mean data are available at ftp://aftp.cmdl.noaa.gov/products/trends/co2/co2_mm_gl.txt (last access: 23 January 2019).

WDCGG global mean data are available at https://gaw.kishou.go.jp/publications/global_mean_mole_fractions (WDCGG, 2019a).

CO₂ records (also including CO and NO) of all GAW observatories which were used in this study are available from the World Data Centre for Greenhouse Gases (WDCGG) at <https://gaw.kishou.go.jp/> (WDCGG, 2019b).

The daily passenger number data for Zugspitze were provided by the Bayerische Zugspitzbahn railway company.

Supplement. The supplement related to this article is available online at: <https://doi.org/10.5194/acp-19-999-2019-supplement>.

Author contributions. YY, LR, HP, and AM designed the study and YY performed the data analyses with help from LR and HP for the data processing and code validation. Atmospheric measurement data were collected, preprocessed, and provided by LR, TT, CC, RS, and FM. Information about data quality assurance and measurement site was provided by LR. YY prepared the manuscript with contributions from all co-authors.

Competing interests. The authors declare that they have no conflict of interest.

Special issue statement. This article is part of the special issue “The 10th International Carbon Dioxide Conference (ICDC10) and the 19th WMO/IAEA Meeting on Carbon Dioxide, other Greenhouse Gases and Related Measurement Techniques (GGMT-2017) (AMT/ACP/BG/CP/ESD inter-journal SI)”. It is a result of the 19th WMO/IAEA Meeting on Carbon Dioxide, Other Greenhouse Gases, and Related Measurement Techniques (GGMT-2017), Empa Dübendorf, Switzerland, 27–31 August 2017.

Acknowledgements. This study was supported by a scholarship from the China Scholarship Council (CSC) under grant CSC no. 201508080110. We acknowledge support from a MICMoR fellowship through the KIT/IMK-IFU to Ye Yuan. Our thanks go to Gourav Misra for the geographical map of the measurement locations. Our thanks go to James Butler and Kirk Thoning from NOAA for their indispensable discussions on the problematic nature of representing and comparing data on different older and current CO₂ scales. The CO₂, CO, and NO measurements at Zugspitze Schneefernerhaus and at Plattform Zugspitze of the GAW global observatory Zugspitze/Hohenpeissenberg and CO₂ measurements at Schauinsland are supported by the German Environment Agency (UBA). The IMK-IFU provided data from the Zugspitze tunnel and summit. Our thanks go to Hans-Eckhart Scheel from the

IMK-IFU for his high-quality data measurement until 2001 at the Zugspitze Summit (ZUG). For a long period, Hans-Eckhart Scheel, who passed away in 2013, led the in situ measurement program at the Zugspitze summit with a high level of expertise and diligence. Former IFU staff members helped us to reconstruct details of the measurements. We would also like to thank the operating team at the Environmental Research Station Schneefernerhaus for supporting our scientific activities and the Bavarian Ministry for Environment for supporting this High Altitude Research Station. Finally, our gratitude goes to the Bavarian Zugspitze railway company for the passenger data for 2016.

This work was supported by the German Research Foundation (DFG) and the Technical University of Munich (TUM) in the framework of the Open Access Publishing Program.

Edited by: Rachel Law

Reviewed by: two anonymous referees

References

- Bader, J.: Aufbau und Betrieb eines automatisierten Gaschromatographen HP 6890 zur kontinuierlichen Messung von CO₂, CH₄, N₂O und SF₆, Universität Heidelberg, 2001.
- Beardmore, D. J. and Pearman, G. I.: Atmospheric carbon dioxide measurements in the Australian region: Data from surface observatories, *Tellus B*, 39, 42–66, <https://doi.org/10.1111/j.1600-0889.1987.tb00269.x>, 1987.
- Bischof, W.: The influence of the carrier gas on the infrared gas analysis of atmospheric CO₂, *Tellus*, 27, 59–61, <https://doi.org/10.3402/tellusa.v27i1.9884>, 1975.
- Bousquet, P., Gaudry, A., Ciais, P., Kazan, V., Monfray, P., Simmonds, P. G., Jennings, S. G., and O'Connor, T. C.: Atmospheric CO₂ concentration variations recorded at Mace Head, Ireland, from 1992 to 1994, *Phys. Chem. Earth*, 21, 477–481, [https://doi.org/10.1016/S0079-1946\(97\)81145-7](https://doi.org/10.1016/S0079-1946(97)81145-7), 1996.
- Carnuth, W. and Trickl, T.: Transport studies with the IFU three-wavelength aerosol lidar during the VOTALP Mesolcina experiment, *Atmos. Environ.*, 34, 1425–1434, [https://doi.org/10.1016/S1352-2310\(99\)00423-9](https://doi.org/10.1016/S1352-2310(99)00423-9), 2000.
- Carnuth, W., Kempfer, U., and Trickl, T.: Highlights of the tropospheric lidar studies at IFU within the TOR project, *Tellus B*, 54, 163–185, <https://doi.org/10.1034/j.1600-0889.2002.00245.x>, 2002.
- Cervený, R. S. and Coakley, K. J.: A weekly cycle in atmospheric carbon dioxide, *Geophys. Res. Lett.*, 29, 15–1–15–4, <https://doi.org/10.1029/2001GL013952>, 2002.
- Ciattaglia, L.: Interpretation of atmospheric CO₂ measurements at Mt. Cimone (Italy) related to wind data, *J. Geophys. Res.*, 88, 1331, <https://doi.org/10.1029/JC088iC02p01331>, 1983.
- Cleveland, R. B., Cleveland, W. S., McRae, J. E., and Terpenning, I.: STL: A seasonal-trend decomposition procedure based on loess, *J. Off. Stat.*, 6, 3–73, 1990.
- Cleveland, W. S., Freeny, A. E., and Graedel, T. E.: The seasonal component of atmospheric CO₂: Information from new approaches to the decomposition of seasonal time series, *J. Geophys. Res.*, 88, 10934, <https://doi.org/10.1029/JC088iC15p10934>, 1983.


- Cundari, V., Colombo, T., Papini, G., Benedicti, G., and Ciattaglia, L.: Recent improvements on atmospheric CO₂ measurements at Mt. Cimone observatory, Italy, *Il Nuovo Cimento C*, 13, 871–882, <https://doi.org/10.1007/BF02512003>, 1990.
- Dettinger, M. D. and Ghil, M.: Seasonal and interannual variations of atmospheric CO₂ and climate, *Tellus B*, 50, 1–24, <https://doi.org/10.1034/j.1600-0889.1998.00001.x>, 1998.
- Francey, R. J., Trudinger, C. M., van der Schoot, M., Krummel, P. B., Steele, L. P., and Langenfelds, R. L.: Differences between trends in atmospheric CO₂ and the reported trends in anthropogenic CO₂ emissions, *Tellus B*, 62, 316–328, <https://doi.org/10.1111/j.1600-0889.2010.00472.x>, 2010.
- Frölicher, T. L., Joos, F., and Raible, C. C.: Sensitivity of atmospheric CO₂ and climate to explosive volcanic eruptions, *Biogeosciences*, 8, 2317–2339, <https://doi.org/10.5194/bg-8-2317-2011>, 2011.
- Frölicher, T. L., Joos, F., Raible, C. C., and Sarmiento, J. L.: Atmospheric CO₂ response to volcanic eruptions: The role of ENSO, season, and variability, *Global Biogeochem. Cy.*, 27, 239–251, <https://doi.org/10.1002/gbc.20028>, 2013.
- Gantner, L., Hornsteiner, M., Egger, J., and Hartenstein, G.: The diurnal circulation of Zugspitzplatt: Observations and modeling, *Meteorol. Z.*, 12, 95–102, <https://doi.org/10.1127/0941-2948/2003/0012-0095>, 2003.
- Gilge, S., Plass-Duelmer, C., Fricke, W., Kaiser, A., Ries, L., Buchmann, B., and Steinbacher, M.: Ozone, carbon monoxide and nitrogen oxides time series at four alpine GAW mountain stations in central Europe, *Atmos. Chem. Phys.*, 10, 12295–12316, <https://doi.org/10.5194/acp-10-12295-2010>, 2010.
- Graven, H. D., Keeling, R. F., Piper, S. C., Patra, P. K., Stephens, B. B., Wofsy, S. C., Welp, L. R., Sweeney, C., Tans, P. P., Kelley, J. J., Daube, B. C., Kort, E. A., Santoni, G. W., and Bent, J. D.: Enhanced seasonal exchange of CO₂ by northern ecosystems since 1960, *Science*, 341, 1085–1089, <https://doi.org/10.1126/science.1239207>, 2013.
- Griffith, D. W. T., Keeling, C. D., Adams, A., Guenther, P. R., and Bacastow, R. B.: Calculations of carrier gas effects in non-dispersive infrared analyzers. II. Comparisons with experiment, *Tellus*, 34, 385–397, <https://doi.org/10.3402/tellusa.v34i4.10825>, 1982.
- Hammer, S., Glatzel-Mattheier, H., Müller, L., Sabasch, M., Schmidt, M., Schmitt, S., Schönherr, C., Vogel, F., Worthy, D. E., and Levin, I.: A gas chromatographic system for high-precision quasi-continuous atmospheric measurements of CO₂, CH₄, N₂O, SF₆, CO and H₂, available at: http://www.iup.uni-heidelberg.de/institut/forschung/groups/kk/en/GC_Hammer_25_SEP_2008.pdf (last access: 23 January 2019), 2008.
- Hernández-Paniagua, I. Y., Lowry, D., Clemitshaw, K. C., Fisher, R. E., France, J. L., Lanoisellé, M., Ramonet, M., and Nisbet, E. G.: Diurnal, seasonal, and annual trends in atmospheric CO₂ at southwest London during 2000–2012: Wind sector analysis and comparison with Mace Head, Ireland, *Atmos. Environ.*, 105, 138–147, <https://doi.org/10.1016/j.atmosenv.2015.01.021>, 2015.
- Huntrieser, H., Heland, J., Schlager, H., Forster, C., Stohl, A., Aufmoff, H., Arnold, F., Scheel, H. E., Campana, M., Gilge, S., Eixmann, R., and Cooper, O. R.: Intercontinental air pollution transport from North America to Europe: Experimental evidence from airborne measurements and surface observations, *J. Geophys. Res.*, 110, D01305, <https://doi.org/10.1029/2004JD005045>, 2005.
- Jones, C. D. and Cox, P. M.: Modeling the volcanic signal in the atmospheric CO₂ record, *Global Biogeochem. Cy.*, 15, 453–465, <https://doi.org/10.1029/2000GB001281>, 2001.
- Jones, C. D. and Cox, P. M.: On the significance of atmospheric CO₂ growth rate anomalies in 2002–2003, *Geophys. Res. Lett.*, 32, L14816, <https://doi.org/10.1029/2005GL023027>, 2005.
- Keeling, C. D., Adams, J. A., Ekdahl, C. A., and Guenther, P. R.: Atmospheric carbon dioxide variations at the South Pole, *Tellus*, 28, 552–564, <https://doi.org/10.1111/j.2153-3490.1976.tb00702.x>, 1976.
- Keeling, C. D., Whorf, T. P., Wahlen, M., and van der Plichtt, J.: Interannual extremes in the rate of rise of atmospheric carbon dioxide since 1980, *Nature*, 375, 666–670, <https://doi.org/10.1038/375666a0>, 1995.
- Keenan, T. F., Prentice, I. C., Canadell, J. G., Williams, C. A., Wang, H., Raupach, M., and Collatz, G. J.: Recent pause in the growth rate of atmospheric CO₂ due to enhanced terrestrial carbon uptake, *Nat. Commun.*, 7, 13428, <https://doi.org/10.1038/ncomms13428>, 2016.
- Le Quéré, C., Raupach, M. R., Canadell, J. G., Marland, G., Bopp, L., Ciais, P., Conway, T. J., Doney, S. C., Feely, R. A., Foster, P., Friedlingstein, P., Gurney, K., Houghton, R. A., House, J. I., Huntingford, C., Levy, P. E., Lomas, M. R., Majkut, J., Metz, N., Ometto, J. P., Peters, G. P., Prentice, I. C., Randerson, J. T., Running, S. W., Sarmiento, J. L., Schuster, U., Sitch, S., Takahashi, T., Viovy, N., van der Werf, G. R., and Woodward, F. I.: Trends in the sources and sinks of carbon dioxide, *Nat. Geosci.*, 2, 831–836, <https://doi.org/10.1038/ngeo689>, 2009.
- Lintner, B. R., Buermann, W., Koven, C. D., and Fung, I. Y.: Seasonal circulation and Mauna Loa CO₂ variability, *J. Geophys. Res.*, 111, D13104, <https://doi.org/10.1029/2005JD006535>, 2006.
- Liu, F., Beirle, S., Zhang, Q., Dörner, S., He, K., and Wagner, T.: NO_x lifetimes and emissions of cities and power plants in polluted background estimated by satellite observations, *Atmos. Chem. Phys.*, 16, 5283–5298, <https://doi.org/10.5194/acp-16-5283-2016>, 2016.
- Liu, Y., Gruber, N., and Brunner, D.: Spatiotemporal patterns of the fossil-fuel CO₂ signal in central Europe: results from a high-resolution atmospheric transport model, *Atmos. Chem. Phys.*, 17, 14145–14169, <https://doi.org/10.5194/acp-17-14145-2017>, 2017.
- Lucht, W., Prentice, I. C., Myneni, R. B., Sitch, S., Friedlingstein, P., Cramer, W., Bousquet, P., Buermann, W., and Smith, B.: Climatic control of the high-latitude vegetation greening trend and Pinatubo effect, *Science*, 296, 1687–1689, <https://doi.org/10.1126/science.1071828>, 2002.
- Manning, M. R. and Pohl, K. P.: Atmospheric CO₂ Monitoring in New Zealand 1971–1985, Institute of Nuclear Sciences, DSIR, New Zealand, Report No INS-R-350, 1986.
- McClure, C. D., Jaffe, D. A., and Gao, H.: Carbon Dioxide in the Free Troposphere and Boundary Layer at the Mt. Bachelor Observatory, *Aerosol Air Qual. Res.*, 16, 717–728, <https://doi.org/10.4209/aaqr.2015.05.0323>, 2016.
- Möller, D.: Chemistry of the climate system, 2nd fully revised and extended edition, De Gruyter, Berlin, 786 pp., 2017.

- Müller, L.: Setup of a combined gas chromatographic system at the stations Schauinsland and Zugspitze for monitoring atmospheric H₂ and other greenhouse gases, University of Heidelberg, 2009.
- Nassar, R., Napier-Linton, L., Gurney, K. R., Andres, R. J., Oda, T., Vogel, F. R., and Deng, F.: Improving the temporal and spatial distribution of CO₂ emissions from global fossil fuel emission data sets, *J. Geophys. Res.*, 118, 917–933, <https://doi.org/10.1029/2012JD018196>, 2013.
- Pales, J. C. and Keeling, C. D.: The concentration of atmospheric carbon dioxide in Hawaii, *J. Geophys. Res.*, 70, 6053–6076, <https://doi.org/10.1029/JZ070i024p06053>, 1965.
- Pearman, G. I.: Further studies of the comparability of baseline atmospheric carbon dioxide measurements, *Tellus*, 29, 171–181, <https://doi.org/10.3402/tellusa.v29i2.11343>, 1977.
- Pearman, G. I. and Garratt, J. R.: Errors in atmospheric CO₂ concentration measurements arising from the use of reference gas mixtures different in composition to the sample air, *Tellus*, 27, 62–66, <https://doi.org/10.3402/tellusa.v27i1.9885>, 1975.
- Pickers, P. A. and Manning, A. C.: Investigating bias in the application of curve fitting programs to atmospheric time series, *Atmos. Meas. Tech.*, 8, 1469–1489, <https://doi.org/10.5194/amt-8-1469-2015>, 2015.
- R Core Team: R: A Language and Environment for Statistical Computing, Vienna, Austria, available at: <https://www.R-project.org/> (last access: 23 January 2019), 2018.
- Reiter, R., Sladkovic, R., and Kanter, H.-J.: Concentration of trace gases in the lower troposphere, simultaneously recorded at neighboring mountain stations Part I: Carbon Dioxide, *Meteorol. Atmos. Phys.*, 35, 187–200, <https://doi.org/10.1007/BF01041811>, 1986.
- Schmidt, M., Graul, R., Sartorius, H., and Levin, I.: The Schauinsland CO₂ record: 30 years of continental observations and their implications for the variability of the European CO₂ budget, *J. Geophys. Res.*, 108, ACL 14-1–ACL 14-7, <https://doi.org/10.1029/2002JD003085>, 2003.
- Sirignano, C., Neubert, R. E. M., Rödenbeck, C., and Meijer, H. A. J.: Atmospheric oxygen and carbon dioxide observations from two European coastal stations 2000–2005: continental influence, trend changes and APO climatology, *Atmos. Chem. Phys.*, 10, 1599–1615, <https://doi.org/10.5194/acp-10-1599-2010>, 2010.
- Slemr, F. and Scheel, H. E.: Trends in atmospheric mercury concentrations at the summit of the Wank mountain, Southern Germany, *Atmos. Environ.*, 32, 845–853, [https://doi.org/10.1016/S1352-2310\(97\)00131-3](https://doi.org/10.1016/S1352-2310(97)00131-3), 1998.
- Stephens, B. B., Brailsford, G. W., Gomez, A. J., Riedel, K., Mikaloff Fletcher, S. E., Nichol, S., and Manning, M.: Analysis of a 39-year continuous atmospheric CO₂ record from Baring Head, New Zealand, *Biogeosciences*, 10, 2683–2697, <https://doi.org/10.5194/bg-10-2683-2013>, 2013.
- Sturm, P., Leuenberger, M., and Schmidt, M.: Atmospheric O₂ CO₂ and $\delta^{13}\text{C}$ observations from the remote sites Jungfrauoch, Switzerland, and Puy de Dôme, France, *Geophys. Res. Lett.*, 32, 2467, <https://doi.org/10.1029/2005GL023304>, 2005.
- Thoning, K. W., Tans, P. P., and Komhyr, W. D.: Atmospheric carbon dioxide at Mauna Loa Observatory: 2. Analysis of the NOAA GMCC data, 1974–1985, *J. Geophys. Res.*, 94, 8549, <https://doi.org/10.1029/JD094iD06p08549>, 1989.
- Trickl, T., Cooper, O. R., Eisele, H., James, P., Mücke, R., and Stohl, A.: Intercontinental transport and its influence on the ozone concentrations over central Europe: Three case studies, *J. Geophys. Res.*, 108, STA 15-1–STA 15-23, <https://doi.org/10.1029/2002JD002735>, 2003.
- Trickl, T., Giehl, H., Jäger, H., and Vogelmann, H.: 35 yr of stratospheric aerosol measurements at Garmisch-Partenkirchen: from Fuego to Eyjafjallajökull, and beyond, *Atmos. Chem. Phys.*, 13, 5205–5225, <https://doi.org/10.5194/acp-13-5205-2013>, 2013.
- Tsutsumi, Y., Mori, K., Ikegami, M., Tashiro, T., and Tsuboi, K.: Long-term trends of greenhouse gases in regional and background events observed during 1998–2004 at Yonagunijima located to the east of the Asian continent, *Atmos. Environ.*, 40, 5868–5879, <https://doi.org/10.1016/j.atmosenv.2006.04.036>, 2006.
- Ueyama, M. and Ando, T.: Diurnal, weekly, seasonal, and spatial variabilities in carbon dioxide flux in different urban landscapes in Sakai, Japan, *Atmos. Chem. Phys.*, 16, 14727–14740, <https://doi.org/10.5194/acp-16-14727-2016>, 2016.
- Wang, Y., Munger, J. W., Xu, S., McElroy, M. B., Hao, J., Nielsen, C. P., and Ma, H.: CO₂ and its correlation with CO at a rural site near Beijing: implications for combustion efficiency in China, *Atmos. Chem. Phys.*, 10, 8881–8897, <https://doi.org/10.5194/acp-10-8881-2010>, 2010.
- Watanabe, F., Uchino, O., Joo, Y., Aono, M., Higashijima, K., Hirano, Y., Tsuboi, K., and Suda, K.: Interannual Variation of Growth Rate of Atmospheric Carbon Dioxide Concentration Observed at the JMA's Three Monitoring Stations: Large Increase in Concentration of Atmospheric Carbon Dioxide in 1998, *J. Meteorol. Soc. Jpn.*, 78, 673–682, 2000. The link to the data has been updated. Please change the link as below,
- World Data Centre for Greenhouse Gases (WDCGG): Global monthly mean mole fractions, available at: https://gaw.kishou.go.jp/publications/global_mean_mole_fractions, last access: 23 January 2019a.
- World Data Centre for Greenhouse Gases (WDCGG): Greenhouse gases and related gases (CO₂, CO, NO), available at: <https://gaw.kishou.go.jp/>, last access: 23 January 2019b.
- Winkler, P., Lugauer, M., and Reitebuch, O.: Alpine Pumping, *Promet*, 32, 34–42, 2006.
- WMO Greenhouse Gas Bulletin: The State of Greenhouse Gases in the Atmosphere Based on Global Observations through 2017, World Meteorological Organization, Geneva, No. 14, 2018.
- Yuan, Y., Ries, L., Petermeier, H., Steinbacher, M., Gómez-Peláez, A. J., Leuenberger, M. C., Schumacher, M., Trickl, T., Couret, C., Meinhardt, F., and Menzel, A.: Adaptive selection of diurnal minimum variation: a statistical strategy to obtain representative atmospheric CO₂ data and its application to European elevated mountain stations, *Atmos. Meas. Tech.*, 11, 1501–1514, <https://doi.org/10.5194/amt-11-1501-2018>, 2018.
- Zhang, F., Zhou, L., Conway, T. J., Tans, P. P., and Wang, Y.: Short-term variations of atmospheric CO₂ and dominant causes in summer and winter: Analysis of 14-year continuous observational data at Waliguan, China, *Atmos. Environ.*, 77, 140–148, <https://doi.org/10.1016/j.atmosenv.2013.04.067>, 2013.



Article

Comparison of Continuous In-Situ CO₂ Measurements with Co-Located Column-Averaged XCO₂ TCCON/Satellite Observations and CarbonTracker Model Over the Zugspitze Region

Ye Yuan ^{1,*}, Ralf Sussmann ², Markus Rettinger ², Ludwig Ries ³ , Hannes Petermeier ⁴ and Annette Menzel ^{1,5}

¹ Department of Ecology and Ecosystem Management, Technical University of Munich, 85354 Freising, Germany; annette.menzel@tum.de

² Karlsruhe Institute of Technology, IMK-IFU, 82467 Garmisch-Partenkirchen, Germany; ralf.sussmann@kit.edu (R.S.); markus.retinger@kit.edu (M.R.)

³ German Environment Agency (UBA), GAW Global Observatory Zugspitze-Hohenpeissenberg, 82475 Platform Zugspitze, Germany; ludwig.ries@gawstat.de

⁴ Department of Mathematics, Technical University of Munich, 85748 Garching, Germany; hannes.petermeier@tum.de

⁵ Institute for Advanced Study, Technical University of Munich, 85748 Garching, Germany

* Correspondence: yuan@wzw.tum.de

Received: 13 November 2019; Accepted: 11 December 2019; Published: 12 December 2019



Abstract: Atmospheric CO₂ measurements are important in understanding the global carbon cycle and in studying local sources and sinks. Ground and satellite-based measurements provide information on different temporal and spatial scales. However, the compatibility of such measurements at single sites is still underexplored, and the applicability of consistent data processing routines remains a challenge. In this study, we present an inter-comparison among representative surface and column-averaged CO₂ records derived from continuous in-situ measurements, ground-based Fourier transform infrared measurements, satellite measurements, and modeled results over the Mount Zugspitze region of Germany. The mean annual growth rates agree well with around 2.2 ppm yr⁻¹ over a 17-year period (2002–2018), while the mean seasonal amplitudes show distinct differences (surface: 11.7 ppm/column-averaged: 6.6 ppm) due to differing air masses. We were able to demonstrate that, by using consistent data processing routines with proper data retrieval and gap interpolation algorithms, the trend and seasonality can be well extracted from all measurement data sets.

Keywords: carbon dioxide; XCO₂; in situ; remote sensing; satellite; time-series analysis; seasonality

1. Introduction

Atmospheric carbon dioxide (CO₂) is the most important anthropogenic greenhouse gas and has increased globally from around 280 parts per million (ppm) since 1850 to over 400 ppm nowadays [1,2]. Measurements of atmospheric CO₂ are performed over the globe and via different measurement techniques. To derive precise CO₂ concentrations at the Earth's surface, representative of lower free tropospheric conditions, continuous in-situ measurements are made with high temporal resolution at either representative ground-based measurement sites or tall towers. Depending on the location, surface measurement sites can provide long-term records that are representative of regional and global scales, e.g., stations within the Global Atmosphere Watch (GAW) network [3]. In addition, to estimate the column-averaged mole fractions of CO₂ (XCO₂), remote-sensing techniques have been operated

at various sites via ground-based Fourier transform infrared (FTIR) measurements within the Total Carbon Column Observing Network (TCCON; [4]). Measurements of such global networks can thus be compared with each other and can be exploited for further use, such as the validation of satellite data and as a-priori input for models. Unlike ground-based measurement systems, satellites are capable of collecting data on the global scale with different spatial and temporal coverages, such as the Greenhouse Gases Observing Satellite (GOSAT; [5]) and the Orbiting Carbon Observatory-2 (OCO-2; [6]). Models, however, can take measurements into account and estimate with regard to only the concentrations global flux exchanges between the surface and atmosphere by simulating the atmospheric transport. As a result, the global carbon cycle could be better understood if all measurement techniques are evaluated and compared.

Many analyses have focused on regional and global surface CO₂ concentrations from selected in-situ measurements. Atmospheric CO₂ records at several central European mountain stations were evaluated, showing their improved representativeness on the CO₂ background levels after data selection [7]. In China, continuous measurements at four GAW regional and global stations were also analyzed, focusing on the characteristics of sampling sites and the influence of local sources [8]. Moreover, remote sites can serve as reference stations in urban studies. A comparison was made for a long-term CO₂ time-series measured from Southwest London with the CO₂ measurements at Mace Head, Ireland, exhibiting a higher growth rate and larger seasonal amplitudes, driven greatly by the anthropogenic emissions [9]. At the same time, inter-comparisons among satellites and cross-validations with ground-based FTIR have also frequently been made. A multi-year comparison of XCO₂ from Scanning Imaging Absorption Spectrometer for Atmospheric Cartography (SCIAMACHY; [10,11]), GOSAT, and Atmospheric Infrared Sounder (AIRS; [12]) was performed with the validation reference of TCCON measurements, and revealed that AIRS data products showed a better performance in both coverage and accuracy [13]. A further study of the comparison of GOSAT and OCO-2 reported that, despite the CO₂ detection capabilities in both satellites, OCO-2 performed better in detection coverage and spatial resolution [14].

However, so far, less attention has been paid to the differences between surface and column measurements at single sites. Column CO₂ from Fourier transform spectrometer was found to be similar to surface CO₂ concentrations from flask, tower, and aircraft observations regarding the amplitude of diurnal and seasonal cycles, but with less variability at both spatial and temporal scales [15]. However, this study focused more on the general patterns resulting from an atmospheric transport model instead of on characteristics of point measurements. However, a systematic comparison was performed at Jungfraujoch, Switzerland, on the in-situ Nondispersive Infrared Analyzer (NDIR) and column FTIR measurements, revealing similar differences in the seasonality (column about one half of surface), but differences that are consistent in the annual CO₂ increase with high correlation [16]. Still, no satellite or model-based results were included. Nevertheless, there were two studies with seasonal and spatial focuses, comparing satellite measurements with ground-based measurements over East Asia and Indian regions [17,18]. In Europe, only the Scanning Imaging Absorption Spectrometer for Atmospheric Cartography sensor (SCIAMACHY) and CO₂ ground measurements at a rural site in the upper Spanish plateau were compared, showing similar seasonal patterns and a satisfying agreement between inter-annual trends, but only with a short studied time period [19]. Surface and column CO₂ data were compared at Ny-Alesund, and a smaller amplitude in the column was found [20]. This was explained by the fact that the processes responsible for the seasonality, namely plant photosynthesis sinks and plant and microbial respiration, take place at the Earth's surface. Besides, co-located column and in-situ CO₂ measurements in the tropics were compared with atmospheric tracer transport model TM3 simulations, which resulted in a good agreement [21].

In this study, we intend to answer the following research questions using a set of CO₂ time-series derived from surface/column-averaged measurements performed in the Zugspitze region of Southern Germany.

1. Can a consistent data processing routine be successfully applied to both continuous in-situ and column-averaged CO₂ measurements for comparisons with increased representativeness?
2. Are the surface and satellite measurements comparable even though they are representative of a single measurement site or a designated region/column average?
3. If significant differences are detected, what are the specific differences in annual growth rates and seasonal amplitudes?

The sections below are organized as follows. Section 2 gives a general description of the CO₂ series. Details in the data processing routine and analyses are given in Section 3. Results and discussion regarding the trend and seasonality are presented in Sections 4 and 5, followed by conclusions on their comparability and applicability in Section 6.

2. CO₂/XCO₂ Data Sets

2.1. Surface In-Situ Measurements

The long-term surface CO₂ records (2002–2018) measured at the GAW global station Zugspitze–Schneefernerhaus, Germany (GAW ID: ZSF) were used in this study. The location of ZSF is at the Southern slope of Mount Zugspitze (47.42°N, 10.98°E) at an elevation of 2670 m above sea level (a.s.l.). Measurements of atmospheric CO₂ at Zugspitze had already started in the 1980s, but were re-located to this research station in 2001. The complete and validated CO₂ time-series has been available since 2002, and thus was used here as CO₂_INSITU_ZSF. For more detailed information regarding the site and experimental instruments, we refer the reader to Yuan et al. [22].

2.2. TCCON

TCCON is the network of ground-based FTS measuring the column-averaged concentrations of atmospheric components such as CO₂ and CH₄ by recording the solar absorption spectra in the near-infrared [23]. Two measurement sites were chosen close to ZSF, i.e., the TCCON sites Garmisch (47.48°N, 11.06°E, 743 m a.s.l.) and Zugspitze (47.42°N, 10.98°E, 2964 m a.s.l.), equipped with the Bruker IFS125HR spectrometer [24]. The data version GGG2014 was used, which is available at <https://tccodata.org/> [25,26]. Temporal coverage was different since XCO₂ time-series have been available at Garmisch since 2007 and at Zugspitze since 2015. The column-averaged dry air mole fractions of CO₂ were extracted in ppm, denoted as XCO₂_TCCON_Garmisch and XCO₂_TCCON_Zugspitze.

2.3. Satellite

Satellite data were taken from a merged CO₂ satellite product described in Buchwitz et al. [27] (available at <https://cds.climate.copernicus.eu/>) from the Scanning Imaging Absorption Spectrometer for Atmospheric Cartography sensor (SCIAMACHY) on the Environmental Satellite (ENVISAT) from 2002 to 2012, and the subunit Fourier Transform Spectrometer of the Thermal And Near-infrared Sensor for carbon Observation sensor (TANSO-FTS) on the GOSAT since 2009, referred to as XCO₂_SAT_Obs4MIPs. To make the satellite XCO₂ time-series more comparable with in-situ measurements on the temporal scale, measurements from the OCO-2 satellite launched and operated since July 2014 were further included [28]. For this study, XCO₂ data from the OCO-2 9 lite product were derived from the CO₂ Virtual Science Data Environment in the Jet Propulsion Laboratory, California Institute of Technology (<https://co2.jpl.nasa.gov/>), abbreviated as XCO₂_SAT_OCO-2. Again, measurements were extracted as column-averaged dry air mole fractions of CO₂.

2.4. CarbonTracker

CarbonTracker ([29], with updates documented at <http://carbontracker.noaa.gov>), the global CO₂ modeling system developed by National Oceanic and Atmospheric Administration Earth System Research Laboratory (NOAA ESRL, USA), was used for validation purposes. It assimilates almost

400 time-series from real CO₂ observations combining both in-situ continuous and flask measurements from the surface, as well as tower, aircraft, and shipboard measurements. The current version CT2017 provides modeled CO₂ mole fractions from 2000 to 2016. For modeling the CO₂ mole fractions for a longer time period, CarbonTracker Near-Real Time (version CT-NRT.v2018-1), which is an extension of CT2017 using real-time meteorology and a different prior flux model with assimilations of fewer CO₂ observations, was chosen. These two data sets were named CO₂_CT2017 and CO₂_CT-NRT.v2018-1, respectively. Figure 1 shows the overall map of measurement sites and sampling grids for all data sets used in the study.

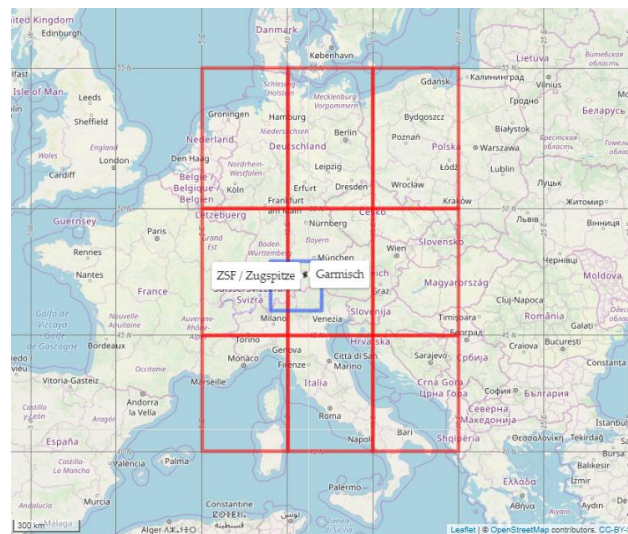


Figure 1. Locations of GAW Global station ZSF and TCCON sites Zugspitze and Garmisch with rectangles representing the spatial coverage of XCO₂ levels extracted in this study for satellite measurements (red) and CarbonTracker-modeled results (blue).

3. Methods

3.1. Data Integration

For a complete and consistent analysis, all data sets were first collected and averaged to monthly values. The surface continuous data set CO₂_INSITU_ZSF used here consisted of 30 min averages from 2002 to 2018, and thus all other data sets were selected in the same corresponding time period. Regarding the TCCON network, agreements in daily measurements between Garmisch and Zugspitze were examined by calculating their difference (XCO₂_TCCON_Garmisch minus XCO₂_TCCON_Zugspitze) for the overlapping time period (April 2015–December 2018). A mean daily difference of -0.24 ± 1.32 ppm (one standard deviation) was derived within the accuracy of 0.2% for the TCCON measurements [30]. Therefore, both data sets were included, but the XCO₂_TCCON_Garmisch data set was used, starting in 2008 due to only 6 months of data being available in 2007.

For satellite measurements, Level 3 product Obs4MIPs Version 3.0 on a monthly scale was first chosen over 2003–2016. To derive the best appropriate mole fractions comparable to the other point measurements, the centered and surrounding eight grids of the Zugspitze region were collected (see Figure 1) and averaged as XCO₂ levels, representative of a broader region and which due to a large amount (34.5%) of missing values at the centered grid. However, the OCO-2 satellite measurements were selected with the customized time period of 2017–2018 and integrated into Level 3 gridded monthly data set with the same spatial and temporal resolutions as XCO₂_sat_Obs4MIPs by the same data

averaging from the centered and surrounding grids. Later, these two satellite data sets were merged and denoted as XCO₂_SAT_merge.

The validation CarbonTracker model data sets were integrated in the following ways. As recommended by NOAA (<https://www.esrl.noaa.gov/gmd/ccgg/carbontracker/CT-NRT/>), the 3 hourly CT2017 data set was used from 2002 to 2016, followed by the CT-NRT.v2018-1 data set used from 2017 to 2018. The inter-comparison between the measurement data sets and the CarbonTracker model was reliable since CO₂_INSITU_ZSF was not included in the CarbonTracker Observational Network. Additionally, the modeled results were representative of different measurement heights because the implemented Transport Model 5 (TM5) used a 25-layer subset in the vertical of ERA-interim transport [31]. We only extracted the modeled CO₂ concentrations at the centered grid (see Figure 1) averaged from Levels 6 to 10 (about 1.2 km to 5.5 km above the ground) as the “free troposphere” (FT, indicated at <https://www.esrl.noaa.gov/gmd/ccgg/carbontracker/index.php>), as well as the total column averages (Levels 1 to 25), representative of XCO₂ concentrations at both Garmisch and Zugspitze. Thus, the overall modeled data sets for comparison are referred to as CO₂_CT_merge_L6-10 and XCO₂_CT_merge_L1-25. A comprehensive description of all data sets regarding instrumentation, temporal, and spatial coverage is given in Table 1.

Table 1. Information on the CO₂ and XCO₂ data sets used in the study.

Measurement Data Set	Time Period	Spatial Resolution (Lon × Lat)	Temporal Resolution	Instrument	Merged Data Set Used in the Study
CO ₂ _INSITU_ZSF	2002–2018	–	half-hourly	GC-FID	CO ₂ _INSITU_ZSF; CO ₂ _INSITU_ZSF_ADV5
XCO ₂ _TCCON_Garmisch	2008–2018	–	daily	Bruker IFS125HR	XCO ₂ _TCCON_Garmisch
XCO ₂ _TCCON_Zugspitze	2015–2018	–	daily	Bruker IFS125HR	XCO ₂ _TCCON_Zugspitze
XCO ₂ _SAT_Obs4MIPs	2003–2016	5° × 5°	monthly	SCIAMACHY/TANSO-FTS	XCO ₂ _SAT_merge
XCO ₂ _SAT_OCO-2	2017–2018	5° × 5°	monthly	OCO-2	XCO ₂ _SAT_merge
(X)CO ₂ _CT2017	2002–2016	3° × 2°	3-hourly	–	CO ₂ _CT_merge_L6-10; XCO ₂ _CT_merge_L1-25
(X)CO ₂ _CT-NRT.v2018-1	2017–2018	3° × 2°	3-hourly	–	CO ₂ _CT_merge_L6-10; XCO ₂ _CT_merge_L1-25

3.2. Data Processing

In order to derive the most representative background CO₂ levels for the lower free troposphere from the CO₂_INSITU_ZSF data set, the data selection method ADVS (Adaptive Diurnal minimum Variation Selection) was applied, which has been proven to be valid for European elevated mountain stations [7], and for long-term continuous measurements [22]. With a nighttime starting selection time window statistically identified based on data variability, the ADVS method selects the best appropriate CO₂ data on a daily basis. The selection threshold criterion at ZSF was set to no more than 0.3 ppm (standard deviation) within a 6-hour time window (22:00–03:00 local time). In total, 14.0% of validated 30-min CO₂ data were selected.

For all monthly averaged data sets, cubic spline interpolation was applied to fill missing values in the time-series, mainly for XCO₂_SAT_Obs4MIPs during winter periods (mostly December and January) due to poor data quality (e.g., cloudiness, shadows, or other factors). Subsequently, all CO₂ time-series were decomposed into trend, seasonal, and remainder components for further analysis using Seasonal and Trend decomposition using Loess (STL) [32]. The STL method applies the moving average technique in an inner loop with seasonal and trend smoothers based on Locally Estimated Scatterplot Smoothing (Loess), and an outer loop weighting the fitted values for the next run of smoothing until convergence is reached [33]. The smoothing parameters $s.window = 5\ years$ and $t.window = 25\ months$ were chosen for the seasonal and trend components, respectively. A periodic window for seasonal extraction was tested and the result was similar. The remainder of the components were assessed for all records, but no systematic signals were detected, indicating reliable decomposed results for further analysis (see Figure A1). The STL-decomposed trend and seasonal components were combined and are shown as curve fitting for all CO₂/XCO₂ time-series.

3.3. Data Analysis

The CO₂ annual growth rate was calculated from the STL-decomposed trend component based on the definition by NOAA [2], following the instructions in Buchwitz et al. [27]. For each month, we calculated the difference in CO₂ or XCO₂ between this month and the same month from the previous year. Thus, 12 values were calculated for each year. Then, the mean annual growth rate was considered as the mean of these 12 differences. The mean annual growth rates were further used for correlation analysis by Pearson's product moment correlation, with error bars defined by the 95% confidence intervals calculated from averaging the 12 values in each year.

However, the seasonal cycle was determined from the STL-decomposed seasonal component with the seasonal amplitude calculated from the monthly maximum minus the monthly minimum of the year. The calculation method of seasonal amplitude has been compared with the curve fitting technique, by Lindqvist et al. [34] applying a skewed sine wave for the seasonal cycle, resulting in the same values. More details can be found in the Appendix A.

All data processing, analyses, and visualizations in this study were done under R programming environment (version 3.6.0) [35], with the implemented packages data.table [36], openair [37], zoo [38], ggplot2 [39], leaflet [40], mapview [41], grid [35], and gridExtra [42].

4. Results

This section first reports the complete CO₂ time-series compared. Then, the results of STL decomposition are shown with inter-annual variations of annual growth rates and seasonal cycles. A statistical summary can be found in Table A1.

4.1. Time-Series of CO₂ and XCO₂

The atmospheric CO₂ and XCO₂ mole fractions from all measurement data sets, including the ADVS-selected surface in-situ time-series CO₂_INSITU_ZSF_ADVS, are given in Figure 2. All time-series are plotted in monthly resolution, together with the fitted curves that are integrated from STL-decomposed trend and seasonal components. CO₂_INSITU_ZSF, CO₂_INSITU_ZSF_ADVS, CO₂_CT_merge_L6-10, and XCO₂_CT_merge_L1-25 covered the complete time period 2002–2018. The first year 2002 was missing for XCO₂_SAT_merge, while XCO₂_TCCON_Garmisch and XCO₂_TCCON_Zugspitze started comparatively later, in 2008 and 2015, respectively. In general, the CarbonTracker-modeled free tropospheric time-series CO₂_CT_merge_L6-10 agreed well with the continuous in-situ measurements (both CO₂_INSITU_ZSF and CO₂_INSITU_ZSF_ADVS). However, CO₂_INSITU_ZSF more frequently exhibited CO₂ concentrations outside the curve fitting and thus represented the local and regional influences, e.g., higher CO₂ concentrations in 2008–2009, 2012–2013, and 2018; lower values in 2013–2014. At the same time, ADVS data selection performed effectively to exclude most of the extreme mean monthly concentrations, except for the lower value in 2005. CO₂_INSITU_ZSF_ADVS was still more similar in the STL-decomposed trend and seasonal fit to CO₂_CT_merge_L6-10 than the original CO₂_INSITU_ZSF series.

Regarding column-averaged measurements, there were far less variations in the time-series compared to the surface measurements, since they are representative of the mean CO₂ levels of the whole vertical atmospheric concentration distribution and not only of the surface concentration as the in-situ measurements. The satellite time-series XCO₂_SAT_merge was slightly higher compared to the point measurements XCO₂_TCCON_Garmisch and XCO₂_TCCON_Zugspitze, while the CarbonTracker-modeled column averages XCO₂_CT_merge_L1-25 showed the opposite. Such deviations could be attributed to differences in the representativeness of the grid values. Unlike TCCON measurements, XCO₂ values averaged from the centered and surrounding grids had the tendency to show a mean XCO₂ level from a much more regional perspective. Additionally, the extracted modeled grid for XCO₂_CT_merge_L1-25 could potentially cover more vegetation signals that were dominant at lower elevations in the Alpine regions nearby. Additionally, it should be noted that the monthly averages for all XCO₂ measurements might not identically indicate the concentrations for the exact same days.

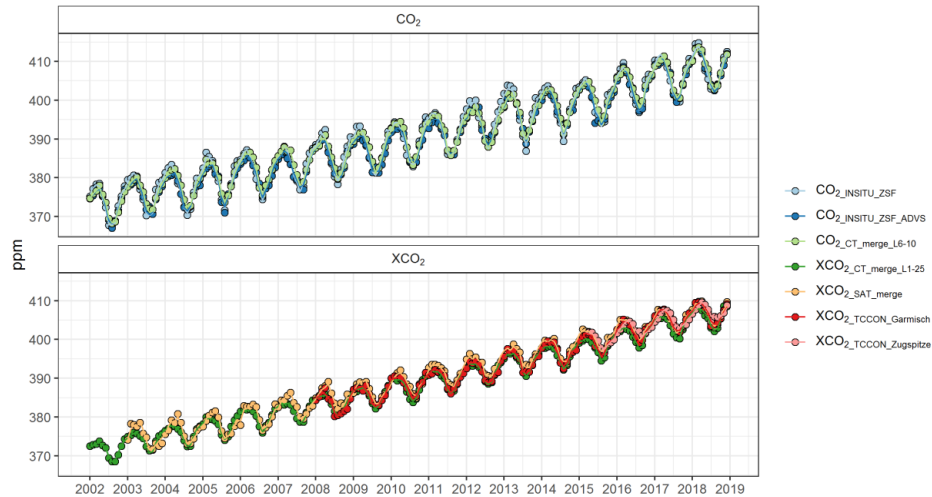


Figure 2. Monthly CO₂ series of all measurements/data products shown as colored points with fitted curves (colored lines) consisting of STL-decomposed trend and seasonal components, divided into CO₂ (upper panel) and XCO₂ (lower panel).

Figure 3 shows the offsets of all six data sets with respect to the continuous in-situ ZSF data set (CO₂_{INSITU_ZSF}), based on the monthly fitted curves. The offsets ranged from -5 to 5 ppm with bimodal distributions. All time-series exhibited negative values for the mean monthly differences relative to CO₂_{INSITU_ZSF} ranging from -0.66 ± 0.15 ppm (CO₂_{INSITU_ZSF_ADVS}) to -2.36 ± 0.32 ppm (XCO₂_{CT_merge_L1-25}), except for CO₂_{CT_merge_L6-10}, which showed a positive difference of 0.01 ± 0.17 ppm (see Table A1).

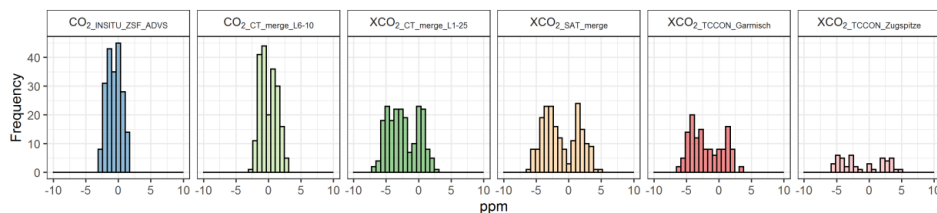


Figure 3. Offsets of six different CO₂ and XCO₂ data sets of this study (monthly fitted curves, STL-decomposed trend plus seasonal components) relative to CO₂_{INSITU_ZSF}.

4.2. Annual Growth Rates

Apart from absolute CO₂ levels, trend analysis is always considered a more promising measure for the comparison of CO₂ time-series, i.e., for assessing whether similar year-to-year increases and inter-annual variations in CO₂ can be detected. The annual CO₂ growth rates are shown as boxplots, together with the mean growth rates connected as lines in Figure 4.

The overall mean annual growth rates of CO₂_{INSITU_ZSF} (2.18 ± 0.10 ppm yr⁻¹), CO₂_{INSITU_ZSF_ADVS} (2.20 ± 0.09 ppm yr⁻¹), and CO₂_{CT_merge_L6-10} (2.21 ± 0.06 ppm yr⁻¹) over 2002–2018 exhibited similar values around 2.2 ppm yr⁻¹ for the free troposphere, while XCO₂_{CT_merge_L1-25} and XCO₂_{SAT_merge} (starting 2003) for the total column of the atmosphere increased at slightly lower rates of 2.15 ± 0.04 ppm yr⁻¹ and 2.13 ± 0.06 ppm yr⁻¹, respectively. Due to the late start of TCCON, significantly higher annual growth rates were observed, namely 2.33 ± 0.08 ppm yr⁻¹ (Garmisch, starting in 2008) and 2.48 ± 0.16 ppm yr⁻¹ (Zugspitze, starting in 2015).

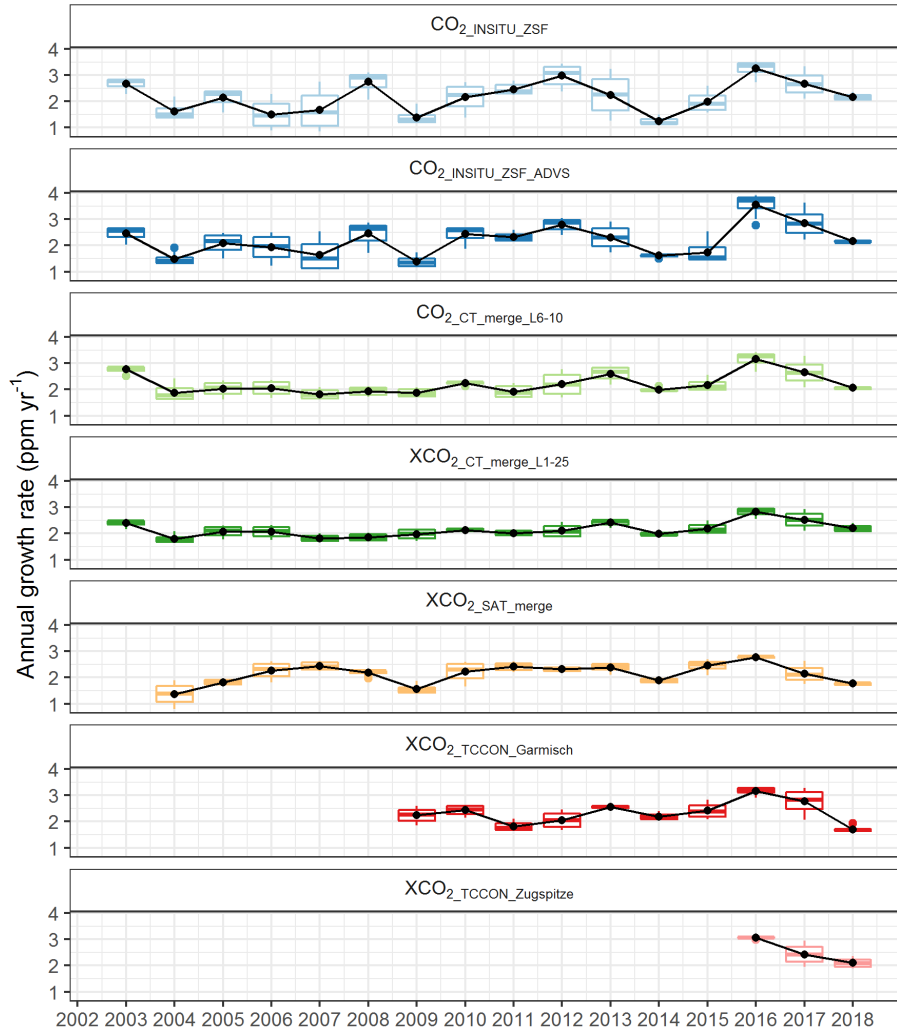


Figure 4. Annual mean growth rates derived from all seven CO₂ and XCO₂ series in this study (STL-decomposed trends, black points, and lines). Colored boxplots represent all 12 values of growth rates from monthly averages.

4.3. Seasonal Amplitudes

Seasonal cycles of all CO₂ and XCO₂ time-series were analyzed in regards to whether they followed comparable annual fluctuations and to identify reasons for potential discrepancies. Clear differences were found between continuous in-situ and column-averaged measurements in the mean seasonal peak-to-peak amplitudes, i.e., annual averages of monthly maximum minus monthly minimum, which were calculated from the STL-decomposed seasonal components shown in Figure 5. The largest mean seasonal amplitude of 13.08 ± 0.52 ppm was calculated for CO₂_{INSITU_ZSF}, indicating a high relevance of local influences at the measurement site. In contrast, the ADVS-selected data set (CO₂_{INSITU_ZSF_ADV}, 10.93 ± 0.45 ppm) agreed well with the modeled CO₂ levels for the free troposphere (CO₂_{CT_merge_L6-10}, 11.05 ± 0.28 ppm), supporting a good performance of the CarbonTracker model in simulating the

surface/free tropospheric CO₂ mole fractions. In this circumstance, an estimation of around 2.0 ppm mole fractions of atmospheric CO₂ is assumed to be associated with short-range carbon sources and sinks.

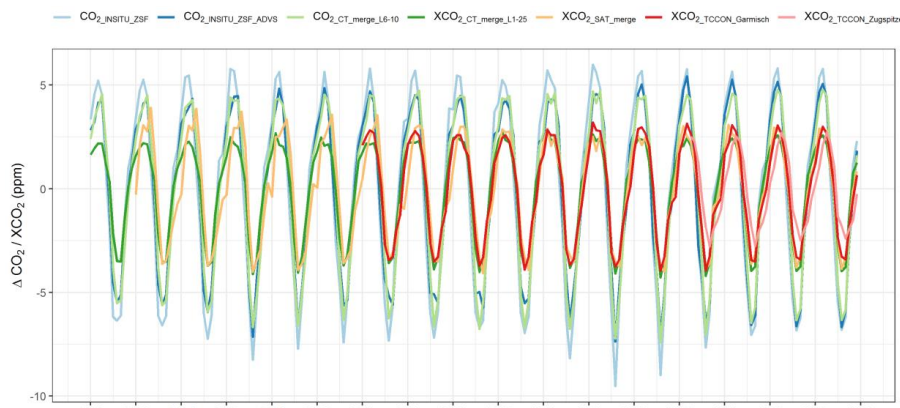


Figure 5. Seasonal cycles from STL-decomposed seasonal components of the different CO₂ and XCO₂ series of this study.

5. Discussion

The atmospheric CO₂ and XCO₂ mole fractions from all measurement data sets were collected and compared (see Figure 2). The differences between FTIR column observations and continuous in-situ measurements (-1.95 ± 0.43 ppm for XCO₂_TCCON_Garmisch, and -1.03 ± 1.01 ppm for XCO₂_TCCON_Zugspitze) were smaller than those found in previous studies, where differences of up to 8% have been reported [20]. This may be explained by the fact that our TCCON column observations were calibrated to World Meteorological Organization (WMO) scale, while the cited column observations were not. Furthermore, the column observations by Schibig et al. [16], showing a difference of 13 ppm with respect to surface measurements at the Jungfraujoch, were performed in the mid-infrared, not in the near-infrared as our TCCON observations. In this context, we note that Buschmann et al. [30] showed that the sensitivity of mid-infrared CO₂ column retrievals is a factor of two lower in the troposphere compared to TCCON-type near-infrared retrievals used in our study.

5.1. Inter-Annual Variation in Trend

The STL-decomposed trend components were calculated into annual CO₂ growth rates and overall mean growth rates (see Figure 4). These results perfectly matched those found by Buchwitz et al. [27], who showed a mean difference between the satellite-derived and NOAA CO₂ surface observation annual mean growth rates of 0.0 ± 0.3 ppm yr⁻¹ (± 1 standard deviation). Their reported “record-large” growth rate over 2015–2016 of around 3 ppm yr⁻¹ due to an El Niño event [43–45] was also clearly observed in all series of our study (ranging from 2.77 to 3.56 ppm yr⁻¹).

Equally, inter-annual variations in the annual growth rates were similar for the different CO₂ series. The continuous in-situ measurements (CO₂_INSITU_ZSF and CO₂_INSITU_ZSF_ADV5) and CarbonTracker free tropospheric model (CO₂_CT_merge_L6-10) agreed well, starting with a noticeably high annual growth rate in 2003 and a decreasing period from 2016 to 2018. They only differed considerably in 2008 and 2009, i.e., both CO₂_INSITU_ZSF and CO₂_INSITU_ZSF_ADV5, but not CO₂_CT_merge_L6-10, which showed high variations in the annual growth rates. Interestingly, also XCO₂_SAT_merge showed this pattern, which might again be attributed to the different spatiotemporal smoothing in the model and satellite grids compared to the local surface measurements. Especially for the period 2004–2009, it is clear that the annual growth rates in CO₂_CT_merge_L6-10 remained stable and the same is true for XCO₂_CT_merge_L1-25.

Regarding column-averaged measurements, smaller variables were expected for the annual growth rates, as shown in Figure 4. Despite much shorter TCCON time-series, the decreasing trends from 2016 to 2018 were still observed in all column-averaged time-series. In 2014, a comparably lower mean annual CO₂ growth rate was depicted across all time-series. Moreover, while the 12 values tended to vary largely in 2017, they did not in 2016 and 2018. Again, this was a result consistent for all seven data sets. However, an increase in growth rates in XCO₂_{SAT_merge} from 2003 to 2007 was not seen elsewhere and thus still remains unclear. However, in general, annual growth rates agreed well among all CO₂ series, particularly in the second half of the study period, and further research should be dedicated to the differences before 2010.

5.2. Correlation of Annual Growth Rates

Figure 6 summarizes correlations of each measurement data set with CO₂_{INSITU_ZSF} and CO₂_{INSITU_ZSF_ADVS}. The ADVS data selection intends to derive more representative CO₂ levels for a broader region, which proved to be valid since the correlation coefficients to CO₂_{INSITU_ZSF_ADVS} were higher than the respective ones to CO₂_{INSITU_ZSF}, e.g., correlation of XCO₂_{TCCON_Garmisch} growth rates to CO₂_{INSITU_ZSF_ADVS} of 0.54 (significant at 0.1 level) instead of 0.38 to CO₂_{INSITU_ZSF} (not significant). Furthermore, the CarbonTracker models also showed improved correlations from 0.66 to 0.78 with improved significance levels (0.01 to 0.001) for CO₂_{CT_merge_L6-10}, and from 0.61 to 0.76 for XCO₂_{CT_merge_L1-25} when applying the ADVS technique. A slight increase (0.57 to 0.62 at 0.05 of the significance level) is also seen for XCO₂_{SAT_merge}, while the highest correlation coefficients of almost 1 were seen for XCO₂_{TCCON_Zugspitze} in both pairs, however, due to a correlation of three points from only 2015 to 2018, this is not comparable. In short, the overall improvements in the correlation coefficients were clearly recognized in all data sets with continuous in-situ measurements at ZSF after ADVS data selection, suggesting a good accordance with the background levels in the atmosphere. Interestingly, the modeled column time-series correlated better with the surface measurements in terms of the trend compared to other column-averaged measurements. Nevertheless, correlations between CO₂_{CT_merge_L6-10} and continuous in-situ measurements as well as between XCO₂_{CT_merge_L1-25} and column-averaged measurements are also provided (see Figure A2) and especially show a good correlation coefficient (0.82 **) between XCO₂_{TCCON_Garmisch} and the modeled column data set.

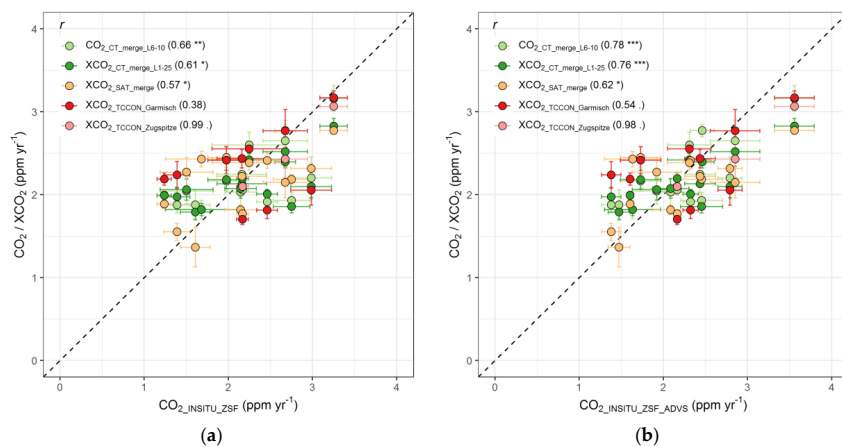


Figure 6. Scatter plots of annual mean growth rates from STL trend components in (a) CO₂_{INSITU_ZSF} and (b) CO₂_{INSITU_ZSF_ADVS} versus CO₂/XCO₂ from other measurement data sets. Pearson's product-moment correlation coefficients (r) are listed accordingly for each pair. The significance levels are shown in symbols as 0.001 (***), 0.01 (**), 0.05 (*), and 0.1 (.). The 95% confidence intervals are shown as error bars on both the x and y-axis with dashed lines representing the 1:1 line.

The levels of correlation coefficients were comparable with similar studies. Buchwitz et al. [27] reported a correlation coefficient of 0.82 between the satellite-derived growth rates and the NOAA global growth rates over 2003–2016. This higher value is assumed to be due to the global averaging effect, while our results show a more specific signature of the Zugspitze region. Equally, Schibig et al. [16] reported that correlations between the FTIR and in-situ NDIR measurements, both with and without seasonality, reached 0.82 as well.

5.3. Seasonality

The mean seasonal amplitudes of column-averaged measurements were only about one half of the amplitudes of in-situ measurements (see Figure 5). It is noteworthy that this factor-of-two amplitude reduction for column-based data sets was nicely reproduced by CarbonTracker, when comparing $\text{CO}_2_{\text{CT_merge_L6-10}}$ with $\text{CO}_2_{\text{CT_merge_L1-25}}$ (6.36 ± 0.18 ppm). A similar effect was also reported by Olsen and Randerson [15] for individual NOAA sites in the Northern Hemisphere. The satellite time-series had seasonal amplitudes of 6.94 ± 0.22 ppm from 2003 to 2018, while 6.58 ± 0.19 ppm was calculated for $\text{XCO}_2_{\text{TCCON_Garmisch}}$ during 2008–2018. Finally, $\text{XCO}_2_{\text{TCCON_Zugspitze}}$ exhibited the lowest mean seasonal amplitude of 5.22 ± 0.14 ppm for the last four years (2015–2018). Taking the same period for the TCCON Garmisch site, the mean seasonal amplitude was still significantly higher (6.64 ± 0.50 ppm for $\text{XCO}_2_{\text{TCCON_Garmisch}}$ during 2015–2018). Therefore, an amplitude difference of around 1.5 ppm can be attributed mainly to the carbon sinks from photosynthesis in the relatively lower elevations of the Zugspitze region compared to the TCCON Zugspitze site (from both the TCCON Garmisch site and the satellite grid coverage perspectives).

In addition, due to different vertical mixing and amounts of air masses measured at the surface or in the column, changes in phase (i.e., timing of seasonal peaks) are expected to be observed as well [7,22]. Olsen and Randerson [15] suggested that the phase delay between surface and column measurements can be up to seven weeks regarding the timing of seasonal maximum and minimum, while Lindqvist et al. [34] showed an up to two–three weeks difference regarding the maximum at the European sites with a smaller difference for the minimum of less than six days. From our study, given that monthly time-series were used, only the shifts in month could be derived here. On average, one–two-month delays were detected in monthly maxima from all column measurements compared to $\text{CO}_2_{\text{INSITU_ZSF}}$, especially in the first half of the satellite time-series ($\text{XCO}_2_{\text{SAT_merge}}$, 2003–2008). Interestingly, the seasonal amplitudes during this period of $\text{XCO}_2_{\text{SAT_merge}}$ also differed greatly from the remaining latter half (2009–2018). This could be probably explained by the fact that the TANSO-FTS/GOSAT satellite measurements included in this merged product ($\text{XCO}_2_{\text{SAT_Obs4MIPs}}$) only started from 2009. In opposition to this, delays of one month at the most can be found for seasonal minima mainly from satellite and TCCON measurements.

At last, inter-annual changes in the seasonality were detected more clearly for continuous in-situ measurements than for the column-averaged measurements, which is in accordance with the anomalies described in Section 4.1. However, some other seasonal patterns are still worthy of further investigations. A slight “shoulder” behavior could be observed for all time-series, usually around November and December, suggesting a slower CO_2 increase during this period. Such a “pause” cannot be fully understood yet, but is probably associated with a known, relatively regular winter warming effect (named “Christmas-thaw weather” over Europe). Meanwhile, the seasonal decrease from monthly maximum to monthly minimum tended to vary rapidly over time, indicating the great influences from vegetation photosynthesis as the carbon sinks during spring to summertime. Such a pattern should be described more precisely in seasonal modeling in the future.

6. Conclusions

This study compared surface CO_2 measurements with column-averaged measurements at a specific site in Southern Germany. Continuous in-situ CO_2 measurements from 2002 to 2018 at Zugspitze–Schneefernerhaus were used and selected by the data selection method ADVS in order

to obtain more representative background levels for a broader region. In order to compare with ground-based FTIR measurements, two TCCON sites, Garmisch and Zugspitze, were chosen at the nearby locations. In addition to providing more comparable results over the region, satellite measurements were included by defining selected grids centered at the specific Zugspitze site. At last, the simulated CO₂ mole fractions from the CarbonTracker models were included and validated for other measurements.

The mean offsets of satellite and FTIR measurements from the continuous in-situ measurements were less than 2.0 ppm, showing generally good agreements. By decomposing each CO₂ time-series into trend, seasonal, and remainder components, the annual growth rates and seasonal amplitudes were compared. Fluctuations of the mean annual growth rates were consistent over the time period, proving that both continuous in-situ and column-averaged measurements are able to capture the CO₂ trend effectively in the atmosphere. The correlation analysis showed lower correlation coefficients than other global studies due to the site-specific focus of this study. However, differences in seasonal cycles were clear with respect to both amplitudes and phases. Column-averaged measurements exhibited smaller seasonal amplitudes and clearly delayed phases regarding both seasonal maximum and minimum. This is most likely due to lessened influences from the local to regional scale as well as to a time lag by the vertical mixing of greater amounts of air masses in the column profile.

With respect to the research questions, the study clearly showed that different types of CO₂ measurements/time-series are comparable by applying a consistent data processing routine. The main differences between continuous in-situ and column-averaged measurements were detected in the seasonal amplitudes, supporting the essential distinction of the measuring objects. However, potential errors should always be noted, especially regarding both temporal and spatial resolutions. Such a comparison provides the basis for a better understanding of these two different types of measurements and is helpful for improved data integration in further research.

Author Contributions: The research aim was developed by Y.Y., L.R., and A.M.; Formal analysis, methodology, and implementation of the programming algorithm were done by Y.Y. under the supervision of L.R., H.P., R.S., and A.M.; The ground-based FTS measurements were performed and collected by R.S. and M.R.; The original draft was prepared by Y.Y. and reviewed and edited by all co-authors.

Funding: Y.Y. is funded by the China Scholarship Council (CSC), grant number 201508080110.

Acknowledgments: We acknowledge support from a MICMoR fellowship through the KIT/IMK-IFU to Ye Yuan. The Obs4MIPs XCO₂ satellite data have been obtained from the Copernicus Climate Change Service (C3S) Climate Data Store (<https://cds.climate.copernicus.eu/>). We thank Michael Buchwitz, University of Bremen, for providing comments on an early draft of this manuscript. OCO-2 satellite data products were produced by the OCO-2 project at the Jet Propulsion Laboratory, California Institute of Technology, and obtained from the OCO-2 data archive maintained at the NASA Goddard Earth Science Data and Information Services Center. CarbonTracker CT2017 and CT-NRT.v2018-1 results were provided by NOAA ESRL, Boulder, Colorado, USA from the website at <http://carbontracker.noaa.gov>.

Conflicts of Interest: The authors declare no conflict of interest.

Appendix A

Figures

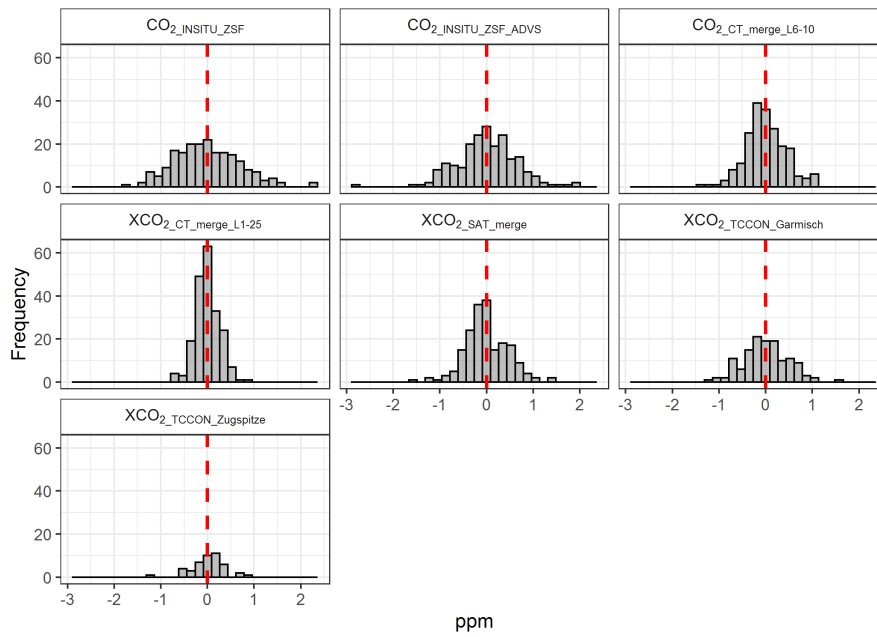


Figure A1. Histogram of STL-decomposed remainder components from all CO₂ and XCO₂ data sets of this study. Red dashed line shows the mean of each distribution.

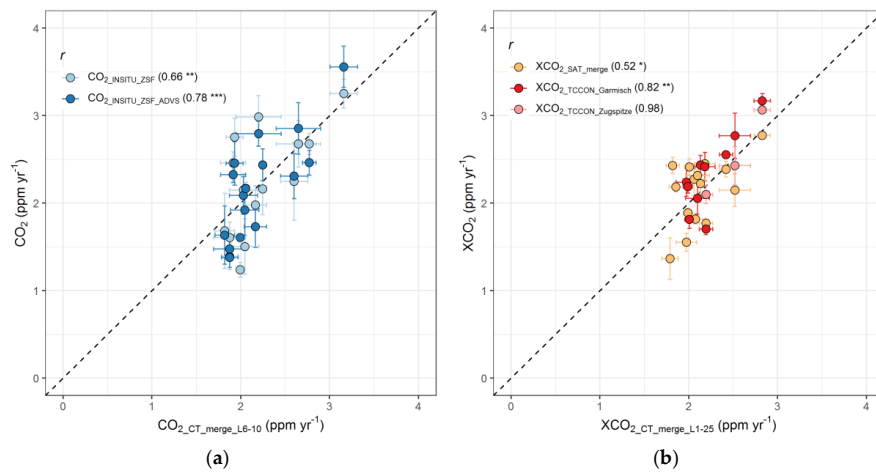


Figure A2. Scatter plots of annual mean growth rates from STL trend components in (a) CO₂ CT_merge_L6-10 and (b) XCO₂ CT_merge_L1-25 versus CO₂/XCO₂ measurements. Pearson's product-moment correlation coefficients (r) are listed accordingly for each pair. The significance levels are shown in symbols as 0.001 (***), 0.01 (**), and 0.05 (*). The 95% confidence intervals are shown as error bars on both x- and y-axis with dashed lines representing the 1:1 line.

Table

Table A1. Statistical summary of all CO₂ and XCO₂ data sets in this study.

Measurement Technique	Offset from CO ₂ _{insitu_ZSF} (ppm ± 95% CI)	Mean Annual Growth Rate (ppm yr ⁻¹ ± 95% CI)	Mean Seasonal Amplitude (ppm ± 95% CI)
CO ₂ _{INSITU_ZSF}	–	2.18 ± 0.10	13.08 ± 0.52
CO ₂ _{INSITU_ZSF_ADV5}	−0.66 ± 0.15	2.20 ± 0.09	10.93 ± 0.45
CO ₂ _{CT_merge_L6-10}	0.01 ± 0.17	2.21 ± 0.06	11.05 ± 0.28
XCO ₂ _{CT_merge_L1-25}	−2.36 ± 0.32	2.15 ± 0.04	6.36 ± 0.18
XCO ₂ _{SAT_merge}	−1.17 ± 0.38	2.13 ± 0.06	6.94 ± 0.22
XCO ₂ _{TCCON_Garmisch}	−1.95 ± 0.43	2.33 ± 0.08	6.58 ± 0.19
XCO ₂ _{TCCON_Zugspitze}	−1.03 ± 1.01	2.48 ± 0.16	5.22 ± 0.14

Comparison of Data Processing Methods

While it is aimed in this study to examine the applicability of the consistent data processing routine to various types of CO₂ measurements, the performance on the column-averaged measurements is focused here since the data processing routine has been applied practically to continuous in-situ measurements in other studies (e.g., [7,22]). Therefore, a re-processing on the same column-averaged data set (XCO₂_{TCCON_Garmisch}) used in Lindqvist et al. [34] but for a different time period (May/2009–Oct/2013) was performed and compared here. The reference study applied a skewed sine wave for the seasonal cycle with an upward linear trend in the following function

$$f(t) = a_0 + a_1 t + a_2 \sin(\omega[t - a_3] + \cos^{-1}[a_4 \cos(\omega[t - a_5])])$$

where a_1 indicates the CO₂ growth rate in trend and $2|a_2|$ denotes the peak-to-peak amplitude for the seasonal cycle. The XCO₂_{TCCON_Garmisch} data subset for the corresponding time period was extracted and decomposed by STL again and resulted in a mean annual growth rate of 2.12 ± 0.11 ppm yr⁻¹, and a mean seasonal amplitude of 6.56 ± 0.27 ppm. Compared to the reference results (2.03 ± 0.04 ppm yr⁻¹ and 6.6 ± 0.1 ppm, respectively), good agreements have been reached. However, small errors can be seen in the reference as daily XCO₂ values were included in the fitted function, while only monthly averaged data sets were used here. Also note that with the fitted sine term, a lack of data would play a minor role in determining the seasonal amplitude. In this case, XCO₂ data in 2009 cannot contribute to the mean seasonal amplitude because this data subset starts in May and the monthly maximum is assumed to be missing so that no seasonal amplitude can be calculated. Nevertheless, inter-annual variations cannot be derived from the function-fitted parameters, which help substantially in evaluating the performance of consistent data processing routines in our study.

References

1. IPCC. Climate Change 2014: Synthesis Report. In *Contribution of Working Groups I, II and III to the Fifth Assessment Report of the Intergovernmental Panel on Climate Change*; Pachauri, R.K., Meyer, L.A., Eds.; Core Writing Team: Geneva, Switzerland, 2014; p. 151. ISBN 978-929-169-143-2.
2. Dlugokencky, E.; Tans, P. Trends in Atmospheric Carbon Dioxide. NOAA/ESRL. Available online: www.esrl.noaa.gov/gmd/ccgg/trends/ (accessed on 21 October 2019).
3. Schultz, M.G.; Akimoto, H.; Bottenheim, J.; Buchmann, B.; Galbally, I.E.; Gilge, S.; Helmig, D.; Koide, H.; Lewis, A.C.; Novelli, P.C.; et al. The Global Atmosphere Watch reactive gases measurement network. *Elem. Sci. Anthr.* **2015**, *3*. [CrossRef]
4. Toon, G.; Blavier, J.; Washenfelder, R.; Wunch, D.; Keppel-Aleks, G.; Wennberg, P.; Connor, B.; Sherlock, V.; Griffith, D.; Deutscher, N.; et al. Total Column Carbon Observing Network (TCCON). In *Advances in Imaging, OSA Technical Digest (CD)*. *Opt. Soc. Am.* **2009**, JMA3. [CrossRef]
5. Hamazaki, T.; Kaneko, Y.; Kuze, A.; Kondo, K. Fourier transform spectrometer for Greenhouse Gases Observing Satellite (GOSAT). *Enabling Sens. Platf. Technol. Spaceborne Remote Sens.* **2005**, *5659*, 73–80. [CrossRef]

6. Crisp, D. Measuring atmospheric carbon dioxide from space with the Orbiting Carbon Observatory-2 (OCO-2). *Earth Obs. Syst.* **2015**, *9607*, 960702. [[CrossRef](#)]
7. Yuan, Y.; Ries, L.; Petermeier, H.; Steinbacher, M.; Gómez-Peláez, A.J.; Leuenberger, M.C.; Schumacher, M.; Trickl, T.; Couret, C.; Meinhardt, F.; et al. Adaptive selection of diurnal minimum variation: A statistical strategy to obtain representative atmospheric CO₂ data and its application to European elevated mountain stations. *Atmos. Meas. Tech.* **2018**, *11*, 1501–1514. [[CrossRef](#)]
8. Fang, S.X.; Zhou, L.X.; Tans, P.P.; Ciais, P.; Steinbacher, M.; Xu, L.; Luan, T. In situ measurement of atmospheric CO₂ at the four WMO/GAW stations in China. *Atmos. Chem. Phys.* **2014**, *14*, 2541–2554. [[CrossRef](#)]
9. Hernández-Paniagua, I.Y.; Lowry, D.; Clemitshaw, K.C.; Fisher, R.E.; France, J.L.; Lanoisellé, M.; Ramonet, M.; Nisbet, E.G. Diurnal, seasonal, and annual trends in atmospheric CO₂ at southwest London during 2000–2012: Wind sector analysis and comparison with Mace Head, Ireland. *Atmos. Environ.* **2015**, *105*, 138–147. [[CrossRef](#)]
10. Burrows, J.P.; Höhlzle, E.; Goede, A.P.H.; Visser, H.; Fricke, W. SCIAMACHY—scanning imaging absorption spectrometer for atmospheric chartography. *Acta Astronaut.* **1995**, *35*, 445–451. [[CrossRef](#)]
11. Bovensmann, H.; Burrows, J.P.; Buchwitz, M.; Frerick, J.; Noël, S.; Rozanov, V.V.; Chance, K.V.; Goede, A.P.H. SCIAMACHY: Mission Objectives and Measurement Modes. *J. Atmos. Sci.* **1999**, *56*, 127–150. [[CrossRef](#)]
12. Aumann, H.H.; Miller, C.R. Atmospheric infrared sounder (AIRS) on the earth observing system. *Adv. Next Gener. Satell.* **1995**, *2583*, 332–343. [[CrossRef](#)]
13. Miao, R.; Lu, N.; Yao, L.; Zhu, Y.; Wang, J.; Sun, J. Multi-Year Comparison of Carbon Dioxide from Satellite Data with Ground-Based FTS Measurements (2003–2011). *Remote Sens.* **2013**, *5*, 3431–3456. [[CrossRef](#)]
14. Liang, A.; Gong, W.; Han, G.; Xiang, C. Comparison of Satellite-Observed XCO₂ from GOSAT, OCO-2, and Ground-Based TCCON. *Remote Sens.* **2017**, *9*, 1033. [[CrossRef](#)]
15. Olsen, S.C.; Randerson, J.T. Differences between surface and column atmospheric CO₂ and implications for carbon cycle research. *J. Geophys. Res.* **2004**, *109*, 419. [[CrossRef](#)]
16. Schibig, M.F.; Mahieu, E.; Henne, S.; Lejeune, B.; Leuenberger, M.C. Intercomparison of in situ NDIR and column FTIR measurements of CO₂ at Jungfraujoch. *Atmos. Chem. Phys.* **2016**, *16*, 9935–9949. [[CrossRef](#)]
17. Shim, C.; Lee, J.; Wang, Y. Effect of continental sources and sinks on the seasonal and latitudinal gradient of atmospheric carbon dioxide over East Asia. *Atmos. Environ.* **2013**, *79*, 853–860. [[CrossRef](#)]
18. Nalini, K.; Uma, K.N.; Sijikumar, S.; Tiwari, Y.K.; Ramachandran, R. Satellite- and ground-based measurements of CO₂ over the Indian region: Its seasonal dependencies, spatial variability, and model estimates. *Int. J. Remote Sens.* **2018**, *39*, 7881–7900. [[CrossRef](#)]
19. Sánchez, M.L.; Pérez, I.A.; Buchwitz, M.; García, M.A. XCO₂ SCIAMACHY Total Column and CO₂ Ground Inter-comparison Results in the Spanish Plateau. In *Proceedings of the ESA Living Planet Symposium, Bergen, Norway, 28 June–2 July 2010*; Lacoste-Francis, H., Ed.; ESA Communications: Noordwijk, The Netherlands, 2010; ISBN 978-929-221-250-6.
20. Warneke, T.; Yang, Z.; Olsen, S.; Körner, S.; Notholt, J.; Toon, G.C.; Velazco, V.; Schulz, A.; Schrems, O. Seasonal and latitudinal variations of column averaged volume-mixing ratios of atmospheric CO₂. *Geophys. Res. Lett.* **2005**, *32*, L03808. [[CrossRef](#)]
21. Warneke, T.; Petersen, A.K.; Gerbig, C.; Jordan, A.; Rödenbeck, C.; Rothe, M.; Macatangay, R.; Notholt, J.; Schrems, O. Co-located column and in situ measurements of CO₂ in the tropics compared with model simulations. *Atmos. Chem. Phys.* **2010**, *10*, 5593–5599. [[CrossRef](#)]
22. Yuan, Y.; Ries, L.; Petermeier, H.; Trickl, T.; Leuchner, M.; Couret, C.; Sohmer, R.; Meinhardt, F.; Menzel, A. On the diurnal, weekly, and seasonal cycles and annual trends in atmospheric CO₂ at Mount Zugspitze, Germany, during 1981–2016. *Atmos. Chem. Phys.* **2019**, *19*, 999–1012. [[CrossRef](#)]
23. Wunch, D.; Toon, G.C.; Blavier, J.F.L.; Washenfelder, R.A.; Notholt, J.; Connor, B.J.; Griffith, D.W.T.; Sherlock, V.; Wennberg, P.O. The total carbon column observing network. *Philos. Trans. A Math. Phys. Eng. Sci.* **2011**, *369*, 2087–2112. [[CrossRef](#)]
24. Sussmann, R.; Schäfer, K. Infrared spectroscopy of tropospheric trace gases: Combined analysis of horizontal and vertical column abundances. *Appl. Opt.* **1997**, *36*, 735–741. [[CrossRef](#)] [[PubMed](#)]
25. Sussmann, R.; Rettinger, M. TCCON Data from Zugspitze (DE), Release GGG2014.R1 [Data set]. *CaltechDATA* **2018**, *r1*. [[CrossRef](#)]
26. Sussmann, R.; Rettinger, M. TCCON data from Garmisch (DE), Release GGG2014.R2 [Data set]. *CaltechDATA* **2018**, *r2*. [[CrossRef](#)]

27. Buchwitz, M.; Reuter, M.; Schneising, O.; Noël, S.; Gier, B.; Bovensmann, H.; Burrows, J.P.; Boesch, H.; Anand, J.; Parker, R.J.; et al. Computation and analysis of atmospheric carbon dioxide annual mean growth rates from satellite observations during 2003–2016. *Atmos. Chem. Phys.* **2018**, *18*, 17355–17370. [[CrossRef](#)]
28. Crisp, D.; Pollock, H.R.; Rosenberg, R.; Chapsky, L.; Lee, R.A.M.; Oyafuso, F.A.; Frankenberg, C.; O'Dell, C.W.; Bruegge, C.J.; Doran, G.B.; et al. The on-orbit performance of the Orbiting Carbon Observatory-2 (OCO-2) instrument and its radiometrically calibrated products. *Atmos. Meas. Tech.* **2017**, *10*, 59–81. [[CrossRef](#)]
29. Peters, W.; Jacobson, A.R.; Sweeney, C.; Andrews, A.E.; Conway, T.J.; Masarie, K.; Miller, J.B.; Bruhwiler, L.M.P.; Pétron, G.; Hirsch, A.I.; et al. An atmospheric perspective on North American carbon dioxide exchange: CarbonTracker. *Proc. Natl. Acad. Sci. USA* **2007**, *104*, 18925–18930. [[CrossRef](#)]
30. Buschmann, M.; Deutscher, N.M.; Sherlock, V.; Palm, M.; Warneke, T.; Notholt, J. Retrieval of XCO₂ from ground-based mid-infrared (NDACC) solar absorption spectra and comparison to TCCON. *Atmos. Meas. Tech.* **2016**, *9*, 577–585. [[CrossRef](#)]
31. Berrisford, P.; Dee, D.P.; Poli, P.; Brugge, R.; Fielding, M.; Fuentes, M.; Kållberg, P.W.; Kobayashi, S.; Uppala, S.; Simmons, A. The ERA-Interim archive Version 2.0. ERA Report, ECMWF, 2011, p. 23. Available online: <https://www.ecmwf.int/node/8174> (accessed on 31 October 2019).
32. Cleveland, R.B.; Cleveland, W.S.; McRae, J.E.; Terpenning, I. STL: A seasonal-trend decomposition. *J. Off. Stat.* **1990**, *6*, 3–73.
33. Pickers, P.A.; Manning, A.C. Investigating bias in the application of curve fitting programs to atmospheric time series. *Atmos. Meas. Tech.* **2015**, *8*, 1469–1489. [[CrossRef](#)]
34. Lindqvist, H.; O'Dell, C.W.; Basu, S.; Boesch, H.; Chevallier, F.; Deutscher, N.; Feng, L.; Fisher, B.; Hase, F.; Inoue, M.; et al. Does GOSAT capture the true seasonal cycle of carbon dioxide? *Atmos. Chem. Phys.* **2015**, *15*, 13023–13040. [[CrossRef](#)]
35. RC Team. R: A Language and Environment for Statistical Computing; Vienna, Austria. 2014. Available online: <https://www.R-project.org/> (accessed on 11 December 2019).
36. Dowe, M.; Srinivasan, A. Data. Table: Extension of 'Data.Frame'. 2019. Available online: <https://CRAN.R-project.org/package=data.table> (accessed on 9 December 2019).
37. Carslaw, D.C.; Ropkins, K. openair—An R package for air quality data analysis. *Environ. Model. Softw.* **2012**, *27–28*, 52–61. [[CrossRef](#)]
38. Zeileis, A.; Grothendieck, G. Zoo: S3 Infrastructure for Regular and Irregular Time Series. *J. Stat. Softw.* **2005**, *14*, 1–27. [[CrossRef](#)]
39. Wickham, H. *Ggplot2: Elegant Graphics for Data Analysis*; Springer-Verlag: New York, NY, USA, 2016; ISBN 978-331-924-277-4.
40. Cheng, J.; Karambelkar, B.; Xie, Y. Leaflet: Create Interactive Web Maps with the JavaScript 'Leaflet' Library. 2018. Available online: <https://CRAN.R-project.org/package=leaflet> (accessed on 16 November 2019).
41. Appelhans, T.; Detsch, F.; Reudenbach, C.; Woellauer, S. Mapview: Interactive Viewing of Spatial Data in R. 2019. Available online: <https://CRAN.R-project.org/package=mapview> (accessed on 13 May 2019).
42. Auguie, B. Gridextra: Miscellaneous Functions for "Grid" Graphics. 2017. Available online: <https://CRAN.R-project.org/package=gridExtra> (accessed on 9 September 2017).
43. Heymann, J.; Reuter, M.; Buchwitz, M.; Schneising, O.; Bovensmann, H.; Burrows, J.P.; Massart, S.; Kaiser, J.W.; Crisp, D. CO₂ emission of Indonesian fires in 2015 estimated from satellite-derived atmospheric CO₂ concentrations. *Geophys. Res. Lett.* **2017**, *44*, 1537–1544. [[CrossRef](#)]
44. Liu, J.; Bowman, K.W.; Schimel, D.S.; Parazoo, N.C.; Jiang, Z.; Lee, M.; Bloom, A.A.; Wunch, D.; Frankenberg, C.; Sun, Y.; et al. Contrasting carbon cycle responses of the tropical continents to the 2015–2016 El Niño. *Science* **2017**, *358*. [[CrossRef](#)]
45. Peters, G.P.; Le Quéré, C.; Andrew, R.M.; Canadell, J.G.; Friedlingstein, P.; Ilyina, T.; Jackson, R.B.; Joos, F.; Korsbakken, J.I.; McKinley, G.A.; et al. Towards real-time verification of CO₂ emissions. *Nat. Clim. Chang.* **2017**, *7*, 848. [[CrossRef](#)]



© 2019 by the authors. Licensee MDPI, Basel, Switzerland. This article is an open access article distributed under the terms and conditions of the Creative Commons Attribution (CC BY) license (<http://creativecommons.org/licenses/by/4.0/>).